PhD Thesis

Responses of epithelial monolayers to an imposed deformation

Author:
Tom Wyatt

Supervisors:
Prof. Guillaume Charras and
Prof. Buzz Baum

A dissertation submitted in partial fulfilment
of the requirements for the degree of

Doctor of Philosophy
of
University College London

UCL CoMPLEX

January 12, 2017

Declaration

I, Tom Wyatt, confirm that the work presented in this report is my own. Where information has been derived from other sources, I confirm that this has been indicated in the report.

This thesis is dedicated with love to Pamela Wyatt and Dudley Robinson.

Abstract

Epithelial monolayers are a class of animal tissue which comprise some of the most basic and important structures in metazoans. Many remarkable morphogenetic events, responsible for determining adult tissue shape, take place in epithelia and they continue to perform crucial functions throughout adult life.

Whether it is the filling of the bladder or during a precise morphogenetic transformation, epithelia must frequently undergo or drive tissue deformations. Therefore, much effort has been directed towards understanding the combination of material properties and cellular behaviours which determine how epithelia respond to the application of stress and strain. The complex biophysical environment of *in vivo* tissues, however, can hinder attempts to understand the underlying mechanisms and principles at play. To address this, a novel and highly simplified system is utilised in which uniaxial strain is applied to epithelia monolayers which are devoid of a substrate.

Application of compressive strain to these suspended epithelia unexpectedly revealed their ability to autonomously flatten buckles and remodel cell shape as the tissue mechanically adapts to a new shorter length over a duration of $\sim$60 seconds. These changes, which are found to be driven by actomyosin contractility, appear fully reversible since the epithelia can readapt to their initial length when it is restored and maintained over a similar time period.

At longer timescales, cell division within the epithelia is also found to be affected by the application of strain. Both compressive and tensile strain causes an alignment of division orientation which is demonstrated to be due to a global realignment of cell long axes combined with orientation of division along these axes, rather than by cells detecting and responding to long-range tissue stress orientation. In turn, these strain-oriented cell divisions homeostatically alter tissue organisation by redistributing cell mass along the direction of division and ultimately restore isotropic cell shape.

Acknowledgements

Thank you firstly to Guillaume and Buzz who have taught me so much, have provided guidance and fun discussions, shared ideas and inspiration and have supported me in every way possible. I couldn't have asked for better of supervisors.

To everyone past and present in both Guillaume and Buzz's labs: Nargess Khalilgharibi, Annaccia Bovissimo, Jigna Patel, Scott Curran, Maxine Lam, Jonathan Fouchard, Clotilde Cadart, Richard Thorogate, Sergey Lekomtsev, Kasa Ciuba, Andre Rosa, Charlotte Strandkvist, Nelio Rodrigues, Majid Malboubi, Helen Matthews, Malti Vaghela, Mario Ruiz Sorube, Julien Bellis, Andrew Harris, Amina Yonis, Jess Davies, Christina Dix, Sushila Ganguli, Jess Davies, Julien Record, Mathilde Richerd, Juanma Garcia, Ginger Hunter, Daniel Gradeci, Elias Barriga, Pelin Candarlioglu, Gautam Dey, Ekaterina Kapitonova, Nunu Mchedlishvili, Nitya Ramkumar, Ana Lisica, Pedro Almada, Guang Yang and Sacha Sarfati, thank you for years of fun, outings, discussion, lessons, help and support. In particular: Andrew for first making suspended monolayers. Julien B for teaching me device making at the start. Rich for making broken things work. Max for help and sharing the joy of division orientation quantifications. Helen for teaching me molecular biology at the start. Nargess for friendship from the beginning. Annaccia for taralli. Clotilde for the maledictions. Kasa for Zubr. Duncan and Si for making so many useful things. Last and probably least, Jonathan for co-founding the illustrious Royal Institution of the Lunch Club Association Society which incredibly now has over 3 members in almost 3 departments throughout UCL and the wider London area.

Many thanks also to collaborators outside UCL, Alexandre Kabla, Qian Cheng and Pierre Recho, for much help, many interesting discussions and many all-you-can-eat Drummond street Indian lunches.

Thank you to my friends and family in London and elsewhere. In particular Ross, Pete, Robbie, Clare, Alex, Nye and Izzy for sharing Camden and Canonbury. Of course

thanks to my lynchpin future child's godfather zen master yo-yo extraordinaire Simon Coplowe. Thanks Ella Ganguli for her careful reading of the thesis and helpful feedback. And everyone at CoMPLEX, Abi, Gemma L, Chris L, Will, Dan, Bobby, Katherine, Tim, Liz, Vic, Rollo, Chris B, Claire, Anne-Marie, Jon, Fintan. Thanks Shaz for the help with my kilim.

Finally, to Mum, Dad, Tash, Grandad and Annie. Thank you for the love and endless support you have given me.

Contents

List of Figures

Thesis overview

This thesis is split into 7 chapters. Chapter 1 introduces the main themes of the thesis by discussing a selection of relevant topics centred around epithelial biology and cell division. Key questions which remain unanswered are highlighted along the way and the goals of the present study are laid out.

Chapters 2 and 3 detail the methods used in the study. Chapter 2 contains general protocols which were used throughout the thesis and is intended to be used as reference. These methods were mainly in existence prior to the start of the project. Chapter 3 describes protocols which were significantly adapted and developed during the study. Each of the following chapters also contain brief methods sections describing procedures specific to those chapters.

Chapters 4, 5 and 6 present the main results of this thesis. Firstly, in chapter 4, the short timescale response of epithelia to uniaxial compressive strain is studied. In chapter 5, the effect of monolayer stretch on cell shape and stress and the effect that this has on cell division orientation is investigated. In chapter 6 the consequences of oriented division in terms of cell packing and cell and tissue shape are explored.

A discussion and interpretation of the results can be found in chapter 7, along with a proposal for future research directions.

Chapter 1

Introduction

1.1 The basics of epithelial tissues

1.1.1 Introducing the epithelium

The word epithelium was coined by Frederik Ruysch in the third volume of his *Thesaurus Anatomicus* [1]. He used it to describe a layered tissue he found on human lip and mouth surfaces and chose the name 'epithelium' from the greek $\epsilon\pi\acute{\imath}$ (epi) meaning 'upon' and $\theta\eta\lambda\eta$ (thēlē) meaning 'teat' due to the nipple-like protuberances which the tissue covered - which today are known as taste buds. The word is therefore a misnomer in literal translation, since in modern usage it refers to one of the four broad classes of animal tissue, that is, those that form layers and only a small subset of epithelia have anything to do with nipples. The misnomer has propagated, such that we have now also adopted the words 'endothelium' and 'mesothelium', which likewise have little to do with nipples.

Epithelial tissues, like those identified by Ruysch, are ubiquitous in animal bodies. Their sheet-like, quasi-two-dimensional structure is incredibly versatile and is used again and again in disparate settings to fulfil the topological, structural and functional demands of complex organisms. They form surfaces, line cavities, encase organs, protrude as villi and form intricate branching networks of tubes from the trunk of the aorta to the tangled

webs of renal glomeruli [2]. They make up the numerous glands of the body which can be tubular, coiled, branched and acinar in shape. Crucially, by encasing and lining, epithelia form the boundaries which partition the body [3]. They define inside from out and so are responsible for deciding what comes in and goes out - for regulating excretion, secretion, absorption and filtration. Simple epithelia are those composed of a single layer of cells (also 'epithelial monolayers') and are classified as squamous, cuboidal or columnar based on whether the cells which form them are wider than they are tall, or taller than they are wide (Fig. 1.1A–C). 'Simple', of course, is another misleading name since many simple epithelia have evolved remarkably complex structure in order to perform highly specialised functions. Podocytes, for instance, form simple epithelia inside nephrons. Their long interdigitating processes encapsulate capillaries and are precisely organised such that the slits between processes can filter the blood, removing water, sugars and urea but leaving behind proteins. Stratified epithelia are those made of multiple layers of cells (Fig. 1.1D). Generally speaking, whereas simple epithelia often specialise in regulating the passage of materials between compartments of the body, stratified epithelia provide robust barriers against the outside world, prohibiting the admittance of microbes and the escape of water and ensuring mechanical protection against mechanical stress and abrasion. Pseudostratified epithelia are an additional class of epithelial monolayers which can appear to be formed of several layers due to the long columnar shape of the constituent cells and the variable positioning of the nucleus (Fig. 1.1E).

Despite their versatility and diversity, epithelia are at the same time the most basic tissues that exist - they are fundamental to all animal bodies. Significantly, an epithelium named the trophectoderm is the first differentiated tissue to form during human embryogenesis. Epithelialness was likely the earliest form of multicellular organisation to evolve, since homologues of the genes which define epithelia are found in all metazoans, including the sponge *Oscarella carmela* [4], which diverged from other animals at the dawn of metazoan evolution, well before the Cambrian explosion. In fact, the relatively recent discovery

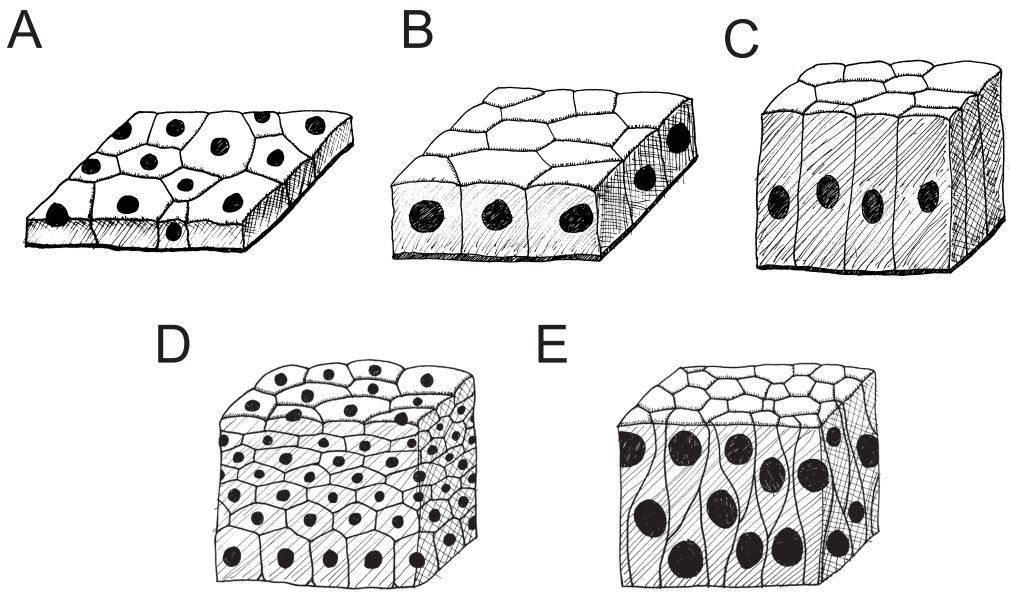

Figure 1.1: Drawings depicting the generic structure of epithelia of various kinds, including (A) squamous, (B) cuboidal, (C) columnar, (D) stratified and (E) pseudo-stratified.

of a simple epithelium in colonies of the not-quite-multicellular amoeba *Dictyostelium discoideum* reveals that epithelia may even predate the evolution of animals [5]. *Dictyostelium discoideum* will at times transition from its solitary unicellular life to form simple multicellular structures called grexes and sorocarps. Astonishingly, a simple epithelium was found in the sorocarp, organised by the proteins α- and β-catenin, which also organise metazoan epithelia. Cadherins, which are also fundamental to metazoan epithelia, were however not found in *Dictyostelium discoideum*. It is, therefore, an intriguing puzzle that the presumed closest single-celled relatives of metazoans, the choanoflagellates, possess cadherins but not catenins [6, 7].

1.1.2 Epithelia polarity and cell-cell junctions

The essence of an epithelial cell is its knowledge of upness from downess, along with its propensity to form cell-cell bonds organised with respect to these notions of 'up' and 'down'. Epithelial cells are thus strongly polarised (for a recent review see [8]) - they have an apical side which, for instance, often possesses a primary cilium and microvilli (Fig.

1.2), and opposite to this, they have a basal side which typically binds tightly to a fibrous substrate called the extracellular matrix (ECM).

This simple axis of polarity (from apical to basal) permeates the entire cell. Organelles such as the Golgi apparatus and the endoplasmic reticulum are polarised, as is the cytoskeleton, and the apical and basal cell membranes are strongly partitioned [8]. The molecular machinery which establishes and maintains polarity has been intensively studied and the number and complexity of the signalling pathways which govern it continues to grow. Among the best studied pathways are the PAR proteins (PARtitioning-defective), including Par-3, Par-6 and Pkc-3 [9]; the SCRIB group of tumour suppressors, including scribble (Scrib), lethal giant larvae (Lgl) and discs-large (Dlg) [10]; the CRB complex, including crumbs (Crb) and stardust (Std) [11]; the Coracle group, including yurt, coracle, neurexin IV and Na^+/K^+-ATPase [12] and the RHO family of GTPases including Cdc42, Rac1 and RhoA [13]. Concomitant with their role in polarity, these proteins localise to defined regions in epithelial cells - the PAR proteins are mostly apical or apical and junctional [14], SCRIB proteins are junctional and lateral [10] and CRB proteins are found apically [15] - although there is naturally plenty of variation between systems. Lipids such as phosphoinositides have also been implicated in organising polarity, with (for example) phosphatidylinositol-3,4,5-trisphosphate found mostly basally [16] and phosphatidylinositol 4,5-bisphosphate found mostly apically [17]. Ultimately, it is this cell polarity which enables opposite surfaces of epithelia to be functionally distinct, allowing for the directed passage of specific materials via endocytic and exocytic signalling pathways [18, 19].

The junctions which bind epithelial cells together, crucially enabling them to function as faithful barriers, are intimately linked with cell polarity since disrupting polarity can lead to disruption of junctions [20] and conversely, the formation of a junction can initiate cell polarisation [21]. Thus, via junctions, polarity can be coordinated across a whole tissue. However, barrier formation and pan-tissue polarity coordination are far from being the only roles played by junctions. As we shall see, cell-cell junctions allow for tissue

coordination in other ways, often transforming the individual cells which form the tissue into a chemical and/or mechanical continuum. Junctions are organised into several distinct types with delineated roles, four of these are briefly described here.

Tight junctions (or septate junctions in invertebrates) are formed from the proteins claudin, occludin and tricellulin, amongst others (for a recent review see [22]). They establish a semi-permeable barrier and thus have a critical role in regulating paracellular diffusion and are usually the apical-most junctions in epithelia. On top of this, they also help to maintain polarity by limiting intra-membrane diffusion of membrane bound proteins, thus partitioning apical and basal surfaces [23].

Usually found just below the tight junctions are the adherens junctions which are built from proteins which include cadherins, catenins and vinculin (for a recent review see [24]). Adherens junctions interact with a contractile network of protein filaments called the actin cortex, they can transmit tension generated extrinsically or by the actin cortex itself [25, 26] and they play a role in mechanosensation via tension-induced unfolding of α-catenin and recruitment of vinculin [27–29]. These attributes make adherens junctions key players in the dynamic movements of epithelia which shape the early embryo.

Thirdly, desmosomes are a family of junctions made up of desmoglein, desmocollin (desmosomal cadherins), plakophilin and plakoglobin (which are the desmosomal equivalents of catenins, for a recent review see [30] or [31]). Fibrous protein polymers named intermediate filaments bind to desmosomes via an adaptor protein named desmoplakin, mechanically integrating cells in the epithelium and helping tissues to resist shear stress. Indeed, mutations of desmosomal genes underlie the aetiology of several diseases associated with skin fragility [30]. As the only class of cytoskeletal filaments without an associated motor protein, intermediate filaments and associated desmosomes are generally considered to play a more mechanically passive role [32]. However, like other classes of junctions, desmosomes are active sites of biochemical signalling [33].

Finally, gap junctions are a class of inter-membrane structures with a rather different

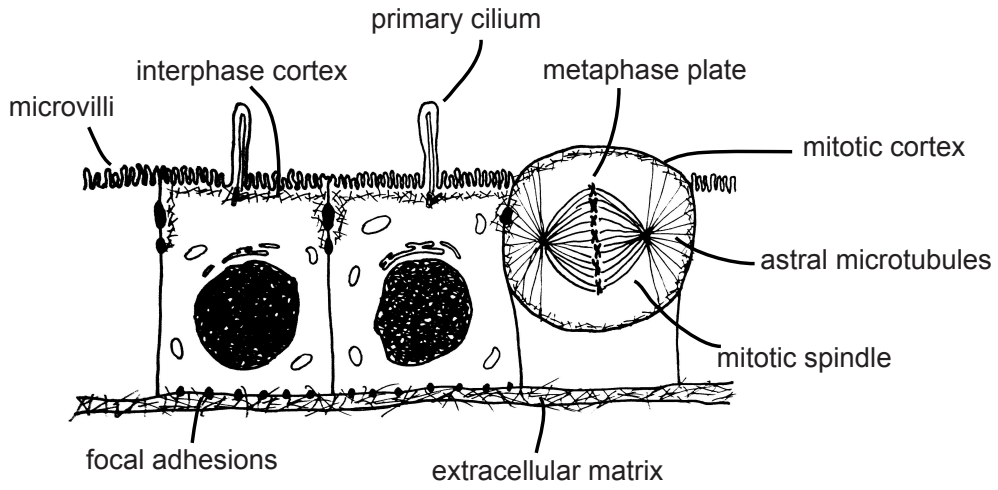

Figure 1.2: A drawing depicting several important features of epithelial cells in interphase and in mitosis.

role. They are formed of proteins called connexins (in vertebrates or innexins in invertebrates). They play little part in the mechanical connection of cells but instead form chemical connections, allowing the passage of various molecules between cells [34]. As such, they can play fundamental roles in fast communication throughout epithelia tissues [34].

1.1.3 Cell culture models of epithelia

Numerous model epithelial tissues have been established and intensively studied in several model organisms, several of which will be mentioned through the course of this introduction. A some-what smaller selection of model epithelia are available in cell culture. One of the best characterised is the Madin-Darby canine kidney (MDCK) cell line isolated in 1958 by S. H. Madin and N. B. Darby from the kidney of a healthy adult female cocker spaniel [35]. Their cow and sheep variants (MDBK and MDOK) never took off [36] but MDCK were later popularised, in particular by the Sabatini lab [37, 38] and the Louvard lab [39] in the 1980s, and have since been used in thousands of studies.

MDCK cells grow on glass and plastic substrates as squamous or cuboidal monolayers which do not become multilayered and exhibit some of the polarised fluid transport characteristics of a renal tubular epithelium [40]. They are tumorigenic, that is, they can

form tumour-like masses when injected into animals [40]. They form spherical cysts when grown in Matrigel [41] or a collagen gel [42] and they exhibit many of the attributes of polarised organisation found in other epithelia [8], both in cysts and when grown in 2D. Importantly for this thesis, they form stable cell-cell junctions and cells divide with many of the characteristics of primary epithelia [43].

Another important epithelial cell line, the HaCaT line, was derived from adult human skin keratinocytes (from the upper half of the back of a "not extensively sun-exposed" 62-yr-old male, to be precise) in 1988 [44]. They are named HaCaT after the low calcium and elevated temperature conditions in which they spontaneously transformed ('Human adult, low Calcium, elevated Temperature') [44]. When cultured in low calcium conditions they can indefinitely maintain a phenotype which most closely matches that of undifferentiated keratinocytes found in the basal layer of the epidermis [45]. In this state the cells express the basal keratinocyte markers keratin 5 and keratin 14 [45] and grow as a monolayer [46]. As in the *in vivo* epidermis, switching to higher levels of calcium triggers the down-regulation of keratin 5 and keratin 14, the up-regulation of keratin 1 and keratin 10, the rapid formation of adherens and tight junctions and the slower onset of stratification [45–47]. HaCaT have therefore become a convenient tool for the study of keratinocyte differentiation and skin morphogenesis [48].

Other important epithelial cell lines in use for various purposes include human corneal epithelia (HCE) cell lines [49] and the spontaneously immortalised human breast epithelial cell line MCF-10 [50].

1.2 The shapeshifting capacities of epithelia

1.2.1 Morphogenetic transformations of epithelia

Despite the large array of critical functions carried out by epithelia in adult bodies, some of which were mentioned in section 1.1, the most impressive are undoubtedly those per-

formed during development. Epithelia are the substrates and drivers of morphogenesis, that is, they shape the embryo. Here, epithelia are incredibly dynamic: they fold, fuse, reshape and reorganise in a dance of escalating complexity which culminates in the generation of much of the structure which defines the adult body. Epithelia migrate, spread and stretch in movements that envelope compartments or indeed an entire embryo, as in zebrafish epiboly [51]. At the completion of such enveloping events, epithelia zip-up and fuse, sealing the envelope in a process best studied in *Drosophila* dorsal closure [52]. The tissue can subsequently undergo refining processes which erase all evidence of the join [53]. To create the intricate tubular networks present in the lungs, pancreas and kidney, epithelia also deform themselves to bud [54] and branch [55] into the surrounding tissue, in processes which even govern the morphogenesis of teeth [56].

One of the most fundamental and perhaps best studied of epithelial morphogenetic processes is invagination. This is the process by which an epithelium folds in on itself, making an incursion into the underlying area. Invagination during gastrulation is the first macroscopic morphogenetic event of embryogenesis for most species in the animal kingdom and is coupled to a dramatic restructuring of the early embryo, from the relatively featureless ball of the blastula to the multi-layered gastrula [57]. After this initial event, epithelial invaginations are repeated again and again in disparate settings, from *Drosophila* eye imaginal discs [58] and tracheal pits [59], to the *C. elegans* vulva [60], to the mouse lens placode [61]. Later on in development, along with cavitation [62], epithelial invagination is a primary mechanism for the formation of glands.

But epithelia do not always fold inwards. The out-folding, or evagination of epithelia has also been studied in several settings. In the human and chick gut, for instance, the first steps of villi morphogenesis involve the evagination of the gut epithelium [63]. Here, the compressive forces applied by the surrounding layers of smooth muscle are what drive the outward buckling [63]. In a rather different setting, the entire *Drosophila* wing imaginal disc evaginates mid-way through wing development [64] and while the driving forces are

less well understood, shape changes within the wing disc epithelium are thought to work in concert with forces produced by a neighbouring tissue [65, 66].

While epithelia achieve an impressive amount through folding, in-plane deformation is of course also important. In the later stages of wing development, for instance, the wing hinge contracts and stretches the attached wing blade epithelium [67]. The combination of this contraction with the specific patterning of boundary constraints is though to determine much of the final shape of the wing [67, 68]. During *Drosophila* germ-band elongation, the increase in width and decrease in length of the germ-band is brought about via a combination of cell-based behaviours (see the next section) and tension generated in neighbouring regions of the embryo [69].

In all, the morphogenetic movements of animal epithelia are probably only outdone by the algae *Volvox globator* embryo, which turns itself entirely inside-out in a spectacular movement [70] which is almost reminiscent of a solution to Smale's veridical paradox [71] (Fig. 1.3).

1.2.2 Cell-level mechanisms which drive epithelial morphogenesis

Underpinning many of the remarkable changes in form that we witness in epithelia during development are choreographed changes in cell behaviour which lead to the spatially and temporally regulated generation of forces which alter cell shape and organisation.

During *Drosophila* gastrulation, the apical areas of a specific subset of cells is gradually reduced by pulsatile constrictions of the apico-medial actomyosin cortex [72]. Beyond apical constriction, the precise mechanical path of invagination is not well understood but various models suggest the requirement of contractile forces along the lateral sides of cells [73] and/or a decay of the basal membrane rigidity [74]. Ultimately, therefore, this morphogenetic event is driven by changes in cell shape.

An alternative method to cell shape change is to rearrange cells within a tissue. Through the regulation of tension and adhesion at individual cell-cell junctions, cells in many sys-

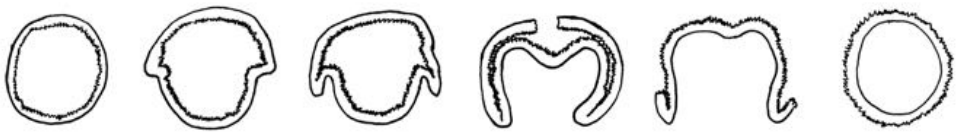

Figure 1.3: A sequence of drawings depicting the shape of *Volvox globator* as it turns itself inside-out. As captured recently by Höhn *et al.* [70]

tems change neighbours by removing and adding entire junctions (termed a 'T1 transition'). During *Drosophila* germ-band extension, by far the best studied system, junction remodelling is polarised across the entire tissue such that anterior-posterior (A-P) junctions are removed and dorsal-ventral (D-V) junctions created [75, 76]. This process relies on orchestration at the cell and tissue scale. Activated non-muscle myosin II is preferentially localised to A-P junctions via Rho-kinase recruitment by RhoA [75, 77]. This generates the tension which drives the shrinkage of A-P junctions. Up-regulation of this tension is accompanied by the down-regulation of adhesion at A-P junctions via Abl tyrosine kinase [78]. Meanwhile, Bazooka and PAR-3 are polarised to the D-V junctions, promoting stability [79]. At the tissue level, this process is in part organised by a set of Toll family receptors which form a tissue-level pattern of partially-overlapping stripes [80].

A third basic class of cell-based morphogenetic mechanisms, in addition to cell shape changes and cell rearrangement, is cell division. Cell division is prolific in epithelia, particularly during development. The *Drosophila* wing disc, for instance, begins life as 50 cells which then proliferate (undergoing rounds of cell growth and division) for several days without differentiation to reach a final size of $\sim$50,000 cells [81]. When coupled to cell growth, differential rates of division in a tissue can result in altered shape and size [82]. But frequent cell divisions do not necessarily result in tissue growth. Cells divide without significant growth during cleavage in early embryos to reduce cell size and cell growth can be balanced by cell loss through apoptosis [83] or cell delamination [53, 84]. Indeed, the loss of cells through such processes is yet another important mechanism which contributes to tissue shape in a range of systems [85, 86]. Cell division is discussed in more

detail in sections 1.3 and 1.4 of this introduction, since it is the subject of the work reported in chapters 5 and 6.

1.2.3 Responses of epithelia to extrinsically applied deformation

Sections 1.2.1 and 1.2.2 above discussed some of the ways in which epithelia produce spatially and temporally regulated patterns of force which induce changes in tissue shape. These processes are intensively studied in a large number of systems as they are crucial to morphogenesis. However, epithelia are also frequently subjected to stresses and deformations which are driven by processes occurring outside of themselves, that is, they are subjected to extrinsically applied deformation. This is true during morphogenesis, where the complex movements of tissues can lead to the deformation of mechanically coupled neighbouring tissues. For instance, endoderm invagination in the *Drosophila* embryo produces a tensile force which is felt throughout the embryo and contributes to germband elongation [87]. Likewise, during pupal stages of the development of the *Drosophila* wing epithelium, contraction of the wing hinge applies a stress to the wing blade epithelium which is crucial for its subsequent morphogenesis [67]. During zebrafish epiboly, the forces which drive the enveloping epithelium to migrate across the entire embryo are mainly generated in the rim of the epithelium, however, an anisotropic stress is observed throughout the tissue [51].

The effects of extrinsically applied deformations are not only important during morphogenesis. In adult tissues too, epithelia are subjected to deformation which varies greatly in magnitude and timescale. Indeed, whereas many tissues (such as the nervous tissue of the brain) are mechanically insulated from their surroundings by bone or other structures, epithelia are frequently found in parts of the body which naturally experience the most extreme of mechanical stimuli. The epithelia which line vasculature experience sub-second deformation with each heartbeat, the alveoli are deformed by up to 40% [88, 89] over a second or so of inhalation, the bladder is stretched as it fills with urine throughout the day

and normal interactions with the environment produce a varied and unpredictable set of deformations on the skin and others tissues.

Epithelia must therefore be designed to respond appropriately to such deformations. First and foremost, since epithelia form crucial boundaries between different tissues, organs and the inside and outside worlds, the risk of rupture must be minimised. As a first defence, in section 1.1.2 above we saw how epithelial cells are tightly bound by a variety of intercellular adhesion molecules which form junctional complexes such as the adherens junctions [24] and desmosomes [30, 31]. The fibrous networks of the cytoskeletons of neighbouring cells meet at these junctions, altogether forming a mechanical syncitium which resists deformation and distributes stresses throughout the tissue [26]. Interestingly, the changes which occur during the formation of an epithelium mean that the tissue is (mechanically speaking) greater than the sum of its cellular parts: the elasticity of MDCK epithelial monolayers was found to be orders of magnitude greater than individual cells [90] and was found to possess an average adhesion strength which is several times the adhesion energy which binds just two cells [90].

Alongside the strength of adhesion, a response which likely contributes to protection against rupture is stress dissipation. Within epithelia, the majority of the stress which is induced by an applied deformation is found to dissipate rapidly [90–92] and so epithelia can in many regimes be considered viscoelastic materials. This dissipation undoubtedly reduces the risk of rupture since the long timescale stress borne by cell-cell junctions for a given strain is reduced. The origin of this stress relaxation is not completely understood but the ubiquitous turnover of molecular structures within the cell [93] is likely a key component. The rapid and continuous assembly and disassembly of stress-bearing structures within the cytoskeleton are a particularly strong candidate [94, 95].

Protecting the plasma membrane against deformation-induced rupture is also crucial. One particularly interesting tissue which has been studied in this context is the urothelium, which is the stratified epithelium which lines the mammalian bladder. Whilst maintaining

the crucial function of storing urine for extended periods (without allowing reabsorption of toxins filtered by the kidneys), the urothelium must also withstand a doubling of its surface area over several hours as the bladder distends. This is later followed by a sudden compression exerted by the detrusor muscle which empties the bladder during urination. To cope with these significant shape changes, the cytoplasms of urothelia are filled with a network of lipid vesicles connected by intermediate filaments [96]. The current working hypothesis [97] is that stretch causes the filaments of this network to straighten and due to their connection with the apical tight junctions [98] they are brought close to the apical membrane where they can be merged, allowing for the required increase of lipid surface area. The connection with the intermediate filaments is maintained so that membrane can be removed upon release of the stretch. The process appears to require ATP during stretch but not unstretch [99].

Specific adaptations also protect the plasma membranes of alveolar epithelial cells against rupture. The cells must increase the surface area of their plasma membrane during inhalation by up to 40% [88, 89]. Fast unfolding of membrane ruffles and slower trafficking of lipids to the membrane both act to allow for this increase. Upon release of the stretch the lipid membrane area decreases with similar dynamics [88].

At longer timescales, of minutes to hours, cell based processes such as cell-cell rearrangements and cell divisions, must also be considered. These processes were discussed in the section above in the context of developmental programmes which actively generate shape, however, they also appear to play a role in responding to extrinsically applied deformation. As mentioned above, tension is applied to the developing *Drosophila* wing blade by the constriction of the wing hinge. Etournay *et al.* [67] demonstrated that this tension specifically induces cell-cell rearrangements and oriented cell divisions which in turn contributes to defining the final shape of the wing by reorganising cellular material. Interestingly, they also noted that the total contribution made by different processes (cell-cell rearrangements, shape change and cell divisions) varied more than the variation in

final wing shape, indicating that the different processes are not specifically programmed but can freely and dynamically compensate for one-another [67]. The ways in which cell divisions can alter epithelial shape and packing are a major topic of this thesis and are investigated in chapter 6. Therefore, our current understanding of such processes is discussed further in section 1.3.

An important class of responses to extrinsically applied forces, which partly overlaps with the processes described thus far, are those processes which involve mechanotransduction. Mechanotransduction is an intensively studied class of processes in which cell behaviours of a great variety can be triggered by mechanical stimuli. Precise terminology is important here, since terms and concepts are easily confused in such a rapidly moving and highly interdisciplinary field. The term 'mechanotranduction' must be reserved for those processes which specifically depend on a pathway of biomolecular signalling which directs cell behaviour. A range of mechanisms for transducing the original mechanical signal into a biomolecular signal have been uncovered, such as the stress-induced conformational change of a protein [100] or the opening of an ion channel [101]. The list of cell behaviours which can be regulated after such a pathway is triggered is much longer [102–104] and is rapidly growing. Mechanotransduction therefore certainly plays important roles in the response of epithelia to mechanical perturbations, for example via the reinforcement of adherens junctions [105] and focal adhesions [100] or reorganisation of the actomyosin cytoskeleton [106, 107]. However, another category of responses must also be recognised, since emergent changes in behaviour do not always need to be overseen by a cascade of biomolecular signalling. These responses are perhaps better described as 'mechanosensitive' and good examples include the automatic mechanical adaptation of the actomyosin cortex to the stiffness of the environment [108] and indeed the automatic delivery of lipids to the apical membrane during stretch of the urothelium described above [96].

Amongst the spectrum of responses to mechanical perturbations discussed in this sec-

tion, a subset may contribute to mechanisms which can be described as homeostatic. That is, they contribute to restoring the state of the tissue to a certain preferred state after it has been perturbed by an extrinsic influence. A perturbation may have changed the cell or tissue size or shape or the level of stress within and molecular and cellular behaviours may then act to restore the original values. An important aspect of tissue homeostasis, defined thus, is that it implies that a memory of the preferred state of the tissue is somehow encoded into the system and that this memory persists when the system is mechanically perturbed, in order to guide homeostasis. Within our current context, the ideal cell (or tissue) shape or stress are attributes which could be stored. An ideal cell shape could be effectively encoded via memory of a preferred cell height, or apical area, for example, and cell stress may in fact mean the stress in the cytoskeleton or the plasma membrane or along cell-cell junctions.

In the majority of systems, the robustness of developing and adult tissues to a great range of perturbations strongly suggests that such homeostatic mechanisms exist yet few have been adequately studied. In many cases it is not yet clear which parameters are being monitored, let alone how they are measured and how homeostatic responses are regulated. In the case of the enveloping cell layer during zebrafish epiboly, however, it is known that a particular ratio of cell height (apical to basal) to cell length (within the epithelial plane) is somehow encoded and measured. Thus, if a cell of the enveloping cell layer is longer than it is wide such that the ratio is greater than 1.3, then the cell divides within the plane, otherwise the division is apical to basal [109] and one daughter cell is removed from the epithelium. This allows for homeostatic control of cell and tissue shape by removing cells when cells become too columnar. The mechanism which defines the ratio is not understood but the authors demonstrate that altering it has a profound effect on morphogenesis and provide evidence that a range of different morphologies found in similar species may be generated simply by altering the ratio [109]. Cell size homeostasis [110], control of the density of cells within a tissue [53, 84] and the regulation of the level of tension in a tis-

sue [111] are further examples of processes in which a specific value of a physical entity must somehow be 'encoded' or 'remembered', even in the face of unpredictable perturbations. Understanding the mechanisms which provide this memory and how they can be tweaked by evolution is a crucial but challenging task which will require a fundamentally cross-disciplinary approach.

Finally, as well as memorising a specific ideal value to any of these physical parameters, so that tissues can respond homeostatically to mechanical perturbations, it may also be asked whether cells and tissues can in any way remember and take into account past mechanical perturbations. If, for instance, a tissue is stretched for just a transient period, is this perturbation remembered for long after the initial state is restored? And can this memory be used to guide a different, perhaps improved, response to the next perturbation? Some well-known phenomena which fall into this category include the increase of muscle mass [112], the reinforcement of bone [113] and the formation of calluses in response to a range of different mechanical stimuli [114]. Here, the long term memory is in the form of changes to cell and tissue structure, via cell hypertrophy, increased mineral deposition and keratinisation, respectively. The memory can persist for months or years but in many cases the absence of further mechanical stimulation will lead to a homeostatic return to the original state. A more dramatic example is found in stem cells in which mechanical stimuli are thought to influence differentiation, thereby permanently changing the identity of the cell. This is thought to take place during gastrulation in the *Drosophila* and zebrafish embryos where stretch has been shown to encourage cells to differentiate into mesoderm [115]. It will now be important to search for more subtle forms of memory in such systems, particularly at the sub-cellular scale. Can, for instance, a transient mechanical perturbation induce long-term changes in the cytoskeleton (see [116] for an excellent, but speculative, discussion) or perhaps epigenetics, which later guide a different response? Of course, it will be important to search for these processes whilst acknowledging that they need not exist *a priori*. For instance, in one particularly elegant experiment Streichan *et*

al. [117] showed that the regulation of cell cycle progression by epithelial deformation has no dependance on previous deformations and is therefore a simple function of the current state of deformation.

1.3 The importance of cell division orientation

1.3.1 Introducing cell division orientation

As already mentioned in the above sections, cell division is a hugely important process which influences the morphogenesis of tissues and is an important focus of this thesis. An adult human body is made from an estimated $\sim 4 \times 10^{13}$ cells [118]. To account for cell turnover, however, the number of cell divisions which occur during the average human lifetime is estimated to be of the order of 1×10^{16} [119]. Such a mammoth process must clearly be carefully controlled and indeed, the result of deregulation is cancer. Thus, cell division is regulated in four basic ways. Firstly, cell division symmetry is controlled. Cell divisions can be symmetric, producing essentially indistinguishable daughter cells, or they can be asymmetric, producing daughter cells of different sizes and/or cell fates. The second and third factors are space and time. Cells grow and divide at different rates, in different places of different tissues, at different time-points during the life of an organism [120, 121]. Mis-regulation of these factors can clearly lead to abnormal tissue shape and size.

The final parameter which must be controlled for each division is orientation. Division orientation is not a precisely defined geometric parameter: it could, for instance, be taken as the direction of the line drawn between the centroids of the new daughter cells or, on the other hand, it could be defined as the normal to the plane of the cytokinetic ring or even the normal to the plane of the new junction which forms between the daughters. These definitions will give similar but not identical orientations. Nevertheless, division orientation has a clear consequence - it determines the position of the daughter cells relative to one-another and relative to the surrounding tissue. In some tissues, post-division

shape change and migration of daughter cells can give them the freedom to reposition themselves in any way required [122]. In other tissues, daughter cells may simply inhabit the same space as the mother cell and there may be little difference between one or two cells inhabiting that space. These extreme scenarios would render division orientation unimportant but, as discussed in this section, there are many examples in which division orientation is in fact critical.

1.3.2 Planar division orientation and cell fate

In epithelia not all orientations are equal. The plane of the epithelium itself defines an *a priori* orientation which is found to have a strong influence on division orientation. Indeed, in many experimental systems, epithelial cells are found to divide in an orientation which is parallel to the epithelial plane (Fig. 1.2). In the mouse small intestine, measurements by Fleming *et al.* demonstrated that cells in this tissue divide within 10° of the plane of the epithelium [123]. Divisions in MDCK are also found to mostly orient within 10° of the plane of the epithelium [43]. The same is true in the *Drosophila* follicular-epithelium which surrounds the germ-line in the *Drosophila* ovary [124] and even in isolated, adherent but non-polarised cells [125] which divide in an orientation aligned parallel to their substrate.

The clearest motive for orienting divisions in the plane of monolayer epithelia is for the generation and preservation of the monolayer structure. Even bacteria make use of this mechanism. The bacteria *Lampropedia hyalina* restricts division orientation to a plane allowing them to form perfect sheet-shaped colonies [126].

Fernández-Miñán *et al.* found that disrupting the planar orientation of the divisions in the *Drosophila* follicular epithelium can cause the monolayer to acquire a stratified structure [124]. Similarly, both MDCK and human intestinal epithelial Caco-2 cells normally form monolayer cysts when grown in 3D but these are misshapen and contain multiple cell layers and multiple lumina when planar division orientation is perturbed [127, 128]. Analogous evidence has also been found in the animal cap of the zebrafish embryo [129].

Altogether, this indicates that daughter cell placement, under the control of division orientation, can be critically important in determining and maintaining epithelial structure. Interestingly, however, Bergstralh *et al.* [122] recently uncovered a mechanism through which misplaced daughter cells can be reintegrated into an epithelium via the action of lateral adhesion.

The link between division orientation and epithelial tissue organisation raises the possibility of a role for division orientation in the progression of cancer. Carcinomas, which by definition begin in epithelial tissues, are often found to lack normal epithelial structure [130, 131]. In addition, the cell-cell interactions resulting from normal epithelial structure can play a role in regulating mitosis and apoptosis [131] meaning that disruption of structure could conceivably lead to mis-regulation of these processes, which are fundamental to cancer. In support of this, Nakajima *et al.* found that perturbing division orientation in the *Drosophila* wing disc could result in tumour-like cell-masses at the basal side of the epithelium [132]. They found that mis-oriented divisions lead to the basal-most daughter cell being removed from the epithelium, usually resulting in apoptosis. However, the tumour-like cell-masses could be induced if apoptosis was inhibited, in addition to perturbing the orientation. In the chick neuroepithelium, perturbing planar division orientation again leads to cells leaving the neuroepithelium and these were found to continue dividing even without inhibition of apoptosis. However, tumour-like aggregates were not reported in this instance [133].

Despite the prevalence of in-plane division orientation in epithelia, many important examples of divisions oriented perpendicular to the plane of the epithelium have been studied. The mouse epidermis starts as an epithelial monolayer in which cell divisions initially align in the canonical in-plane orientation. However, later in development cells begin to divide in the perpendicular direction [134]. Interestingly, this begins at the onset of epithelial stratification, suggesting that the perpendicular divisions could promote stratification in analogy to the ectopic stratification induced by mis-oriented divisions in [124]. A direct

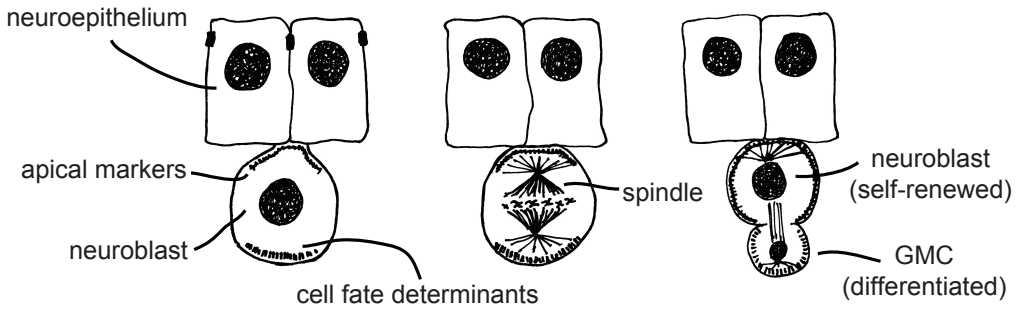

Figure 1.4: A sequence of drawings depicting *Drosophila* neuroblast self-renewal.

causal relationship, however, is yet to be established. More recently, it was shown that cells in the zebrafish presumptive enveloping layer (pre-EVL) can also divide in both the planar and perpendicular orientation. The authors propose and experimentally validate a model whereby division orientation regulates cell shape in the pre-EVL by increasing cell number (in the case of planar divisions) or decreasing pre-EVL volume (in the case of perpendicular divisions) [109].

Epithelial divisions in the out-of-plane direction are also known to play a role in the regulation of stem cell populations and the generation of cellular diversity. The mouse epicardium is an epithelial monolayer which covers the myocardium. Epicardium cells either divide in the plane of the epicardium, thereby staying integrated in the monolayer, or divide perpendicular to the plane, in which case one of the daughters migrates into the subepicardial space where it differentiates into a fibroblast or a vascular smooth muscle cell [135]. Deletion of either the cell fate determinant Numb or the junctionally associated protein β-catenin leads to loss of control of division orientation along with loss of the ability of cells to migrate [135].

Details of the relationship between division orientation and fate determination in the mouse epicardium are yet to be elucidated. However, it is tempting to draw comparisons with the *Drosophila* neuroblast system, where the relationship is well established (Fig. 1.4, for a review see [136]). Here, the neuroblasts are derived from the neuroepithium, a tissue in which cells divide symmetrically in the plane of the epithelium. When a neuroblast is

formed it partially delaminates from the epithelium and divides in the orthogonal, apical-to-basal direction [137]. By doing so it partitions cell fate determinants unequally between the daughters, giving rise to one neuroblast and one ganglion mother cell (GMC) [137]. In the regulation of stem cell populations in the *Drosophila* male germ-line, division orientation is again important. Here though, it is thought that the main cue to differentiate comes from the surrounding tissue and that divisions are oriented such that one cell remains in contact with this environment (or "niche"), enabling it to retain stem cell character, whereas the other is positioned outside of the niche, leading to cell differentiation [138].

Importantly, a link between cancer and division orientation has emerged in the study of stem cell divisions. In humans and mice, in both the small intestines and colon, invaginated structures called crypts harbour a small number of stem cells at their base. Unlike the epithelial cells which line the rest of the crypt, which divide in the plane of the epithelium, stem cells in the crypt divide in the apical to basal direction [139]. Loss of adenomatous polyposis coli tumour suppressor (APC) protein, however, causes disruption of this pattern of division orientation [139]. This loss leads to the mis-segregation of DNA, such that the old, template DNA strand is no longer exclusively partitioned into the daughter cell which is fated to remain a stem cell [139]. Drawing on Cairns' hypothesis [140], which proposed that retention of the old, template DNA protects stem cells from accumulating replication errors in the DNA, the authors therefore suggest that the strong oncogenic effect of APC mutations may in part be explained by its effect on division orientation [139].

1.3.3 The azimuthal orientation, geometric order and tissue shape and stress

Epithelial cells which divide in the plane of the epithelium still have one remaining degree of freedom with regard to orientation - they still have a choice of within-plane orientations, also known as the azimuthal orientation or "in-plane" orientation. The choice of azimuthal orientation has profound consequences, separate from the effects of the out-of-

plane orientation. The effects of this choice of division orientation are a key topic of this thesis and they are explored within a simple epithelium in chapter 6.

In-plane division orientation affects epithelial topology, this can be understood as follows. An epithelium viewed apical-side-on can, for some purposes, be considered as a two-dimensional tiling of polygons. The 'topology' of this simplified model of an epithelium describes which polygons neighbour which others. Cell division alters the topology by turning one polygon into two, both of which will have a new number of sides. On top of this, the division adds one side to two neighbouring cells as a result of the junctions bisected by the newly formed junction. The cells which gain a side are thus determined by the azimuthal angle of the division. Surprisingly, Gibson *et al.* found that epithelial topology was similar over a broad range of metazoan epithelia [141]. Although the topology was irregular, consisting of a disordered mix of shapes including everything from squares to decagons, all of the examined epithelia contained a similar distribution of shapes. Ultimately the authors were able to demonstrate that this distribution was consistent with a randomly distributed azimuthal angle [141], showing that simply a lack of regulation of this parameter can produce an important emergent pattern. Interestingly, it was later demonstrated that epithelial topology can itself feed back on division orientation, via control of cell shape [142].

Despite a broad range of epithelia sharing this distribution of polygons, the choice of the azimuthal orientation of cell division is frequently not random at all and its regulation has important consequences in epithelial morphogenesis (for a detailed review see [143]). Indeed, there are many examples where all divisions in a tissue, or a particular section of a tissue, orient along the same axis.

During zebrafish gastrulation, cells of the epiblast initially divide along the animal-vegetal axis [144]. A little later, after the start of neurulation, the preferred direction of division changes. Now divisions align in the medio-lateral direction [145]. Likewise, divisions align along the anterior-posterior axis during primitive streak formation in chick

embryos [146]. During *Drosophila* germ band elongation, divisions at the posterior end of the embryo orient along the anterior-posterior axis [147]. In the *Drosophila* wing disc, cells in the centre of the tissue divide along the proximal-distal axis, whereas cells at the proximal edge divide perpendicular to this axis [148]. Cells near the dorsal ventral compartment border divide along this border, whereas cells far from the border divide perpendicular to it [149]. Such patterns are also seen in the eye imaginal disc [149].

Later on in development, divisions again take on stereotyped azimuthal orientations during the morphogenesis of tubules of various kinds. In rat and mice kidney tubules [150], rat retina blood vessels [151] and mouse lung tubules [152], divisions orient preferentially along the length of the tubule. In the mouse fore-stomach, divisions align along an axis called the cephalocaudal axis [153].

Such distinct patterns, found over such a broad range of tissue across the animal kingdom, are unlikely to have no role. It is compelling that in all of the examples above the stereotyped division orientation is aligned with the direction of tissue shape changes. This has led several authors to propose that oriented divisions may drive tissue elongation. This has been supported by the observation of clone shapes which are elongated in the direction of division orientation during *Drosophila* germ band elongation and in the wing and eye imaginal discs. Such shape is lost when division orientation is randomised [147–149]. The plausibility of this model of tissue elongation, in which oriented divisions drive a change in tissue shape, was confirmed via computational modelling [154]. Importantly, the randomisation of division orientation also perturbed the shape of the fully-developed wing and eye [148, 149]. In a similar fashion, randomisation of division orientation leads to cephalocaudally shortened fore-stomachs in mice as well as short and dilated blood [151] and lung vessels [152] and kidney tubules [150] in mice and rats. In addition, the dilation of kidney tubules due to ectopic division orientation has been proposed to be characteristic of the first stages of Polycystic kidney disease [150].

Despite this large body of evidence, there is still debate over the degree to which po-

larised division orientation can instructively drive tissue elongation. Many of the studies mentioned above interfered with division orientation by altering genes that have pleiotropic effects. Tissue elongation can be driven by many factors including cell intercalation [76] and extrinsic forces [155] and it is difficult to know which factors are affected by a given perturbation. Furthermore, some direct evidence against a role for oriented division has emerged. The avian primitive streak can form without defect in embryos in which cell division is inhibited [156]. Similarly, in zebrafish embryos, Quesada-Hernández *et al.* showed that body-axis elongation during gastrulation was not perturbed by the inhibition of division or by the inhibition of the motor protein dynein, which randomises division orientation [157]. In kidney tubules, it has more recently been observed that tubule dilation in mutants can occur before the randomisation of division orientation, casting doubt on a causal link between division orientation and Polycystic kidney disease [158].

Rather than instructively driving tissue elongation, it is therefore possible that in some settings oriented cell division could play a permissive role, allowing tissues subjected to forces to elongate without causing damage. Campinho *et al.* used laser ablations to show that a highly anisotropic tension builds up in the zebrafish enveloping cell layer during epiboly [51]. They found that cell divisions aligned with this direction of tension and, by examining the tissue recoil after laser cuts made adjacent to divisions, they showed that cell division could relieve tissue stress in the cell layer. They therefore proposed that tension-oriented cell division permits tissue spreading by reducing tension anisotropy. This hypothesis was supported by the reduction in layer spreading caused by the inhibition of cell division and the oriented cell fusions which occurred when division orientation was randomised.

1.4 Controlling the orientation of the mitotic spindle

1.4.1 Moving the mitotic spindle

Given the biological community's ongoing exposition of the important effects of division orientation, a key question is how division orientation is regulated by the cell and its environment. This is a topic which has been intensively studied but which still contains a host of unanswered questions.

During mitosis, several conspicuous structures form within epithelial cells which play roles in the faithful completion of division. Early on in mitosis, the mitotic spindle (Fig. 1.2) assembles from tubular polymers called microtubules, which are themselves formed from heterodimers of α- and β-tubulin (Fig. 1.5). First seen by 19th century cytologists [159], the spindle has been studied with great interest ever since. We now know that the spindle is nucleated from structures called centrosomes, that it is responsible for capturing chromosomes and arranging them into an orderly structure called the metaphase plate and that later it pulls the sister chromatids apart and carries them into the newly forming daughter cells [160] which are generated by a cytokinetic ring which drives division. This contractile annulus constricts to a point, bringing with it the membrane which physically separates the two daughter cells. The cytokinetic ring is formed from another filament-forming globular protein, called actin, along with myosin motor proteins. These two structures must collaborate closely and be carefully coordinated in time and space in order to complete their task. In fact, it has been shown that the spindle usually takes the lead and determines the position of the cytokinetic ring according to the spindle mid-zone [161, 162]. The question of how division orientation is regulated therefore becomes the question of how the spindle is oriented and this is the focus of this section.

Key players in the regulation of the spindle orientation are the microtubules which emanate radially from the centrosomes, on the opposite side to the DNA, and travel through the cytoplasm towards the cell boundaries. These are known as astral microtubules and

spindles do not orient correctly when they are removed in *Drosophila* neuroblasts [163], rat kidney cells [164], yeast [165], HeLa cells [166], sea urchin eggs [167] and the *C. elegans* embryo [168], amongst others.

A particularly simple mechanism for controlling the positioning of the spindle is the 'search and capture' mechanism. Here, astral microtubules form stable attachments to specific sites at the cell cortex which stabilise the position of the spindle. A large collection of proteins are known to localise to the plus-ends of microtubules and to have some role in spindle orientation. Collectively they are known as +TIPS and these can take the role of 'prey' which search for and bind to cortical 'bait' (for a recent review see [169]). +TIPS known to influence spindle positioning include ZYG-9 in *C. elegans* [170]; the end-binding protein 1 (EB1) [125]; the dynactin subunit p150, known as Glued in *Drosophila*, which is brought to microtubule plus-ends by EB1 [171] and kinesin-13 MCAK, a member of the kinesin family of microtubule associated motors which walk towards the plus-ends of microtubules [172]. There are many more besides. However, due to the strong effects which +TIPS have on microtubule dynamics and spindle structure, dissecting the precise mechanisms through which +TIPS act is challenging. One +TIP which has been convincingly shown to play a part in spindle orientation is the kinesin Khc-73 [173]. Here, phosphorylation of a protein called Partner of Inscuteable (Pins) by Aurora A at the start of prophase leads to the cortical localisation of Dlg which directly binds Khc-73 at the end of astral microtubules in an interaction which appears to stabilise the spindle position [173].

In addition to putative search and capture mechanisms, astral microtubules also appear to be the substrates for the application of forces which move the spindle in order to orient it. However, there are multiple possible origins for these forces and it is likely that they are generated via different mechanisms in different systems.

Microtubules are highly dynamic structures, they rapidly polymerise and depolymerise in a behaviour termed 'dynamic instability' [174] (Fig. 1.5). Hill and Kirschner [175] proposed that polymerisation of a microtubule at the cell boundary would push on the bound-

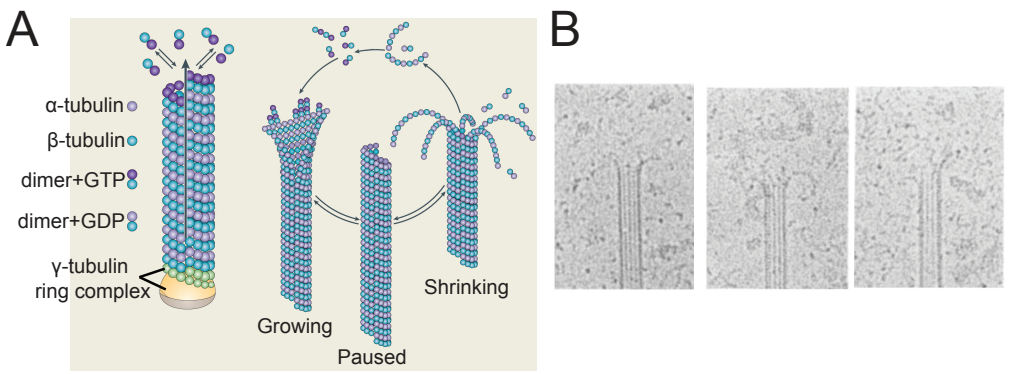

Figure 1.5: The dynamics of microtubules. (A) A diagram showing the structure and dynamics of microtubules. Source: http://www.nature.com/scitable/topicpage/microtubules-and-filaments-14052932. (B) Cryo-electron microscope images of 3 depolymerising microtubules. Source: [179]

ary and they derived an expression for the force that this would produce, thus theoretically verifying that it could be of significant magnitude. This phenomenon has been reconstituted *in vitro* using a centrosome to nucleate purified tubulin [176] and the force produced by a single polymerising microtubule has been measured [177] (for a review see [178]).

While these forces are likely to be relevant in some circumstances, particularly in yeast cells, which are small [180], it has been shown that pushing via polymerisation is not the dominant mechanism in a range of animal systems. By locally inactivating the microtubule depolymerising drug colcemid with UV irradiation, Hamaguchi *et al.* demonstrated that the dominant force on sand dollar sperm centrosomes was pulling rather than pushing [181]. This has also been confirmed in early zebrafish and *Xenopus* embryos [182] and *C. elegans* [183].

Importantly, microtubules do not have to do all the work by themselves. The motor protein dynein, which is a minus end directed motor, has been shown to play a role in many animal cell types [164, 184–187]. The nature of the force transmission from dynein to the spindle is still an open question and different mechanisms appear to exist in different systems. These mechanisms can broadly be separated into two groups based on the location of the dynein, which is either in the cytoplasm or at the cortex.

In favour of a cytoplasmic dynein model, Hamaguchi *et al.*'s [181] colcemid experi-

ments (described above) were the first to demonstrate the existence of a pulling force in the cytoplasm. In fact, in many of the large cells of early embryos astral microtubules do not reach the cortex, so forces must originate in the cytoplasm [188]. As might be expected, these pulling forces appear to be generated by dynein since in the one cell stage of the *C. elegans* embryo dynein is found throughout the cytoplasm and is required for positioning of centrosomes [184]. Similar patterns are found in many cell types, including MDCK cells [189]. However, to transmit force to the spindle, cytoplasmic dynein must be anchored in some way. Kimura and Kimura [190] identified a dynein light chain subunit called Dyrb-1 required for force transmission. They showed that Dyrb-1 mediates a link between astral microtubules, cytoplasmic dynein and intracellular organelles. They also showed that the proteins Rab7 and RILP (which are also found in mammals) take part in this interaction. Finally, they provided evidence that the reaction force produced by dynein transiently dragging organelles through the viscous cytoplasm is sufficient to account for the pulling forces which centre the centrosome [190].

Dynein-generated forces located at the cell cortex form a separate set of spindle-orienting mechanisms which appear to be as important as cytoplasmic forces, if not more so. Dynein is found at the cortex and is required for spindle orientation in one cell *C. elegans* embryos [183, 191, 192], *Drosophila* neuroepithelial cells [193] and male germ-line cells [138], chick neuroepithelium [133], MDCK cells [194] and HeLa cells [195], amongst others. An elegant demonstration of cortical based forces was provided by Redemann *et al.* in the single cell *C. elegans* embryo where disruption of the actin cortex lead to tubular invaginations at points where dynein and microtubules met at the cortex [196].

There are two main modes by which cortical dynein could transfer force to the spindle. In the first, microtubules reaching the cortex are bent and so have ends which run parallel to the cell boundary. Many dynein molecules anchored at the cortex could then bind along the length of the microtubule and processively pull the microtubule to move the spindle. Contrary to this intuitive model, microtubules at the cortex of many cells appear

as dots, rather than lines, so seem to meet the cortex end-on [197]. In this arrangement, the immobilised dynein could produce a force by pulling the microtubule past it, which would require coupling of depolymerisation to pulling. Interestingly, however, it has been demonstrated that an idiosyncratic property of microtubule depolymerisation can lead to the generation of pulling forces through depolymerisation alone [176, 198, 199]. During microtubule assembly, tubulin heterodimers bind GTP, which they hydrolyse after being incorporated into the microtubule (Fig. 1.5A). But not all the energy stored in the pre-hydrolysis GTP molecule is released. Instead, some is mechanically stored in the tubulin dimer which is constrained from forming its preferred bent conformation by the surrounding polymer [200]. Later, during depolymerisation, this energy is released when dimers are made free to bend. This is seen as curled strands at the end of microtubules cryo-electron microscope images [179] (Fig. 1.5B). The curling action can allow microtubules to pull on something if the force generated by the curling strands can be transmitted. Indeed, this phenomenon has been shown *in vitro* to produce forces up to ten-fold larger than those produced by an individual motor and can lead to the centring of microtubule asters confined inside simple geometries [176].

Regardless of the precise mechanisms of dynein-mediated force production at the cortex, an important aspect is how dynein is cortically recruited and anchored to the cortex, since dynein has no membrane or actin binding domain. This appears to be achieved by a conserved complex of proteins called Gα/GPR-1/2/LIN-5 in *C. elegans* [192, 201], Gαi/Pins/Mud in *Drosophila* [202, 203] and Gαi/LGN/NuMA in mammals [133, 195, 204, 205] (Fig. 1.6).

Gαi is the i subtype of the α subunit of a heterotrimeric G-protein complex (for a review, see [206]). Best known as signalling proteins, Gα proteins can bind and hydrolyse GTP due to a Ras-like small GTPase domain. This is a process controlled by G protein-coupled receptors (GPCRs) which act as guanine nucleotide exchange factors (GEFs). Normally, GTP-bound Gαi is associated with an active state, which disassociates

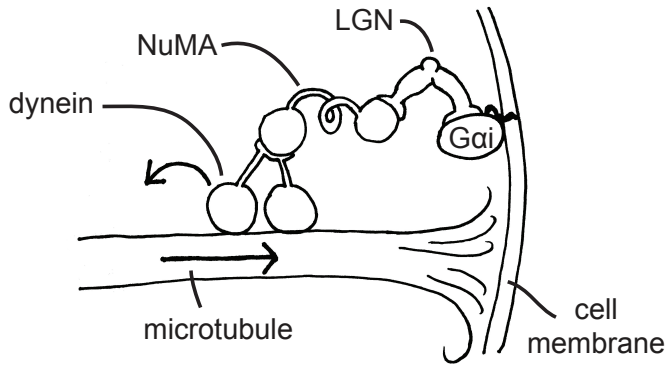

Figure 1.6: A drawing depicting dynein generated force transmitted to microtubules via the Gαi/LGN/NuMA complex at the cell cortex. The arrows show the force applied by dynein and the reaction force on the microtubule.

from the β and γ subunits of the complex. Regulation of spindle orientation therefore represents an unusual role for a Gα protein since no dependence on extra-cellular signalling or GPCRs has been found and because here the active form is the GDP-bound state [207]. Instead, the role of Gαi-GDP here is to recruit and bind Leu-Gly-Asn repeat enriched protein (LGN) which in turn recruits and binds the nuclear mitotic apparatus protein (NuMA) which binds dynein. NuMA is located in the nucleus during interphase and is only released at nuclear envelope breakdown. Release into the cytoplasm then allows NuMA to interact with LGN, which resides there throughout the cell cycle and is strongly upregulated during mitosis [208, 209]. The binding of NuMA activates LGN by interfering with a head-tail self-interaction which otherwise keeps LGN in a closed conformation. In the open active conformation, LGN can bind Gαi allowing the formation of the Gαi/LGN/NuMA/dynein/microtubule complex at the cortex [208]. This complex is crucial for generating the movements which orient the spindle in a large variety of studies in varied organisms [192, 201, 207–209].

1.4.2 Responding to molecular, geometric and mechanical cues

Armed with a detailed (yet still incomplete) knowledge of the molecular mechanisms through which force is applied to the spindle, the final question addressed in this intro-

duction is how these force-producing mechanisms can be regulated to align the spindle to a biologically relevant orientation.

In cells and tissues with pre-existing polarity, a possible spindle orienting mechanism is to couple the polarity machinery to the cortical force generators so that the location of force generators can be regulated. For example, in MDCK cells, Par3 keeps the atypical protein kinase (aPKC) at the apical cortex which in turn phosphorylates LGN leading to the inhibition of its interaction with Gαi via 14-3-3 proteins [194]. This interaction of LGN with the apicobasal polarity pathway therefore prevents astral microtubules binding the apical surface of MDCK cells which ensures planar division. Similarly, PAR proteins regulate the localisation of dynein which controls the first asymmetric division in the *C. elegans* embryo, however, the mechanism here appears to work via PAR dependent recruitment of Gα proteins (GOA-1 and GPA-16), leading to division towards PAR proteins rather than away from them [185, 191]. In *Drosophila* neuroblasts, force generators are again coupled to the PAR complex but this time a protein called inscuteable (Insc) is a key mediator. Produced in neuroblasts but not their neuroepithelial precursors [210], Insc is localised to the apical cortex by the polarity protein Bazooka (the *Drosophila* homologue of Par-3). Here, Ins binds Pins (Partner of Insc) to orient the spindle along the apico-basal axis [211–213].

Another polarity pathway which interacts with cortical force generators is the *SCRIB* pathway. In the *Drosophila* wing disc Dlg and Scrib are required to localise Mud and all three are required for planar spindle orientation [132]. In the *Drosophila* follicular epithelium Pins, Mud and Dlg are all required for planar orientation, as is the interaction between Dlg and Pins which is thought to relocalise Pins from the apical to the lateral membrane during mitosis [214]. Importantly, in this system a link between spindle orientation mechanisms and the cell cycle has recently been established. It was demonstrated that the kinase Aurora A, which is most active in early prophase, phosphorylates Lgl leading to its release into the cytoplasm. This frees the Pins binding site on Dlg, which is essential for planar orientation. In an impressive cell culture system involving the artificial induction of polar-

ity in *Drosophila*-derived S2 cells, Johnston *et al.* revealed a complex relationship between the Gαi/Pins/Insc/Mud/dynein pathway and the Pins/Dlg/Khc-73 pathway [173]. Interestingly, the Mud/dynein pathway was required for fast and directed spindle movements but couldn't work without the simultaneous action of the Dlg/Khc-73 pathway [173].

Many other couplings have been demonstrated in a range of systems. They include pathways involving E-cadherin and APC tumour suppressor protein [138, 193] and the *frizzled* and *dishevelled* pathway [144, 215], amongst others. These tissue- and cell-specific mechanisms are crucial for our understanding of development and morphogenesis and will no doubt continue to be the subject of many fruitful studies. However, mechanistically they are equivalent to one another in that they all simply require coupling of cortical force production to some other, pre-existing signal, be it cell or tissue polarity. The details are different and complex but the principle is the same. Of particular interest to this thesis, hoewever, are mechanisms which operate in the absence of a tissue specific signal. Of course such mechanisms need not exist *a priori* but it happens that in many instances, in the absence of specific signalling, certain other default cues appear to guide reproducible patterns of spindle alignment. The ability of such cues to control the orientation of cell divisions is a key topic of this thesis and is here investigated within a simple model epithelium, as reported in chapter 5.

The most prominent of these default cues is that of cell shape. Over 100 years ago, Oskar Hertwig took some recently developed theories on plant cell division orientation [216–219] and adapted them according to his observations in echinoderms and frog eggs [220]. The rules which had been formulated in plants stated that a new cell wall is positioned so as to divide the cell volume into two equal volumes while minimising the area of the new cell wall ('Sach's rule' and 'Errera's rule', respecitvely). The equivalent basic rule which Hertwig formulated for animal cells still stands today: mitotic animal cells tend to divide so as to bisect their long axis. This has been shown to hold true in a plethora of systems [51, 164, 166, 167, 221].

One problem with Hertwig's rule, however, was that the cell long axis was not unambiguously defined for the arbitrarily shaped cell. In an ellipsoid the long axis is unequivocally clear but many cells do not take on such regular shapes. Even in a cuboid the definition of 'long axis' is not immediately obvious - does it correspond to the longest axis of four-fold rotational symmetry or to the longest line which can be drawn, which connects the most distant corners? These question were addressed in an elegant series of experiments by Minc *et al.* [167]. The authors explored the subtleties of Hertwig's long axis rule by altering the shape of sea urchin eggs by placing them inside micro-fabricated moulds. The moulds could be made to arbitrary shape and the eggs adapted their shape to the moulds. Using cuboidal and L-shaped moulds, Minc *et al.* found that the division was oriented along the longest axis of symmetry, so that the division plane passed through the centre of mass of the cell. On top of this, they identified and quantified the noise in the system, i.e. the division did not always align perfectly with the long axis and instead divisions occurred in a distribution of orientations centred around the longest axis of symmetry. The width of this distribution decreased with increasing cell aspect ratio, showing that the cell geometry can control both the target division orientation and the accuracy to which it can is achieved. Analogous refinements of the old shape-based rules of division orientation have also recently been developed in plant cells. Besson and Dumais [222] demonstrated that different potential cell wall orientations with similarly minimal areas compete against each other with a strength which increases inversely with their relative area according to an exponential probability distribution [222]. The methods which allowed the precise manipulation of cell shape in Minc *et al.*'s study, however, are yet to be recapitulated in systems other than eggs and early embryos where the large cell size makes manipulation easier. Therefore equivalent methods for the control of shape in smaller mammal cells would be an important advance.

So how is it that cells can know their own shape and orient their spindles accordingly? In many bacteria, a set of proteins called the MinCDE system is thought to define the lo-

cation of the point of septation at the centre of the cell via a sophisticated shape-sensing reaction-diffusion mechanism [223] but no analogue to this system has been found in Eukaryotes. Instead, the search for Eukaryotic mechanisms has led to the cell cytoskeleton. In plant cells, the division plane is prefigured by a cytoskeletal structure, known as the phragmosome, which spans the distance between the soon-to-divide nucleus and the cell cortex [224]. The observation that the cytoskeletal strands which make up this structure are put under tensile stress provides a simple explanation as to how the minimal area configuration could be achieved [225]. Similarly, in animal cells, explanations have been found which depend on the distributions of forces applied on astral microtubules by dynein. In a first class of models, mainly based on experiments on the large cells of early embryos, a basic fact has been established: the mitotic spindle will be centred and oriented with cell shape if the force on a particular astral microtubule is dependent on its length.

A range of functional relationships between the force exerted on a microtubule (F) and its length (L) have been shown to recapitulate shape alignment [167] and several molecular mechanisms have been proposed. In early models based on pushing generated by microtubule polymerisation, length dependence results from the buckling of longer microtubules and gives a $F_{push} \propto L^{-2}$ and this was shown to align the spindle to cell shape in simulations [226], provided the spindle length was short enough. The cytoplasm based forces generated via dynein-powered organelle transport, proposed by Kimura *et al.* [190], simply give $F_{pull} \propto L$ since every extra unit of microtubule length provides an equally sized substrate onto which dynein can bind. Perhaps surprisingly, Grill *et al.* realised that even force generators uniformly distributed along the cortex can provide a length dependence, provided the astral microtubules are significantly greater in number than the force generators [183]. If there are fewer astral microtubules than cortical force generators, then every microtubule receives the same force and the spindle is stable at every position. If force generators are the limiting factor, however, then there are always more force generators in the direction of the longest distance of cytoplasm, which leads

to a $F_{pull} \propto L^2$ relationship. More complex microtubule dynamics including length dependent catastrophe rates [227], length dependent depolymerisation by kinesin [228] or accumulation of microtubules in long axis as a consequence of polymerisation and depolymerisation times [229] can also generate such length dependent forces. Through careful comparison of their experimental results with their model, Minc *et al.* were able to estimate that a $F \propto L^3$ was at work in their sea urchin eggs [167]. This rules out one of these simple mechanisms working in isolation. Instead they concluded that several mechanisms may act co-operatively in the sea urchin egg. They noted, however, that limited force generators in the cytoplasm would give a $F \propto L^3$ 'volume-sensing' relationship.

In HeLa cells some more sophisticated regulation of cortical force generators have been found which could play a role in shape sensing [186, 230]. Kiyomitsu *et al.* found that the protein Polo kinase 1 (Plk1), which decorates HeLa spindle poles, causes dissociation of dynein/dynactin from the Gαi/LGN/NuMA complex when it comes close to the cortex, causing a reduction in force. A GTP-Ran gradient from the chromosomes was also found to remove LGN and NuMA (and therefore dynein) from the cortex, ensuring centring in the perpendicular direction. In these studies, the molecular mechanisms uncovered were explored in the context of positioning the spindle centrally in the cell. It is not a large step, however, to imagine how these mechanisms could be used for shape sensing.

A crucial problem with the shape-based mechanisms proposed thus far is that most animal cells round up during mitosis and therefore the shape information is lost [231]. Although spindle position (or at least centrosome position) could in theory be set before the completion of rounding, this is unlikely to be robust since rounding is one of the first events to initiate at mitosis and involves dramatic and rapid morphological and mechanical changes [232, 233]. Rounding is an essential part of mitosis in many cell types as it plays vital roles in spindle morphogenesis [234] and chromosome capture [235]. Inseparable from the cell shape and mechanical changes during rounding are the changes in the actin cortex, driven by Ect2 [232] and ERM proteins [234]. These changes too will

likely impact spindle positioning. Indeed, actin is required to maintain dynein [189] and the Gαi/LGN/NuMA complex at the cell boundary, preventing its transport to the spindle poles [187] and loss of actin disrupts both planar [125, 132] and azimuthal [166] orientation of cell division. Additionally, ERM proteins, which link actin to the cell membrane, are required for a stable spindle orientation [166, 236] and may play a more direct role together with actin in localising NuMA and LGN [237].

Given the importance of cell rounding and the associated changes in the actin cortex in mitosis and spindle orientation, an important question is then how the spindle can orient to the interphase cell shape during mitosis, when this shape information appears to have been lost. One mechanism for interphase shape memory may function through the actin-rich membrane tubes, called retraction fibres, which connect the metaphase cortex of a rounded cell to the interphase adhesion sites. In an elegant series of experiments, Théry *et al.* demonstrated the effect of these retraction fibres on spindle orientation using micro-patterning of fibronectin to create a range of reproducible cell adhesion shapes [166]. The patterns were shown to lead to bias in the distribution of locations where retraction fibres met the cell cortex, which lead to cortical patterns of cortactin and ezrin and biasing of the spindle orientation. Importantly, a physical model based on the uneven distribution of cortical force generators, governed by retraction fibre locations, was able to quantitively reproduce the spindle orientations in experiments over a range of adhesion shapes [238].

Further evidence of the role of retraction fibres was provided by Fink *et al.* who grew HeLa cells on micro-patterned stretchable substrates [221]. When elliptical cells were stretched along their short axis, to create an isotropic cell shape, cells divided in the direction of stretch. They used optical tweezers and laser ablation to show that retraction fibres exert a significant stress on the cell (up to $\sim 7\,\mathrm{nN}$) which appears to guide spindle orientation [221]. This demonstrates the possibility of a mechanosensitive pathway playing a role in spindle orientation which could have far-reaching ramifications for the organisation of cell divisions during embryogenesis. Indeed, in the fly wing disc [148, 154] and during

zebrafish epiboly [51] tension is known to orient divisions via its effect on cell shape. In plants too, recent evidence suggests that tension may play a direct role in orienting cell division [239–241] and indeed may even supersede cell geometry as the favoured generic cue [242]. A tension-based pathway independent of shape would allow further coordination of division orientation across an embryo since tensions are automatically transmitted over long distances due to the strong mechanical coupling within tissues [243]. Uncovering the molecular mechanisms behind this mechanosensitvity is an important next step which has begun with a recent study which implicated focal adhesion kinase (FAK) and paxillin in the transduction process [129].

1.5 Aims of this study

This introduction has aimed to provide an overview of the main themes of this thesis. As highlighted in section 1.2, epithelia are crucial structures in metazoans which are frequently subjected to deformation during developmental morphogenesis, normal physiology and disease. While the mechanisms which govern the regulation of morphogenetic forces in epithelia are intensively studied, the responses of epithelia to extrinsically applied deformation can be just as important but are somewhat understudied. In this thesis, such responses are investigated within the context of the highly simplified *in vitro* model system of suspended epithelial monolayers.

Firstly, in chapter 4, the short timescale (seconds and minutes) response of epithelia to a compressive strain is studied. Secondly, section 1.4.2 of this introduction described how both cell shape and stress signals have been found to influence the orientation of divisions in single cells. The relative contributions of these signals in orienting cell divisions in a deformed epithelium is assessed in chapter 5. Thirdly, section 1.3.3 discussed the various ways in which the particular orientation of cell division is known to impact a tissue and how this may play a role in some morphogenetic processes. The effect of cell division orientation on the organisation and shape of an epithelium is investigated in chapter 6.

Chapter 2

General methods and reagents

This section gives details of general methods which were used throughout this thesis and is intended to be used as reference. These protocols were mostly pre-existing. For methods which were optimised or changed during this work see chapter 3. For detailed descriptions of methods for specific experiments see the methods sections at the start of each chapter. Another account of many of the procedures detailed here can be found in [244].

2.1 Cell culture

Wild-type (WT) MDCK-II cells were cultured at 37°C in 5% CO_2. They were cultured in high glucose Dulbecco's Modified Eagle Medium (DMEM; Invitrogen) supplemented with 10% (vol/vol) fetal bovine serum (Invitrogen) and penicillin-streptomycin (100 U/ml; Invitrogen) - hereafter this prepared media is referred to as supplemented DMEM. Cells were passaged (using standard cell culture procedures) at a ratio of 1:5 when they reached ∼80% confluency (every 3 or 4 days). They were disposed of after 25 passages. MDCK-II cells stably expressing E-cadherin–GFP were used to visualise cell-cell junctions and to measure cell shape. Details on the generation of this cell line can be found in [90]. E-cadherin–GFP cells were cultured in the same condition as WT except for the addition of 500 ng/mL puromycin as a selection agent. HaCaT cells were cultured using a similar

protocol except that during routine culture they were maintained in media with a low calcium content.

2.2 Stretching device production

Exact details of stretching device manufacture varied depending on the context. For experiment-specific devices see chapter 3 and chapter-specific methods sections. What follows is a general outline of the manufacture of generic stretching devices. The bodies of the stretching devices were made from a borosilicate capillary (inner diameter of 0.5 mm, outer diameter of 1 mm; Sutter Instruments). Capillaries were bent into shape using pliers after heating the centre for 2 seconds with a micropen blowtorch (Gosystem). The bent capillaries could then be cut to size by gently gripping and snapping with pliers. One capillary 'arm' was left long (∼34 mm) and was therefore rigid during experiments. The other arm was cut short (∼4 mm). To form a hinge, a small length of (∼6 mm) nickel-titanium ('nitinol' or 'NiTi'; Euroflex) wire of diameter 0.2–0.3 mm was threaded into the short arm and adhered with UV curing glue (Loctite Glassbond). The glue was cured by ∼ 2 min exposure to UV light using a UV transilluminator (VWR). In the same fashion, a ∼30 mm straight length of capillary was adhered to the free end of the NiTi wire to form the hinged arm. Completed devices were washed in 70% ethanol and fixed to sterile plastic bottomed Petri dishes (Sterilin) with either hot glue or plasticine (Blu Tak).

2.3 Monolayer culture on stretching devices

MDCK cells were cultured on a sacrificial collagen scaffold which formed a bridge between the two arms of the stretching device. To form the bridge, collagen was reconstituted on ice by mixing 5 parts collagen type 1A (Cellmatrix) with 2 part sterile H_2O, 2 parts 5X-DMEM and 1 part reconstitution buffer. $100\,\mathrm{ml}$ of reconstitution buffer was made from $100\,\mathrm{ml}$ of 0.02 N NaOH, with $200\,\mathrm{nM}$ HEPES buffer (Invitrogen) and $2.2\,\mathrm{g}$ of $NaHCO_3$.

The solution was thoroughly mixed with a pipette, taking care not to introduce bubbles. Reconstitution buffer was the last to be added since this initiates rapid cross-linking of the gel. The reconstituted collagen was used immediately by placing 16 µl of the solution between the rods of each device, which was held in place by capillarity. The suspended collagen was then dried out by carefully transferring the devices to a 37 °C incubator for 90 minutes. By the end of the drying period, the collagen formed a thin, dehydrated bridge between the stretching device arms. The collagen bridge was then rehydrated by placing a 10 µl drop of DMEM on the collagen and incubating for 30 minutes at 37 °C. ∼500 µl of DMEM was included at the bottom of the dish during this period to maintain a humid atmosphere. Note that it was clear that this rehydration step did not return the collagen scaffold to its pre-drying, droplet-like state, presumably because the drying process caused changes in the collagen micro-structure which were not directly reversed. The rehydration step, however, was critical for the survival of seeded cells in the following steps. Flasks of MDCK cells at ∼80% confluence were trypsinised and resuspended in DMEM at 5 million cells per ml. The DMEM droplet used during rehydration was then removed from the top of the collagen and a 5 µl droplet of cell suspension was put in its place. The devices were incubated for another 30 minutes at 37 °C by which time the cells were securely adhered to the collagen scaffold and supplemented DMEM was then added the Petri dishes to cover the devices. The completed devices were then incubated, at 37 °C and 5% CO_2, for 48-72 hours until the monolayers covered the whole of the collagen scaffold and part of the glass capillaries or glass coverslips. The same overall protocol was used for HaCaT cells, except that the low calcium media used for routine culture was replaced with standard supplemented DMEM once cells were plated on devices. This stimulates the generation of intercellular junctions.

2.4 Collagenase treatment

To remove the collagen substrate, leaving only the suspended monolayer, the devices were incubated for 30 minutes at 37 °C in a collagenase solution consisting of 250 units/ml of type 2 collagenase (Worthington) dissolved in supplemented DMEM. Once the enzymatic treatment was finished the monolayers were extremely fragile so handling was minimised. To avoid damage incurred by surface tension upon complete removal of the media, the collagenase solution was removed by serial dilution.

2.5 Live imaging of suspended monolayers

Two separate live imaging setups were used in the studies presented here. Both were contained in environmental chambers (custom built) which were maintained at 37 °C using a temperature control system (Life Imaging Services). A stage top incubator connected to a gas mixer and humidity regulator (Life Imaging Services) was used to maintain an atmosphere saturated in humidity (preventing media evaporation) and containing 5% CO_2. The spinning disk confocal microscope setup consisted of a Yokogawa spinning disk head (CSU22; Yokogawa) and an iXon camera (Andor) interfaced to an IX81 Olympus inverted microscope. Image acquisition was controlled by iQ software (Andor). An Olympus 30X N.A. 1.05 silicone oil immersion objective and an Olympus 60X N.A. 1.2 water immersion objective were used. The second setup consisted of a FV-1000 scanning laser confocal microscope interfaced to an IX-71 microscope (Olympus) using the same objectives.

To image suspended monolayers the devices were carefully removed from plastic-bottom dishes at the end of the 72 hour incubation and before collagenase treatment. They were then affixed to glass-bottom petri dishes with hot glue applied to the U-bend in the devices. Prior to attaching the device to the glass dish, $\sim$150 µl of warmed collagenase solution was put on the glass dish at the position where the monolayer would rest. This was to avoid the monolayer coming into contact with dry glass during the handling and

attachment. $\sim 3\,\mathrm{ml}$ of warmed collagenase solution was then carefully added immediately after application of the hot glue. Any delay in adding this solution could result in the heat of the hot glue causing damage to the monolayer. For live imaging, the collagenase solution was exchanged for $\sim 3\,\mathrm{ml}$ of imaging media made from the normal supplemented DMEM with no phenol red (Invitrogen).

2.6 Application of strain to suspended monolayers

While it is possible to use the system described here to maintain a constant tissue stress, the approach used in all experiments reported in this thesis was to control tissue strain. Uniaxial strain was applied to the suspended monolayers using either a manual micro-manipulator or a M-126 high-resolution translation stage (Physik Instrumente). The glass-bottomed Petri dish was fixed to a custom built microscope stage with hot glue and in some instances a notch was cut out of the side of the plastic dish using a heated metal wire or a small hand drill. The micro-manipulator was attached to the microscope stage and positioned via a custom built magnet system that clamped to a metal plate fixed onto the microscope stage. A steel wire probe was then bent into shape according to the geometry of the microscope setup, it was connected to the micro-manipulator and positioned at the far end of the stretching device. The monolayer was imaged using bright field illumination with a 2.5x objective so that the total strain applied could be accurately controlled. Once the desired strain was applied, the probe could be fixed in position with hot glue and detached from the micro-manipulator. For more complex or fast time series of applied strains, the motorised stage was controlled via a computer running custom routines written in LabView (National Instruments).

Chapter 3

Method development: a device for mid-term live imaging at high resolution

3.1 Motivation

As discussed in section 1.5, the Charras laboratory experimental system for generating and stretching suspended epithelial monolayers is ideal for studying the response of epithelial tissues to mechanical perturbations. Prior to the beginning of this project, however, the system had only been used to study short timescale mechanical properties of epithelial monolayers, using mainly low magnification imaging [90]. High magnification fluorescence imaging of monolayer and cell shape was challenging with the set-up and long-term live imaging was impossible.

One crucial requirement was that the setup would allow capture of time lapse images of cells passaging through mitosis. However, the combination of a transient inhibition of division at the start of experiments and a relatively low division rate after the inhibition (see section 5.5) gave just $\sim$3% of cells dividing within 5 hours of collagenase treatment.

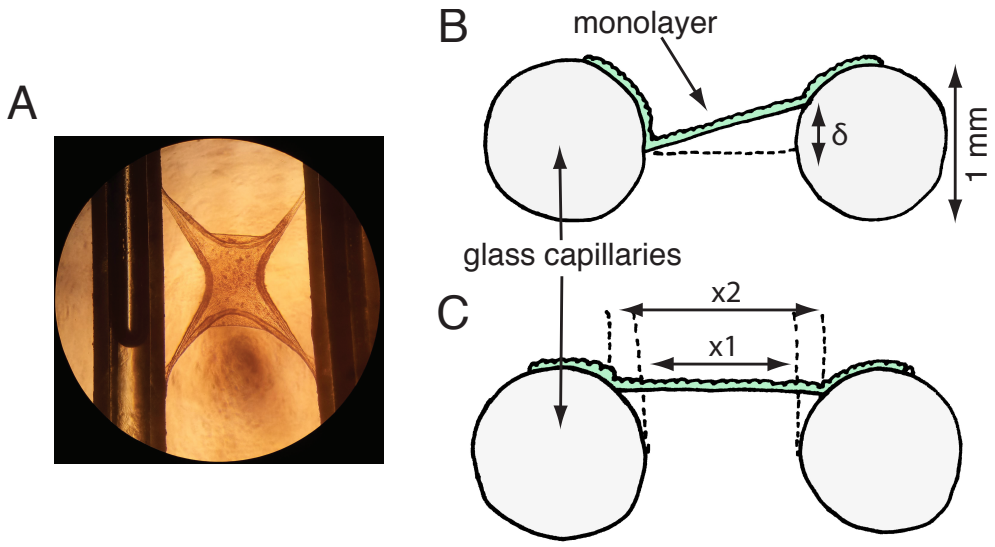

Figure 3.1: Problems with the existing system. (A) After severe hours, holes formed at the test rods as cells delaminated from the glass. (B) Variation in the position of attachment to the glass frequently led to a significant slope in the plane of the monolayer (δ). (C) Uncertainty in the location of the attachment points on the test rods could lead to significant errors in the strain applied (x1 vs x2).

This dictated that experiments had to last a minimum of 2-3 hours. Over these durations, however, it was found that holes formed in >50% of the monolayers (Fig. 3.1A), which appeared to be caused by cells delaminating from the test rods as a result of sustained tissue contractility. The geometry of the stretching devices also made it difficult to create monolayers which were sufficiently parallel to the plane of imaging due to variation in the points of attachment of the monolayer to the test rods (Fig. 3.1B). This meant that confocal stacks that were many times the thickness of the monolayer would have to be acquired in order to image a large area of the tissue (i.e. to account for the slant), thereby increasing photo-toxicity and decreasing temporal resolution (Fig. 3.1B). Furthermore, confocal stacks which were obtained would need to be processed to remove the slant in order to make measurements of cell shape but the naturally lower resolution along the z-axis would reduce the quality of resulting images. An additional problem associated with the point of monolayer attachment was that, as well as being highly variable, it was also difficult to determine. This meant that the total length of the tissue (x2, Fig. 3.1C) was not

known with satisfactory accuracy (x1 vs. x2, Fig. 3.1C) leading to significant errors in the magnitude of applied strains.

The necessary use of inverted microscopes also created a working distance issue. In the worst case scenario the monolayer could attach to the test rod at the centre line of the cross-section (Fig. 3.1B, left test rod, note that the devices are flipped over before imaging, therefore the Petri dish bottom would be above the device in this figure). This would lead to a $500\,\mu m$ distance between the tissue and Petri dish glass. The difficulty in controlling the distance between the stretching device and the bottom of the Petri dish could add another $100\,\mu m$ between the two. A custom device made from thinner components had previously been implemented to overcome this problem [90], however, since this only just brought the monolayer within the limits of the focal range of 60x objectives, small amounts of drift during long timescale imaging frequently took the monolayer out of range.

Further to these problems for high magnification live imaging, two additional improvements were required. Firstly, it was important to generate devices in which the initial length of the monolayer could be both accurately controlled and chosen from a large range of possible lengths. In the existing devices the initial length was, in the first instance, determined by the shape of the U-bend formed after heating the capillary with a blowtorch and this could not easily be controlled. Secondly, it would be important to have precise control of both tensile and compressive strain during fast and complex time series of manipulations. The existing system controlled strain with a probe which only made contact with the device on one side and relied on the elasticity of the NiTi hinge to restore length once a strain was removed. Compressive and tensile strains could not be applied in the same experiment. All of these points were addressed via a number of adaptions to the design and manufacture of the existing stretching device and live imaging protocol, which are described in section 3.2.

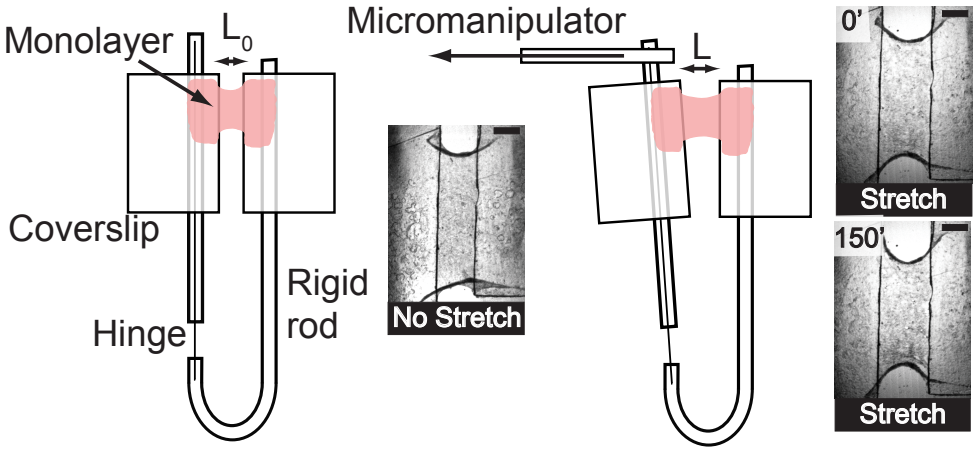

Figure 3.2: A diagram of the adapted stretching device. The insets show brighfield images of monolayers a various stages throughout an experiment. (Scale bars: 1 mm)

3.2 An adapted stretching device for mid-term and high resolution live imaging

The limitations of the original device, described above, were addressed with a number of simple changes to the geometry of the stretching device (Fig. 3.2). The arms were moved further apart from one another by forming a much larger (but not carefully controlled) U-bend of $\sim$10 mm. Rectangular glass coverslips were then attached to the arms with UV curing glue (Loctite Glassbond), positioned as in diagram 3.2. The collagen drop was then placed to form a bridge, as before, between the two coverslips.

In this newly adapted device the initial length of the tissue is determined by the position of the glass coverslips, rather than by the shape of the U-bend formed by the blow-torch. The positioning of coverslips could be controlled with a higher degree of accuracy than the shape of the U-bend. If, for a given experiment, accuracy was not important, then the coverslips could be positioned by hand. For many experiments, a precisely controlled length of 350 µm was desirable. This could be achieved by positioning the coverslips under a microscope. Reference devices were constructed using a graticule. The prepared coverslips were then placed adjacent to the reference device under a microscope so that

minor adjustments could be made with tweezers before fixing the position with UV glue. It was found that placing a small droplet of water between the coverslips and work surface allowed for much more precise movements to be made. Following this procedure, the only limiting factor which restricted the range of lengths that could be produced was the ability of the collagen drop to support itself across the gap. Overall, following this procedure, devices could be built with initial lengths between $150\,\mu m$ and $2000\,\mu m$, with an error of $\sim\pm 20\,\mu m$ (see Fig. 4.2).

By growing a monolayer between two thin flat platforms, instead of between two cylindrical rods, the maximum possible slant in the monolayer was drastically reduced, since the area of the lateral surface presented to the collagen drop (Fig. 3.3A vs. B) was reduced. In addition, this geometry allowed the monolayer to be brought closer to the bottom of the Petri dish (Fig. 3.3C). Further reductions in the distance between the monolayers and the glass surface of the Petri dish could be achieved by carefully placing a small weight on the device. This weight was made by cutting microscope slides into several $1\,cm$ by $0.5\,cm$ rectangles and glueing them on top of one another. For some applications, such as when observing monolayer buckling during compression, the monolayer could come too close to the Petri dish glass. To prevent this, glass spacers were glued to devices to precisely control the monolayer to Petri dish distance (Fig. 3.3C).

The reduction in monolayer slant made it possible to image a large area of the monolayer by using a motorised stage to create a montage of the tissue. Within the 5 minute intervals between image acquisitions it was possible to image up to 50 positions. This significantly increased the amount of data which could be collected. This also made it possible to image the majority of the tissue rather than just one small window, giving a global perspective.

As expected, the adapted device also greatly reduced the number of monolayers in which holes were formed, since the cells had a much larger area over which to grow and form a robust attachment to the glass, continuous with the growth on the collagen bridge.

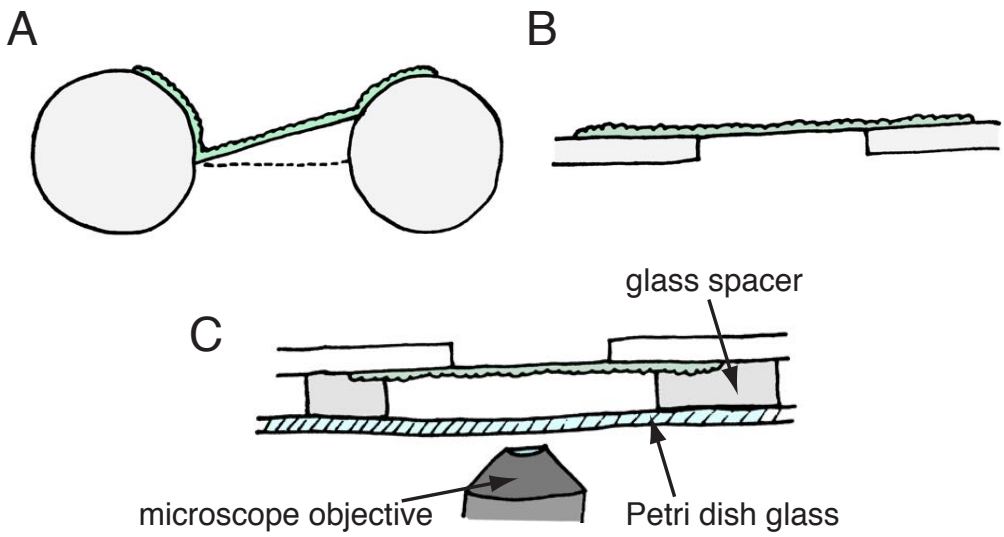

Figure 3.3: Improvements of the new system. (A) An example of slant in the original system. (B) Slant is reduced in the new system. (C) Spacer glass can be attached to the devices to precisely control the distance to the coverslip.

This reduced the number of devices which needed to be prepared and the number of experiments which failed, therefore significantly increasing throughput. The clearer view of the attachment surfaces presented by the flat geometry also facilitated fast pre-experiment screening of devices to check for damage.

Overall, these changes required some minor adjustments to the protocol for generating suspended monolayers. One problem which arose was, before drying, the collagen drop bridge would break and spread over one of the glass coverslip platforms. To prevent this, a hydrophobic layer was painted on the coverslip with a PAP pen (Sigma-Aldrich) which prevented the collagen from spreading over the glass. Once the collagen had dried, the devices were flipped over and cells were deposited on the other side. Slightly different quantities of various liquids were needed in the new devices due to the altered geometry. 16 µl collagen was used, along with 8 µl DMEM to rehydrate after drying and 10 µl of cell mix at a density of 4000 cells/µl.

One final adaptation was made to the device to allow for more precise control over both compressive and tensile tissue strains. A small additional piece of glass capillary was

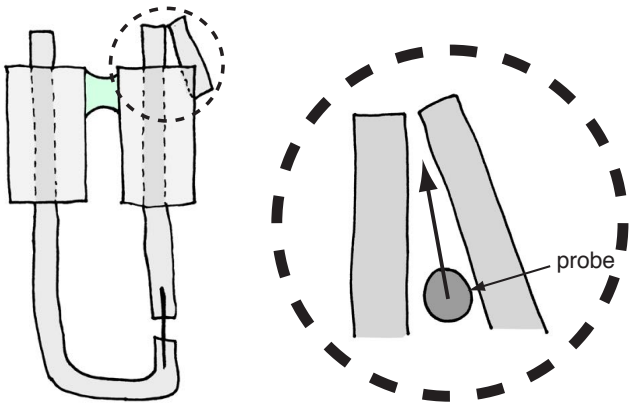

Figure 3.4: Probe positioning in the new system. An extra section of glass is added to the device for added contact with the probe. The probe is positioned between the two glass rods and moved upwards and sidewards until it makes contact with both rods.

added to the hinged side of the device at a small angle to the axis of the test rod (Fig. 3.4, left). The probe which controlled movement of the device (either via manual manipulators or a motorised stage) could then be lowered into the wide end of the gap between the capillaries (Fig. 3.4, right). Finally, the probe could be moved upwards and across (Fig. 3.4, arrow) until it made contact with both capillaries at the same time (Fig. 3.4, right). While a more secure attachment could be made by pushing the probe a small amount further into the angle, thereby jamming it in place, this was found to cause problems when obtaining confocal stacks of images. In both microscope setups used, confocal stacks were obtained by moving the sample relative to the main stage which supported the probe and manipulator. This relative motion caused artefacts in the obtained images if the probe-device contact was attached rather than proximal.

The devices could be recycled after cleaning, similar to the original devices. However, here it was particularly important to clean the hydrophobic pen and cell debris off with a cotton wool bud before washing in ethanol.

3.3 Video data processing using automated image analysis

Once the setup had been adapted and optimised for mid-term live imaging, an additional set of challenges emerged concerning the processing of images obtained during experiments. In the case of experiments involving live imaging of cell division, in order to obtain large numbers of cell divisions, a large area of tissue was imaged ($\sim$500 µm x 500 µm x 40 µm) with high spatial resolution (60x objective, $\sim$2 µm thick confocal slices), at 5 minute intervals, for relatively long durations ($\sim$3 hours). This resulted in relatively large image files of $\sim$30 GB. Extracting image sequences suitable for quantitative analysis from these files presented a unique combination of challenges. The main obstacles were drift in all three dimensions and the large size of the files. Drift in the x-y plane appeared to be caused by uneven contractile forces in the tissue which caused movements of over one cell diameter between time points. The x-y drift was not uniform across the tissue, so a correction could not be applied globally. In the z-direction the drift was more steady and directional but varied from experiment to experiment and manual correction of drift during experiments produced sudden jumps in the resulting video. The source of the drift in the z-axis is still unknown.

Since no existing software package from the scientific community was found which could meet the specific set of requirements demanded by these experiments, combinations of pre-existing image processing and analysis algorithms were assembled into workflows in Mathematica (Wolfram Research) and manual analysis was used as a substitute in instances where existing algorithms were not adequate (development of basic image analysis algorithms was not undertaken, since this was not the aim of the project and was unlikely to be time-efficient). To reduce the file sizes to something more manageable, divisions in the tissue were identified and cropped out of the original data. A nuclear marker was not used in the majority of experiments so that only one wavelength would be imaged, in order to limit photo-toxicity. No software could be found which could reliably identify cell divisions from the membrane signal, in a crowded tissue environment. Therefore, divi-

sions had to be identified and tracked manually, although this was aided by the automatic preparation of cleaned maximum projected videos, as well as by FIJI's Manual Tracking plugin. Once divisions were identified and extracted, correction of remaining x-y and z drift aided the automatic measurement of cell shapes using Tissue Analyzer [245].

Chapter 4

Actomyosin contractility drives autonomous buckle flattening and length adaptation in epithelia in response to compressive strain.

4.1 Introduction

Many functions performed by epithelial tissues, during both embryonic development and adult life, demand that they endure and adapt to deformations of varying magnitude, timescale and configuration. Compressive stresses and strains are common and can be driven, for example, by the contraction of muscles or can arise when neighbouring tissues grow at different rates during development [148, 246] or disease [247, 248]. They can also be the result of the shifting of tissue boundaries which necessarily accompany many complex movements performed by tissues during embryonic morphogenesis [249]. Importantly, compression has been found to play a central role in determining the final form of many tissues, from the villi of guts [63] to the sulci and gyro of the human cortex [250].

Over a timescale of hours and days, compression alters a number of aspects of cellular behaviour. When applied perpendicular to the plane of an epithelial monolayer, for instance, compression was shown to cause changes in cell-ECM adhesion and cytoskeletal organisation in mammary carcinoma cells, leading to the emergence of a migratory phenotype [251]. Compressive strain oriented in the plane of the monolayer, on the other hand, can trigger live cell extrusion [53, 84]. In MDCK epithelia monolayers, it was proposed that this relies on stretch activated ion channels to restore the preferred cell density [84]. In a similar vein, cell cycle progression is related to cell density [252]. This is thought to be mediated, in part, by activation of the Hippo pathway, since the mitogenic transcription factor YAP is excluded from the nucleus when the cell density of an epithelium increases beyond a certain threshold [253]. In tumour spheroids, a reduction in proliferation in response to uniform compressive stress was found to depend on the CDK inhibitor $p27^{Kip1}$ [254].

At shorter timescales of seconds and minutes, most research into the response of epithelia to deformation has focussed on tensile strain [255]. In the stretched epithelium of a distended bladder or alveolus, for instance, plasma membrane ruffles can rapidly unfold to accommodate an increase in surface area and within minutes additional phospholipids are added via trafficking from cytoplasmic vesicles [88, 96–98]. The risk, however, is not limited to the plasma membrane. Stress accumulation throughout the cell can lead to epithelial fracture by causing the cell-cell junctions which bind tissues to fail [90, 256]. Ectopic cell fusions caused by stretch have also been observed [51]. In general, however, such risks are minimised since large stresses are not maintained in stretched epithelia for long periods. Instead epithelia are found to behave viscoelastically [90–92] such that stresses induced by a stretch are rapidly relaxed in a process which is not completely understood. Instances of specific reorganisations of the actomyosin cytoskeleton in response to stretch [106], mechanoaccumulation of cytoskeletal components [257, 258] and reinforcement of adherens junctions [105] and focal adhesions [100, 259], may also play important roles in

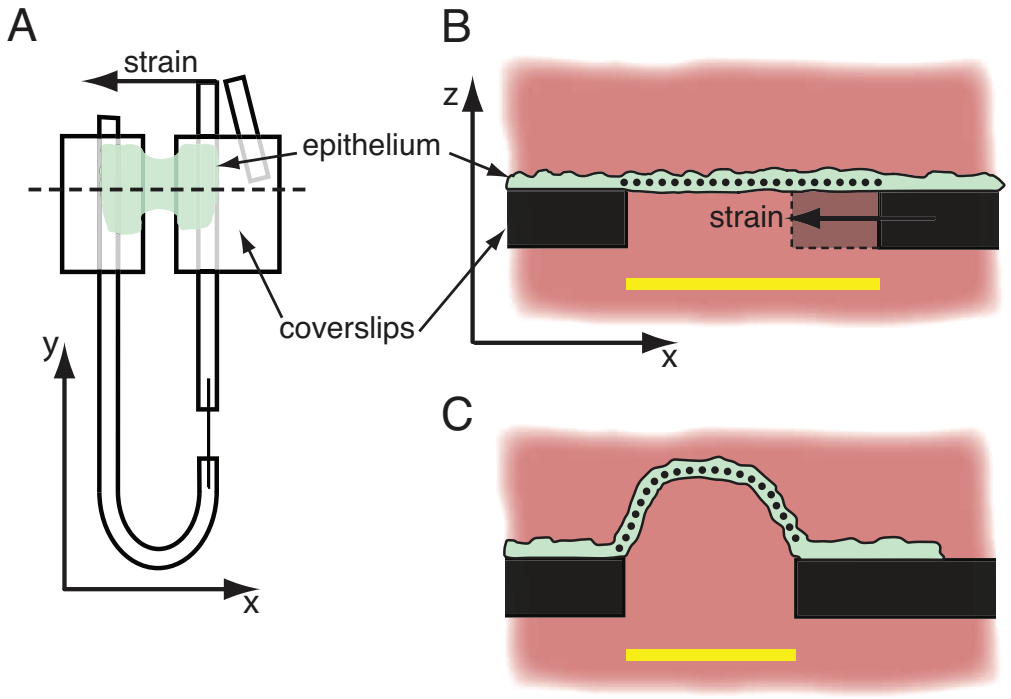

Figure 4.1: Experimental set-up for the application of compressive strain. (A) Diagram depicting the stretching device described in section 3.2 along with the epithelial tissue grown on the device (green). Uniaxial compressive strains were applied oriented with the axis labelled x. (B) Diagram depicting the x-z cross-section of a device and epithelial tissue. To visualise the cross-sectional shape of the tissue at high time resolution during deformations, confocal scans were acquired along the dotted line in (A). Plasma membranes of epithelial cells were fluorescently labelled with CellMask (green) and the medium was labelled with fluorescently conjugated dextran (red) to reveal, by exclusion, the coverslips on which the cells grew (black). The dotted line demarks the contour length of the suspended epithelium and the yellow solid line demarks the distance between the coverslips, which is manipulated to apply strain. (C) Diagram of a suspended epithelium which has buckled as the result of an applied strain. Note the contour length (dotted line) is longer than the distance between the coverslips (yellow solid line).

adaptation to stress.

While the risks of compression in single cells are known to include mitotic errors [235, 251] and DNA damage [260], the short timescale response of compressed epithelia has not been studied. Yet understanding the response of epithelia to compression is vital for the interpretation of many morphogenetic events - for understanding why an epithelium may bulge, buckle or wrinkle under compression. Here, to investigate this, a uniaxial planar compressive strain was applied to suspended epithelial monolayers (Fig. 4.1A and B). The basic geometric arrangement of the suspended epithelium system [244], along with the

absence of developmental processes and an ECM, provides a highly simplified biophysical setting compared with that of any *in vivo* system, allowing for more straightforward interpretation of how the cells adapt to application of compressive strain. Furthermore, the system is further simplified by the lack of basal substrate, which decouples changes in structure which are driven by the tissue itself from those which may result from coupling with a substrate.

Using this set up, the application of a constant 40% compressive strain at a high strain rate caused immediate buckling of suspended epithelia. Remarkably, however, buckled tissues rapidly and autonomously decreased their contour length to restore a flattened morphology. This is accompanied by a change in cell shape and was observed in epithelia made up of Madin-Darby canine kidney (MDCK) cells, as well as human keratinocyte (HaCaT) cells. The response was found to be driven by actomyosin contractility and was unaffected by Gadolinium(III) Chloride (a treatment thought to block stretch activated ion channels).

Changes in cell and nuclei shapes and the heights of cell-cell junctions were accompanied by mechanical adaptation to the new tissue length, since buckles flattened much faster when the compressive strain was removed and immediately reapplied. These changes, however, could be reversed by restoring the tissue to its original length for over 60 seconds. Overall these results demonstrate that simple epithelia lacking a basal substrate possess a surprising ability to autonomously adapt to compressive strains. This is likely to be relevant in a range of morphogenetic and physiological processes involving epithelial deformation.

4.2 Methods

4.2.1 Experimental setups and live imaging

Wild type MDCK cells, MDCK cells expressing Ecadherin–GFP and HaCaT cells were cultured as described in section 2.1. Stretching devices were assembled as described in sections 2.2 and 3.2. Except where stated otherwise, devices were made with coverslips separated by a target length of $350\,\mu\mathrm{m}$. The true length, as measured by confocal microscopy, was generally within $10\,\mu\mathrm{m}$ of this target length (Fig. 4.2A). MDCK cells and HaCaT cells were cultured on sacrificial collagen scaffolds on the stretching devices as described in section 2.3. After approximately 72 hours of growth, confluent epithelial tissues were formed. Due to factors which are difficult to control during the seeding of the cells, the final tissues varied significantly in cell density. Therefore the cell density of every monolayer used in an experiment was directly measured using confocal microscopy (Fig. 4.2B) so that any possible effect of this variation could be identified (Fig. 4.2C).

To prepare fully grown epithelia for live fluorescent imaging the collagen scaffold was removed via enzymatic digestion (section 2.4) and the devices were attached to glass bottom Petri dishes (section 2.5). Cell plasma membranes were stained via a 10 minute incubation in 1X CellMask plasma, a membrane stain (Thermo Fisher Scientific), to visualise the shape of the tissue and its constituent cells. Alexa Fluor-647-conjugated dextran, 10,000 MW (Thermo Fisher Scientific) was added to the imaging medium in order to visualise the coverslips on which the epithelia were grown. The edges of these coverslips delimited the region of the tissue which is suspended and therefore the region to which a compression is applied (see Fig. 4.1).

Two microscope set-ups were used which are described in section 2.5. To obtain three dimensional image stacks, the spinning disc live imaging set-up was used, whereas the scanning laser live imaging set-up was used to obtain two-dimensional images of the epithelia's cross-sectional shape (Fig. 4.1).

Various strain routines were applied via a motorised stage controlled through custom written LabView scripts (see section 2.6). The distance between the motorised stage contact point (i.e. the point at which the strain was controlled) and the stretching device's hinge point was greater than the distance between the tissue and hinge - this led to the requirement that the motorised stage must move a slightly greater distance than the distance that was required for the coverslips. Although this additional distance could be calculated exactly for a known device geometry, the devices were hand-made so variation in the geometries led to some error on the final strain applied (see Fig. 4.1D). Strains were applied at either the relatively low strain rate of 0.5%/s or at a much higher rate of >100%/s, depending on the experiment. Note that in these experiments tissue strain is the parameter which is controlled rather than tissue stress.

4.2.2 Quantification of cell and nuclei shapes

Three dimensional confocal stacks of live tissues in which plasma membranes were stained with CellMask and nuclei were stained with Hoechst were acquired on the spinning disc live imaging set-up (section 2.5) at various compressive strains. The cell outlines were automatically segmented and hand-corrected using the FIJI [261] plugin Tissue Analyzer [245]. Measurements of cell shape were extracted from the resulting outlines via Mathematica (Wolfram Research). Cell length measurements were obtained by calculating the minimum bounding box of the cell outline, where the bounding box is oriented with respect to the experimental x- and y-axes. Measurements of cell and nuclei height were obtained by hand in FIJI from cross-sectional slices through the image stack along y-z planes. Measurements of nuclei shape in the x-y plane were obtained manually in FIJI and the same bounding box measurements were used.

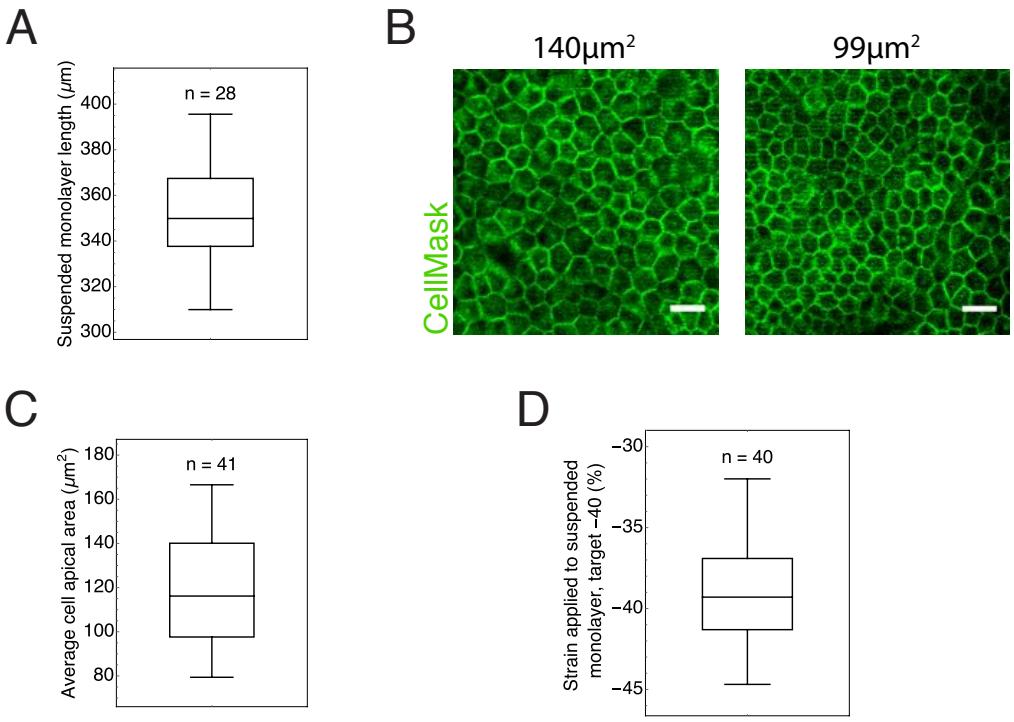

Figure 4.2: Potential sources of error in the experimental system. (A) The distances between coverslips of stretching devices used in the experiments. The target length was 350 µm. (B) Suspended MDCK monolayers with cell membranes labelled using CellMask. Examples of a tissue with low (left) and high (right) cell density are shown. The average cell area of the tissues is given above the image. (Scale bars: 20 µm) (C) The distribution of the average cell apical area in suspended MDCK monolayers used in experiments. (D) The true compressive strain applied to suspended tissues in experiments for a target compressive strain of 40%. The horizontal line and top and bottom of boxes represent the median, 75th percentile, and 25th percentile in all box plots, respectively. The whiskers demarcate the range.

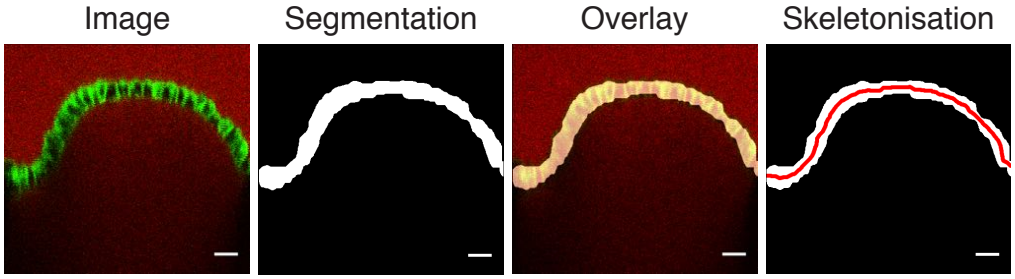

Figure 4.3: Segmentation and calculation of contour length using cross-sectional images of suspended monolayers. Confocal images of suspended epithelial monolayers (left) with membranes visualised with CellMask (green) and surrounding medium visualised with fluorescently conjugated dextran (red) where segmented using Chan-Vese algorithm (midlle-left). The middle-right image shows the overlay of the segmentation with the original image. This segmented mask was converted to a line via morphological thinning and morphological pruning (right). (Scale bars: 20 µm)

4.2.3 Segmentation of monolayer profiles

An implementation of the Chan-Vese algorithm [262] in Mathematica (Wolfram Research) was used to segment the monolayers from the videos (Fig. 4.3, middle-left). The Chan-Vese binarisation assigns each pixel of an image domain Ω, into one of two groups, either $\mathcal{D}$ or $\Omega/\mathcal{D}$. The contour of $\mathcal{D}$ is denoted $\Gamma = \partial\mathcal{D}$. The final segmentation is defined as the minimum of the functional F, of image f, which is given by:

$$F(c_1, c_2, \Gamma) = \mu Length[\Gamma] + \nu Area(\mathcal{D}) + \lambda_1 \int_{\mathcal{D}} |f - c_1|^2 dxdy + \lambda_2 \int_{\Omega/\mathcal{D}} |f - c_2|^2 dxdy,$$

where μ, ν, λ_1 and λ_2 are free parameters which define the magnitude of the length penalty, area penalty and pixel value difference penalty, respectively. The choice of pixel targets c_1 and c_2 depends on the desired segmentation but setting $c_1 = \int_{\mathcal{D}} f dxdy$ and $c_2 = \int_{\Omega/\mathcal{D}} f dxdy$, as it was here, will generally produce a segmentation of the two most mutually distinct regions. For the given application, this was found to be a particularly efficient approach and it achieved accurate segmentation of the monolayer region (Fig. 4.3, middle-left) combining the presence of the membrane fluorophore (CellMask Orange Plasma membrane Stain, Thermo Fisher Scientific or E-cadherin–GFP) and the lack of background (Alexa Flour-647-conjugated dextran, Thermo Fisher Scientific). The generally small movement in the monolayer position between time frames in videos meant that the search for each minimum could be initialised using the segmentation of the previous time frame.

4.2.4 Quantification of monolayer unbuckling

To quantify the changes in the contour length of the epithelial cross section during experiments, a range of possible metrics could be applied to the segmentation of the image. One potential metric to quantify the degree of buckling is the furthest perpendicular distance

between the monolayer and the plane in which the compression is applied. This measurement, however, is sensitive to details of the shape of a buckle. It can be used if buckles take a very stereotyped shape, such as a single arch (the 'fundamental mode'), however, the measurement is harder to interpret when more complex and varied buckled shapes are produced. The total contour length of the epithelium's x-z plane cross-section was found to provide a more meaningful measure (see Fig. 4.1B and C, dotted lines). For instance, the contour length is approximately unchanged from the rest length if the deformation consists of simple buckling out of the plane, whereas it can take a minimum value of the distance between boundary points if the deformation is entirely in-plane (see Fig. 4.1B and C, dotted lines and yellow lines). This is independent of the shape of the buckle.

In order to convert each binary mask generated by segmentation (which defines an area) into a line, morphological thinning [263] was applied to the mask repeatedly until it was skeletonised (Fig. 4.3, right). This process can produce smaller isolated lines so the largest morphologically connected component was selected. The skeletonisation could also produce a line with branches, introducing an error in the measurement of contour length. These were also removed using morphological pruning [263]. The length of the shortest path between opposite edges of the image via foreground pixels thus constituted a measure of the cross-sectional contour length of the monolayer. These algorithms were assembled in Mathematica.

4.2.5 Generation of Myosin–GFP cell lines

To investigate the localisation of myosin in suspended MDCK monolayers, plasmids encoding GFP-tagged myosin were stably transfected into wild-type MDCK cells. Non-muscle myosin II (NM II) is formed of three pairs of proteins - two 'heavy chains', two 'regulatory light chains' and two 'essential light chains' [264] and is a class of myosins which is essential for a large range of functions performed by non-muscle cells [265]. Three isoforms of NM II arise from variations in the heavy chain. They are named NM IIA,B and

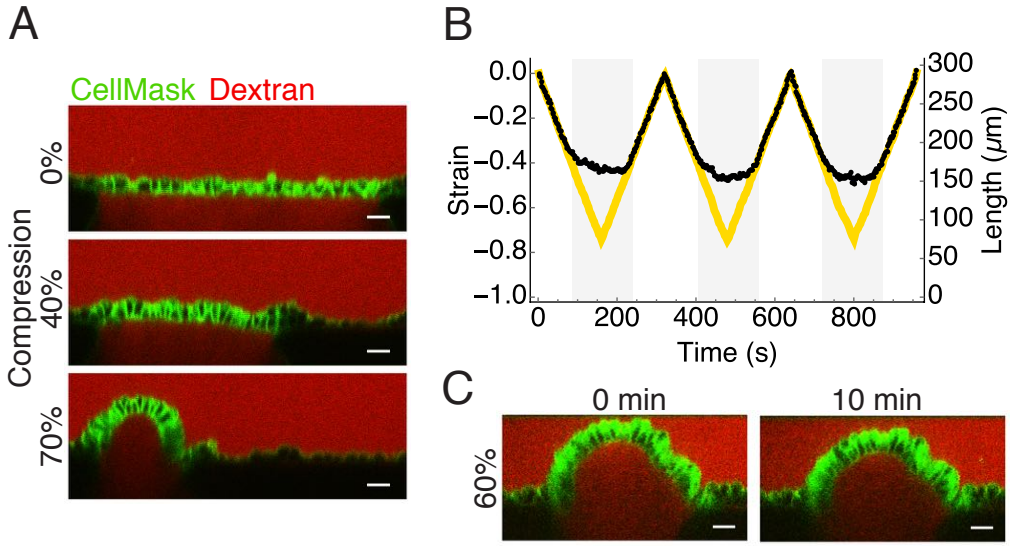

Figure 4.4: Changes in tissue shape upon compression. (A) Cross-sectional perspectives of suspended MDCK monolayer visualised with CellMask live membrane stain (green). The medium contained fluorescently conjugated dextran (red) to show the location of coverslips (black). A 75% compressive strain was applied at a rate of 0.5%/s. (B) The contour length (black dots) of the monolayer and the distance between coverslips (yellow solid line) during three triangle wave cycles of compressive strain. The grey shaded regions demark to times in which the monolayer was buckled. (C) Cross-sectional perspectives of a suspended MDCK monolayer with a constant 60% compressive strain maintained over a time period of 10 minutes. (Scale bars: 20 μm)

C [264]. In MDCK monolayers, NM IIA and NM IIB have been found to play important non-redundant roles in establishing and regulating tension at adherens junctions [266]. Therefore GFP-tagged non-muscle myosin heavy chain IIA and IIB (NMHCIIA–GFP and NMHC IIB–GFP) were chosen to image myosin localisation.

Plasmids encoding either the human NMHCIIA–GFP or the human NMHCIIB–GFP gene were linearised and transfected into wild-type MCDK cells using electroporation (Lonza). 1×10^6 cells were transfected using $10\,\mu g$ of plasmid. The transfected cells were then amplified and selected with Geneticin ($1\,mg/ml$). Flow cytometry was used to select a population of cells with a relatively homogenous level of fluorescent expression.

4.3 Changes in tissue shape induced by compressive strain

A planar compressive strain applied to a sheet of any material may lead to out-of-plane deformation in the form of a buckle. Alternatively, the deformation may be confined within the plane of the sheet. The combination of these two behaviours in response to a given strain will ultimately depend on properties of the sheet, such as its flexural rigidity, and on details of the applied strain, such as the speed at which it is applied.

The response of a suspended epithelial monolayer to planar compression was initially tested by applying a 75% uniaxial compressive strain to the tissue at a relatively slow strain rate of 0.5%/s. An object which is slender (i.e. has a thickness much smaller than the length of the other dimensions) and/or has low bending stiffness, is expected to buckle at low strains. At these strains rates, however, suspended MDCK monolayers were found to accommodate compressive strains of up to 40% without buckling (Fig. 4.4A, top and middle). Beyond a strain of 40%, a transition in behaviour was observed and the monolayers now buckled (Fig. 4.4A, bottom).

To quantitatively assess this behaviour, the evolution of the cross-sectional contour length of the tissue (see Fig. 4.1B, black dotted line) was measured using a custom built image analysis pipeline (see sections 4.2.3 and 4.2.4). Comparison of such measurements of contour length with the accompanying evolution of the applied strain, demonstrated that there was a sharp transition between the two regimes. During the initial regime of in-plane deformation, changes in tissue contour length exactly matched changes in the applied strain (as is required for entirely in-plane deformation) (Fig. 4.4B, white regions). However, this behaviour stops quite suddenly when the strain passes $\sim$40%, at which point buckling begins and the contour length remains almost constant (Fig. 4.4B, grey regions).

Despite the large magnitude of the compressive strain and high level of curvature during buckling, the compression did not appear to cause irreversible changes in the monolayer. Indeed, the behaviour described above was repeated identically over several triangle wave cycles of strain application (Fig. 4.4B).

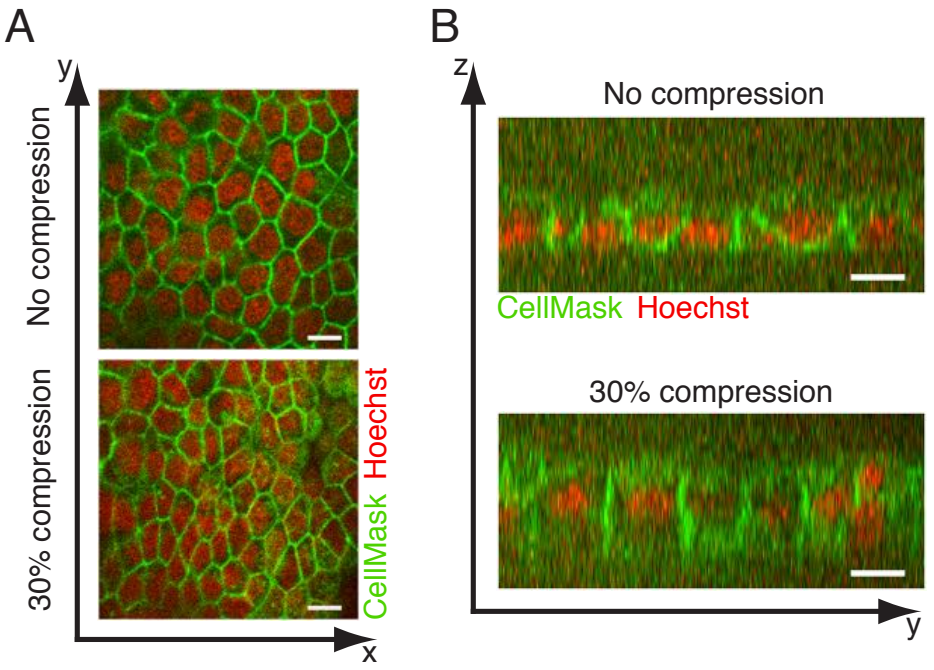

Figure 4.5: Changes in cell and nuclei shape upon compression. (A) Confocal section of a monolayer with plasma membranes visualised using CellMask (green) and nuclei labelled with Hoechst (red) showing shape change in the plane of the monolayer upon 30% uniaxial compression along the axis labelled x. The images are taken 20 minutes apart. (B) A cross-section of the same tissue showing shape change orthogonal to the plane of the monolayer. (Scale bars: 10 µm)

The constant contour length observed during strains of >40% showed that no further deformation occurred within the plane of the tissue - neither due to the changing applied strain nor due to active processes from within the tissue. However, this apparent lack of active processes was not entirely clear in these experiments due to the continual evolution of applied strain and the rather short time period (∼160 seconds) during which strains of >40% were applied. To test whether the buckles retained truly stable shapes, a 60% compressive strain was applied at a rate of 0.5%/s and maintained for 10 minutes. The buckles which formed in these experiments did indeed appear to be stable in shape (Fig. 4.4C), however, a very slight but reproducible contraction of the shape suggested there may be some active processes acting at much longer timescales (Fig. 4.4C). These were not investigated further in this study.

4.4 Changes in cell shape induced by compressive strain

During the initial phase of in-plane deformation, the global change in tissue shape could possibly be accounted for at the cellular level by changes in cell shape, by cell extrusions, by cell rearrangements or by a combination of all three. Indeed, in many morphogenetically active epithelia a combination of all three processes frequently contributes to overall changes in tissue shape [67]. Over these relatively short timescales, however, cell extrusions and cell rearrangements were not observed, although they may have occurred at a low rate (Fig. 4.5, images were compared using clear reference points between the tissues such as dividing cells). Instead, cell shape change accounted for the majority of the global change in tissue shape (Fig. 4.5). While the reduction in cell length along the axis of compression (x-axis) almost matched the global reduction in tissue length (Fig. 4.6A), there was no detectable change in length along the y-axis (Fig. 4.6B). Instead, cells increased dramatically in height (Fig. 4.6C). Interestingly, this change consisted of an increase in the height of the cell-cell lateral interfaces, as well as an increase in the distance between apical and basal membranes (Fig. 4.5B). Overall the ratio of change in cell height to change in length along the x-axis was 1.03 indicating that there was no significant change in the volume of the tissue following compression.

While nuclei are known to be stiffer than the cytoplasm that surrounds them [267], enabling them to resist deformation, the shape of nuclei in suspended MDCK monolayers closely followed the shape of cells during compression (Fig. 4.7). As with cell shape, the length of nuclei along the x-axis decreased with compression (Fig. 4.7A), while the length along the y-axis remained constant (Fig. 4.7B) and the height of nuclei increased (Fig. 4.7C).

Altogether, whereas cells changed from an approximately isotropic shape to a highly anisotropic shape (Fig. 4.5D), nuclei began and ended with an anisotropic shape with a similar aspect ratio but oriented along a different axis (Fig. 4.7D). It is worth noting that the lack of change of cell and nuclei shape along the y-axis compared with the change in height

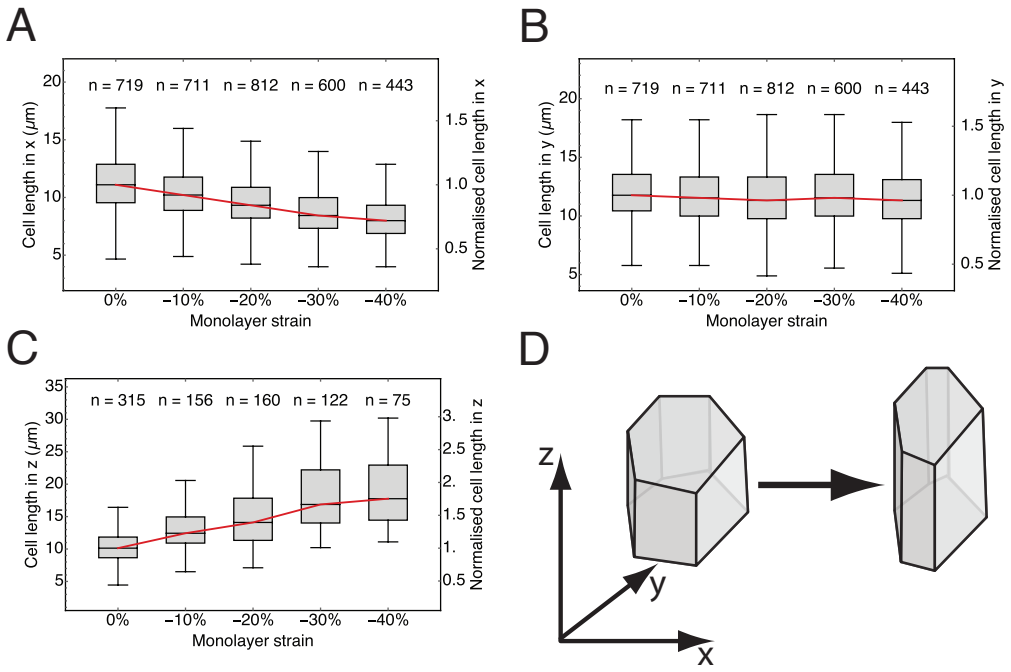

Figure 4.6: Changes in cell shape upon compression. (A) Cell length along the x-axis during tissue compression. (B) Cell length along the y-axis during tissue compression. (C) Cell length along the z-axis (i.e. cell height) during tissue compression. In all charts, the right-hand axis shows the length normalised by the median length at zero strain. The horizontal line and top and bottom of boxes represent the median, 75th percentile, and 25th percentile in all box plots, respectively. The whiskers demarcate the range. The number of cells measured for each strain is given in the chart. N = 4 tissues. (D) Schematic showing the change in cell shape induced by tissue compression in the average cell.

does not imply an intrinsic anisotropy in cell mechanical properties. The experimental system does not provide a fair test of Poisson ratio since the tissue is physically attached to the coverslips along its boundaries along the y-axis. While the remaining boundaries are free to deform, this attachment can limit the global deformation which can occur along the y-axis throughout the tissue and could contribute significantly to the lack of shape changes observed along the y-axis.

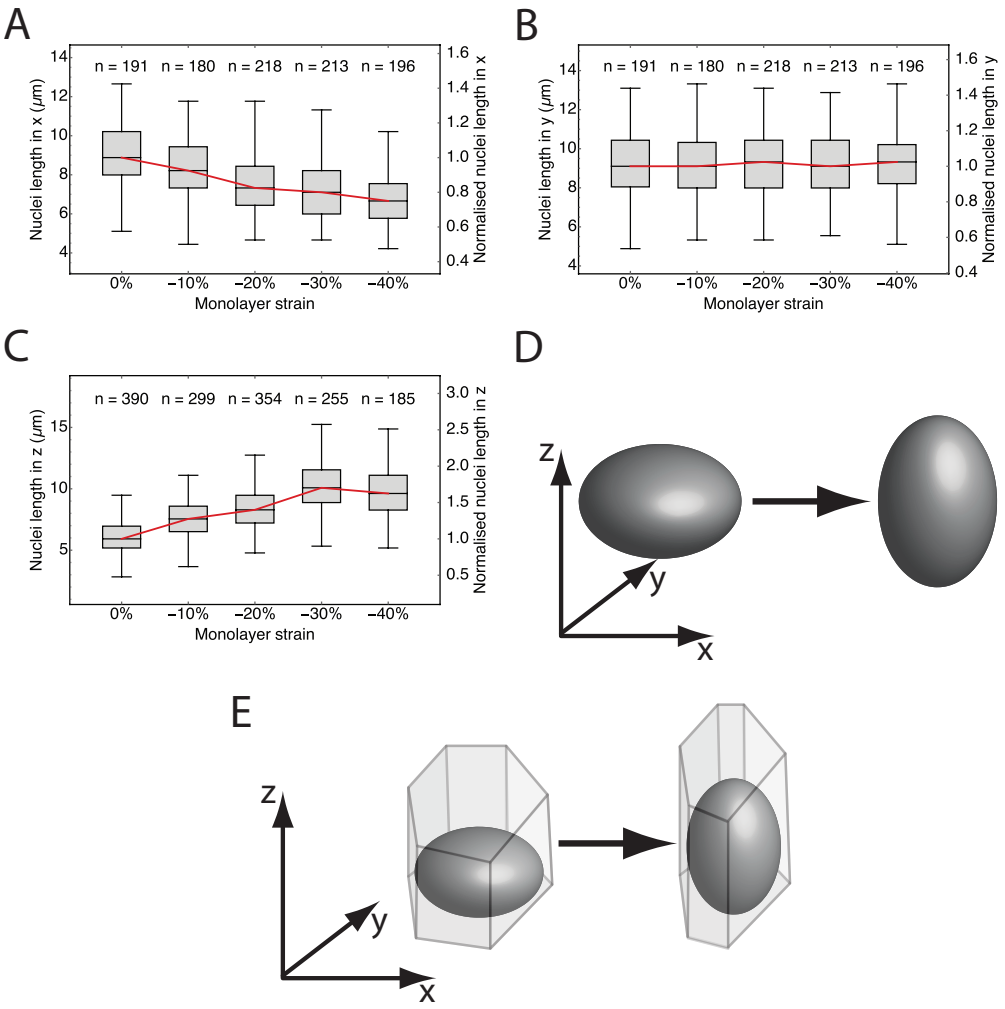

Figure 4.7: Changes in nuclei shape upon compression. (A) Length of nuclei along the x-axis during tissue compression. (B) Length of nuclei along the y-axis during tissue compression. (C) Length of nuclei along the z-axis during tissue compression. The horizontal line and top and bottom of boxes represent the median, 75th percentile, and 25th percentile in all box plots, respectively. In all charts, the right-hand axis shows the length normalised by the median length at zero strain. The whiskers demarcate the range. The number of cells measured for each strain is given in the chart. N = 4 tissues. (D) Schematic showing the change in the shape of nuclei induced by 30% tissue compression in the average cell. (E) Schematic showing the change in the shape of both cells and their nuclei induced by 30% tissue compression in the average cell.

4.5 Suspended epithelia autonomously flatten buckles induced by compressive strain

The changes in tissue, cell and nuclei shape described above (sections 4.3 and 4.4), which occurred during the application of compressive strain at a slow low strain rate, could be

passive, i.e. they could be forced upon the tissue and constituent cells by the application of strain. On the other hand, cells could play an active role, adapting to the changes in boundary conditions by actively altering their shape. To differentiate between these two scenarios, compression was applied at a much faster strain rate (>100%/s), in the hope that the application of strain may outpace the rate of active processes in the tissue. Indeed, this change in strain rate produced a very different result in terms of the immediate response of the tissue. A 40% planar compressive strain applied at a rate >100%/s resulted in immediate tissue buckling (Fig. 4.8). Therefore, the immediate response of an epithelium to a compressive strain depends strongly on strain rate.

In the majority of experiments, the buckle took the shape of a single arc with no points of inflection of curvature (Fig. 4.8 top row and bottom right). This was true for 69% of cases (18 out of 26 tissues). Of the tissues which buckled with a single arc, all but 2 of them (89%) buckled so that the apical side of the tissue was on the outside of the curve. This bias in direction may result from an asymmetry in the mechanical properties of the tissues along the z-axis, however, it could also result from asymmetries in the boundary conditions of the experimental setup. For example, the coverslips extend basally in the z-direction and not in the apical direction and the glass boundary of the Petri dish is on the apical side of the tissue whereas there is no such boundary on the basal side. The relative mechanical properties of the apical and basal sides of the monolayer are explored further in section 4.8. The remaining 31% of tissues buckled to give rise to more complex shapes which contained one or more points of inflection in the curvature (Fig. 4.8 bottom left and middle).

Remarkably, the buckles formed by the fast application of 40% strain were not stationary structures. Instead they rapidly flattened, returning the monolayers to a planar configuration (Fig. 4.9A). Given the absence of other influences, this behaviour could only be explained as being autonomously driven by the tissue itself. This may be considered particularly surprising given the change from an isotropic to an anisotropic cell shape which accompanies tissue flattening, along with the substantial deformation of stiff nuclei

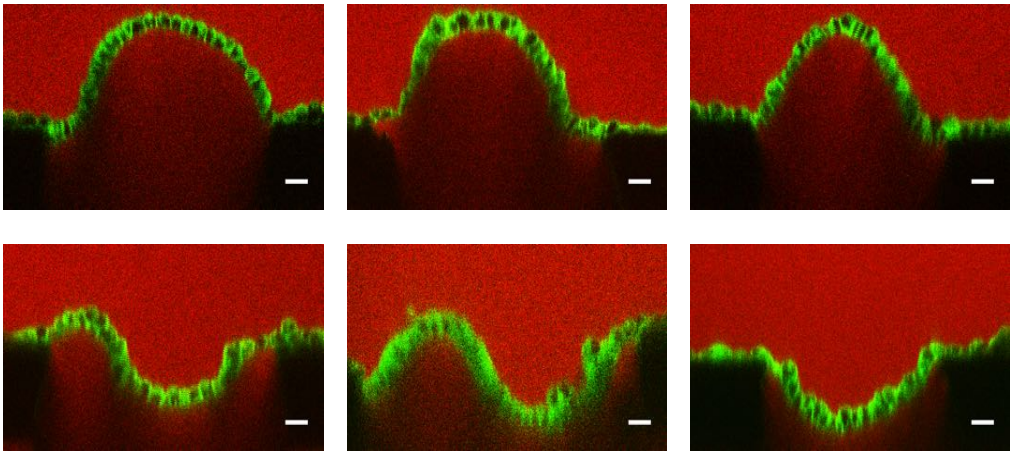

Figure 4.8: Fast application of 40% strain induces tissue buckling. Tissue shape immediately after application of a 40% compressive strain. A variety of buckle shapes were observed. The majority of tissues produced a single buckle in the apical direction (top row). In some cases buckles with multiple points of inflection were produced (bottom left and middle). Tissues rarely buckled basally (bottom right). (Scale bars: 20 μm)

which is required (Figs. 4.6 and 4.7). Indeed, this is very different to the behaviour of single cells which make exactly the opposite transformation in shape when their boundaries are freed from attachment - they become spherical.

Tissue flattening was further examined by measuring the contour length of the tissue's cross-section during the process. The effectively instantaneous reduction in length between the tissue's boundaries (i.e. the application of strain, Fig. 4.9B, yellow line) was accompanied by a decrease in the cross-sectional contour length of the tissue over several minutes (Fig. 4.9B, black points). The rate of length contraction was fastest at the start, with an average 15% decrease in length within the first 2 seconds. Thereafter the flattening rate quickly decayed as the tissue length approached the distance between the boundaries (Fig. 4.9B). While there was substantial variation in the rate of flattening between tissues, the overall behaviour was very reproducible (Fig. 4.9C).

In order to quantitatively compare the dynamics of flattening between tissues in varying experimental conditions it is necessary to identify a simple mathematical function to describe the changes in contour length. However, while the overall pattern of the behaviour was similar between tissues, a simple function could not be identified which ac-

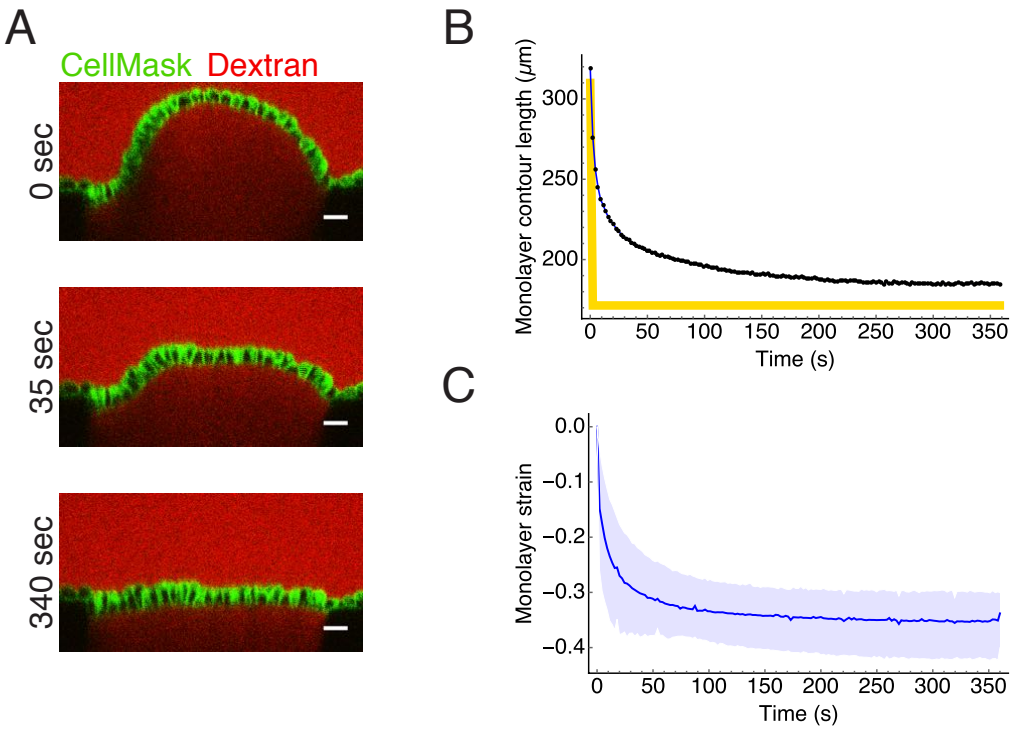

Figure 4.9: MDCK monolayers rapidly flatten buckles induced by a 40% compression. (A) Confocal cross-sections of an MDCK monolayer after the application of a 40% compressive strain. The buckle which is formed immediately after application of compression flattens over a period of several minutes. (B) Temporal evolution of the contour length of the tissue cross-section (black points) after a 40% reduction in the distance between the coverslips (yellow line). (C) The average temporal evolution of strain of the tissue cross-sectional contour length of n = 16 tissues. The solid blue line is the mean, the blue shaded region demarks the total range. (Scale bars: 20 μm)

curately described the dynamics of tissue flattening in all experiments. Some curves were approximated well by a simple exponential decay function (Fig. 4.10A), however, others were better approximated by a sum of two exponentials (Fig. 4.10B). Some decayed slower than exponentially throughout but were not well approximately by a power law either (Fig. 4.10C). More complex functions with additional fit parameters were explored but ultimately this did not help to provide a more meaningful measurement of flattening rate.

Since a simple function could not be found to fit the entire time course of flattening, attention was focused on the first 20 seconds of the process, to determine the initial rate of flattening. The fits of linear, exponential and power law functions to the data within this time frame were compared (Fig. 4.10D). A linear model fit least well, producing the largest

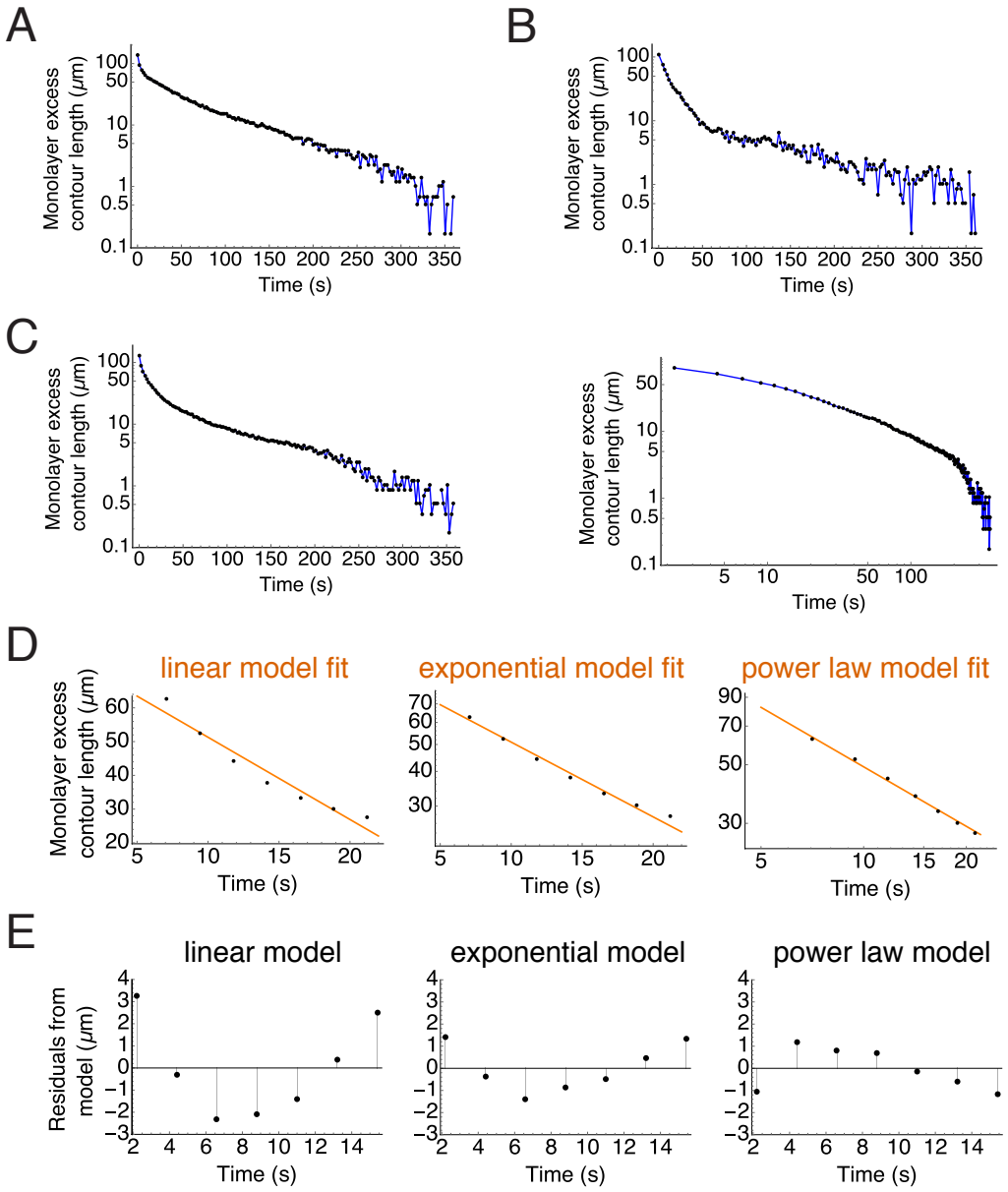

Figure 4.10: Quantifying the rate of flattening in buckled tissues. (A-C) Examples of the evolution of tissue cross-sectional contour length plotted on logarithmic y-axes to visually assess whether the behaviour can be described by an exponential decay function. In each case, the minimum tissue contour length is subtracted from the true measured length to give the 'excess length'. (A) shows an example in which the decay is well approximated by an exponential function throughout. In (B) there appears to be two regimes of exponential decays with different rate. In (C) the decay is slower than exponential so the data is also plotted on log-log axes to test for a power-law function. (D) A linear (left), exponential (middle) and power law (right) model is fit to the first 20 seconds of tissue flattening. (E) The mean residual of linear (left), exponential (middle) and power law (right) model fits to all experiments (N = 14 tissues).

residual errors. These errors followed a characteristic pattern which showed that linear functions approached zero too fast (Fig. 4.10E, left). Exponential and power law models fit the data much better and residual errors were small (Fig. 4.10E, middle and right). As with the linear models, both the exponential and power law models gave systematic patterns of error, here showing that the exponential functions approached zero too fast and whereas the power law functions approached zero too slowly (Fig. 4.10E, middle and right). While the exponential and power law models clearly fit the data better than linear models, there was no meaningful difference in the fit between exponential and power law models, as is expected when fitting over a small time span.

Given the above analysis (Fig. 4.10), the measure chosen to describe the initial rate of flattening was the rate constant of an exponential fit to the first 20 seconds of the data. Altogether, suspended MDCK monolayers flattened with an initial rate of $0.049 \pm 0.049\,\mathrm{s}^{-1}$ ($mean \pm standard\ deviation$) (Fig. 4.11A), corresponding to a half-life of $15\,\mathrm{s}$. As discussed in section 4.2.1, both the length of the tissue and cell density of the tissue were subject to variation due to limitations in experimental control. Both these factors could conceivably impact the flattening rate, contributing to the variation between experiments (Fig. 4.11A). Cell contractility and the assembly of stress fibres, for instance, is known to depend on the cell spread area [268] and the total tension produced in a muscle fibre depends strongly on muscle length [269]. Strikingly, however, neither the cell density of the tissue (Fig. 4.11B) nor the total tissue length (Fig. 4.11C) correlated with the initial rate of flattening.

4.6 Human keratinocyte epithelia also autonomously flatten buckles induced by compression

To test whether the flattening behaviour was specific to MDCK monolayers, the behaviour of a human keratinocyte cell line, HaCaT, was examined. Whereas MDCK cells grow ex-

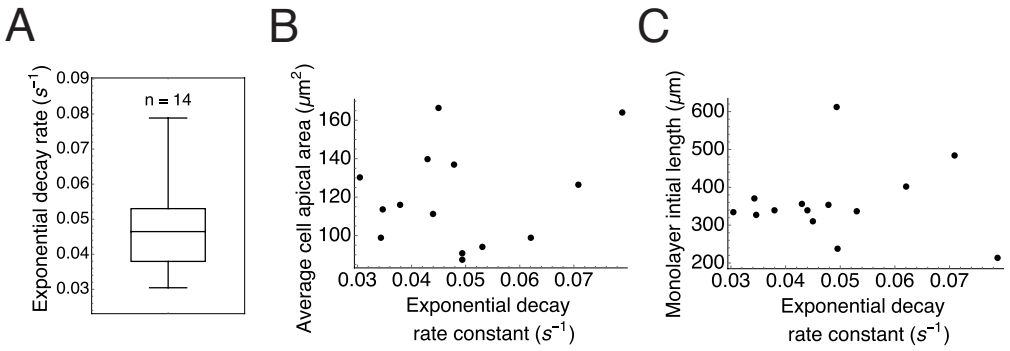

Figure 4.11: The initial rate of flattening in MDCK monolayers. (A) The initial rate of tissue flattening was measured as the rate constant of the exponential decay function fit to the first 20 seconds of the evolution of tissue contour length during flattening. Suspended MDCK monolayers flattened with a median rate of $0.046\,\mathrm{s}^{-1}$. The horizontal line and top and bottom of boxes represent the median, 75th percentile, and 25th percentile, respectively. The whiskers demarcate the range. (B) The average cell area for a tissue does not correlate with the initial rate of flattening. (C) The total length of the tissue does not correlate with the initial rate of flattening.

clusively as monolayers, HaCaT only grow as monolayers in low calcium conditions which prevent the formation of cell-cell junctions. When calcium is added, cell-cell junctions are formed within a few hours and over several days the tissue stratifies and expresses keratins which are typical of the apical section of the human epidermis [47].

Accordingly, HaCaT cells grown on the collagen scaffolds of stretching devices in the presence of calcium formed tissues which were clearly not a single layered structure (Fig. 4.12A). Cells at the apical side of the tissue were densely packed compared to those at the basal side (Fig. 4.12A). While these tissues were clearly different in structure to MDCK monolayers, they behaved in the same manner when subjected to a rapid 40% compressive strain. Once again buckles induced by the compression were rapidly flattened, returning the tissue to a planar configuration (Fig. 4.12B and C).

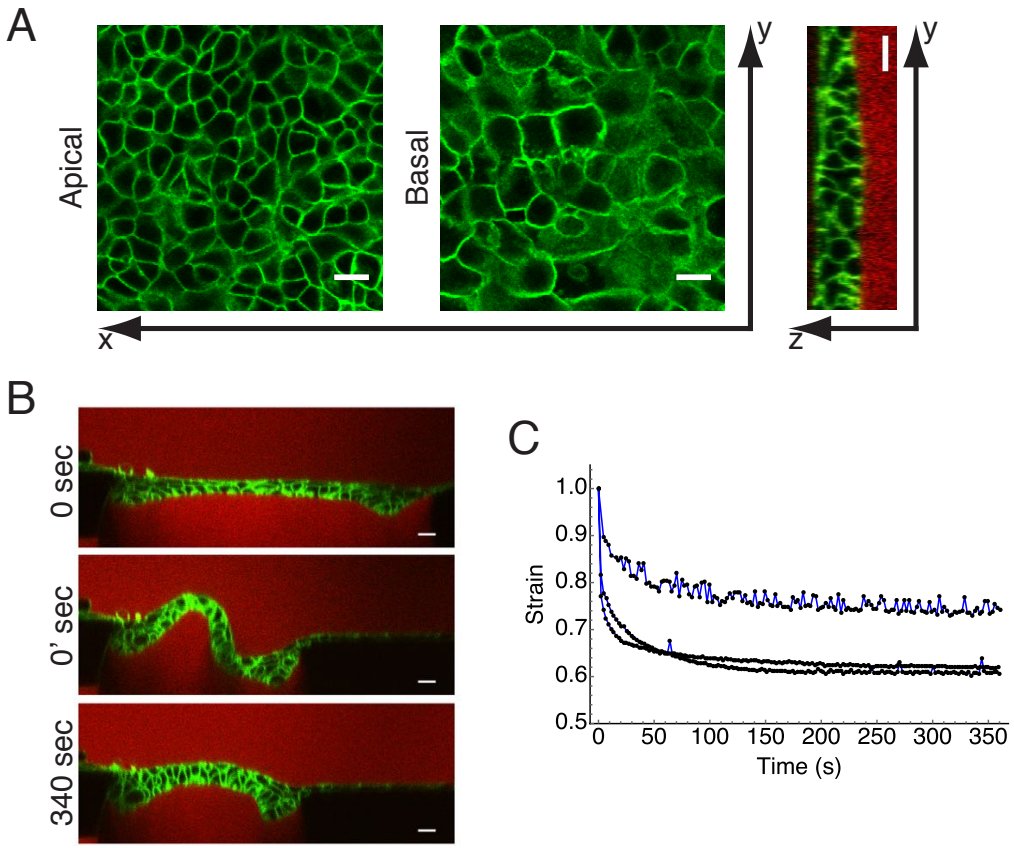

Figure 4.12: HaCaT epithelia behave similarly to MDCK monolayers when compressed. (A) Confocal slices of HaCaT cells grown on collagen scaffolds on stretching devices. Cell membranes are marked with CellMask (green) and the medium is labelled with fluorescently tagged dextran (red). The cells formed multilayered tissues which were more densely packed apically than basally. (B) and (C) A 40% compressive strain applied to the tissue caused tissue buckles which were rapidly flattened. (C) shows the change in length of three different HaCaT tissues. (Scale bars: 20 µm)

4.7 Flattening of tissue buckles requires actomyosin generated contractility

Many changes in the shape of eukaryote tissues and cells are driven by forces produced by the actomyosin cytoskeleton [72, 270]. To test the role of actomyosin in the cell and tissue shape changes triggered here by tissue compression, the actomyosin cytoskeleton was perturbed in suspended epithelia prior to, and during compression using pharmacological treatments.

Three drugs were used to perturb actomyosin function - blebbistatin, Y27632 and la-

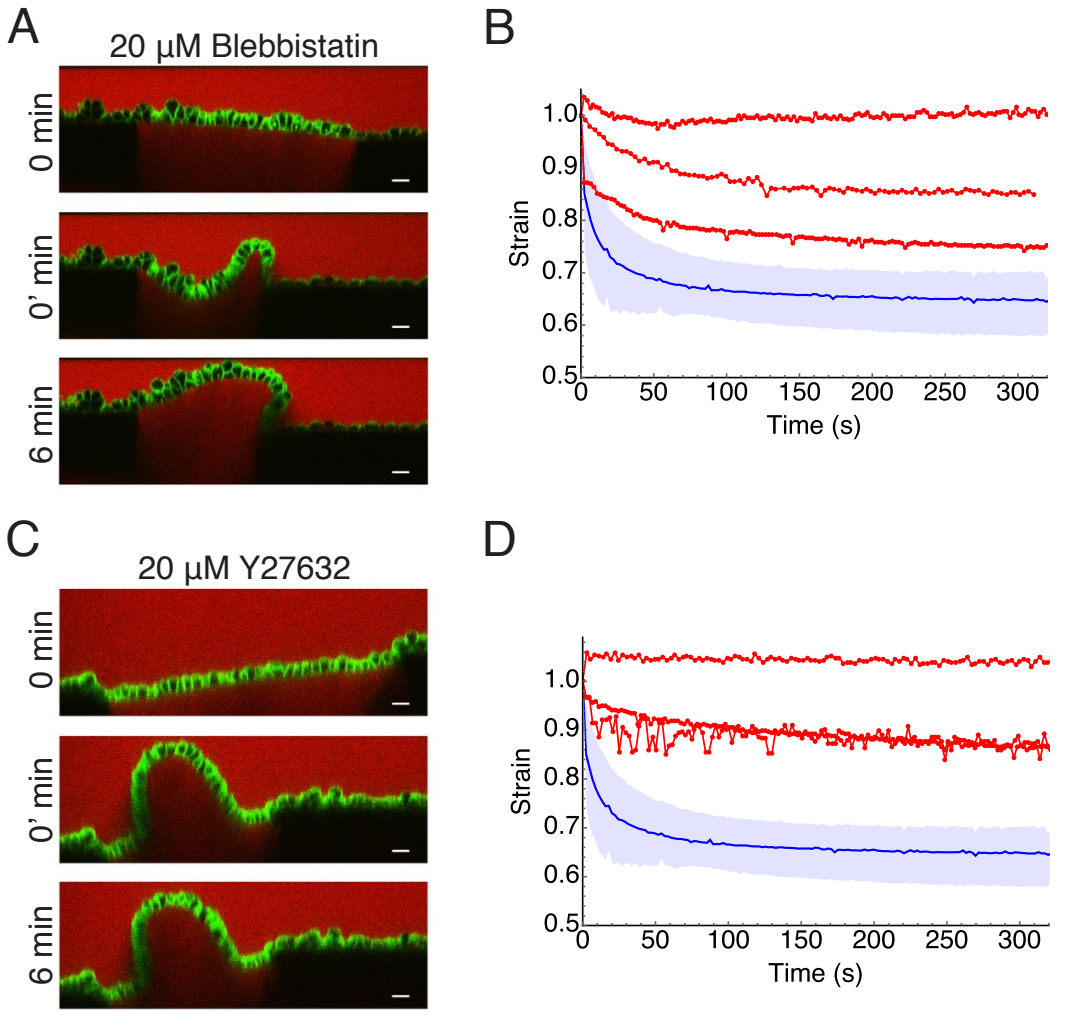

Figure 4.13: Flattening of buckles induced by compression requires active myosin. (A) Cross sectional image of a suspended MDCK monolayer (green) treated with 20 μM blebbistatin, immediately before compression (top), immediately after compression (middle) and 6 minutes later. (B) Evolution of the cross sectional contour length of tissues treated with 20 μM blebbistatin (red) compared to the control (blue). (C-D) As in (A-B) but monolayers were treated with 20 μM Y27632. (Scale bars: 20 μm)

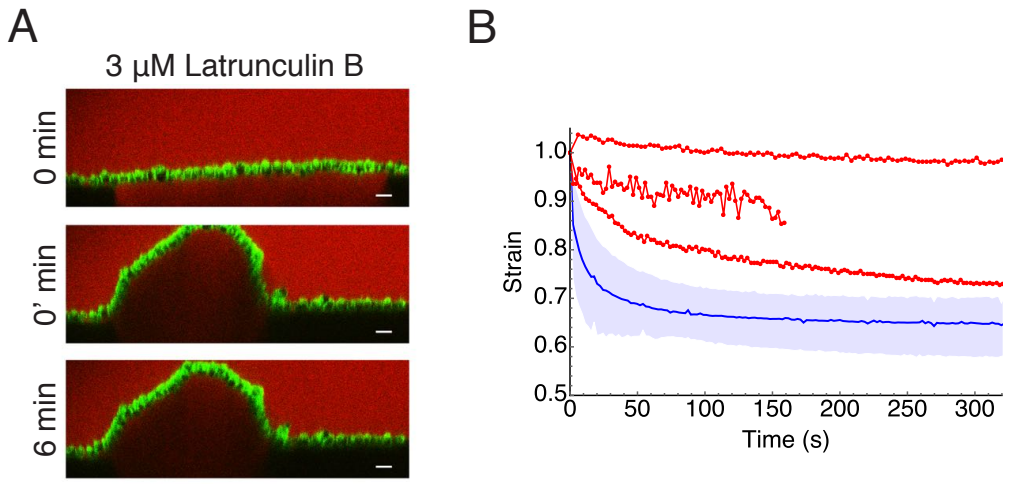

Figure 4.14: Flattening of buckles induced by compression requires an intact actin cytoskeleton. (A) Cross sectional image of a suspended MDCK monolayer (green) treated with 3 μM latrunculin B, immediately before compression (top), immediately after compression (middle) and 6 minutes later. (B) Evolution of the cross sectional contour length of tissues treated with 3 μM latrunculin B (red) compared to the control (blue). (Scale bars: 20 μm)

trunculin B. Both blebbistatin and Y27632 reduce the activity of non-muscle myosin II. Blebbistatin binds preferentially to myosin when it is in the ADP and phosphate-bound intermediate state [271], which has a low affinity for actin filaments [271]. It slows the release of the phosphate, thereby delaying cycle progression and reducing motor activity [271]. Y27632 reduces myosin-driven contractility through the less direct route of reducing the activity of Rho-associated protein kinase (ROCK). ROCK is an effector of the small GTPase RhoA and when active it phosphorylates the myosin II regulatory light chain, thereby increasing contractility by increasing the affinity of myosin to actin [272]. Y27632 binds to the catalytic domain of ROCK and so reduces its kinase activity by competing with ATP binding [273]. At the cellular level both of these drugs have been found to reduce contractility in MDCK cells at concentrations ranging from 10 to 50 μM [274–277].

Latrunculin B, a toxin secreted by the sea sponge *Negombata magnifica* to paralyse potential predators, targets actin filament dynamics. It binds to the nucleotide binding cleft of monomeric actin, preventing incorporation into actin filaments [278]. Thus, at sufficient concentrations latrunculin sequesters enough monomeric actin to prevent new

filaments from replacing the ones which naturally depolymerise. Accordingly, concentrations ranging from 0.75 to $20\,\mu\mathrm{M}$ have been found to mechanically perturb MDCK cells, dramatically reducing stiffness [90, 279].

All three of the above drugs had a strong effect on the response of the tissue to a 40% compressive strain. The suspended monolayers were treated with $20\,\mu\mathrm{M}$ blebbistatin, $20\,\mu\mathrm{M}$ Y27632 or $3\,\mu\mathrm{M}$ latrunculin B for 10 minutes, 10 minutes or 30 minutes prior to compression, respectively. As before, fast application of the strain led to immediate buckling of the tissue (Fig. 4.13A,C and 4.14A, middle panel). However, perturbation of the actomyosin cytoskeleton dramatically slowed tissue flattening. In some cases stopped flattening altogether (Fig. 4.13 and 4.14, bottom panels and plots). Therefore, these data show that the actomyosin cytoskeleton plays a crucial role in tissue flattening after a compressive strain.

4.8 Apical-basal asymmetry in mechanical properties of suspended epithelia

In section 4.5 it was noted that tissues which were compressed at a high strain rate buckled preferentially to the apical side of the tissue, suggesting a possible apical-basal asymmetry in the mechanical properties. If true, mechanical asymmetry may be an important part in understanding the overall mechanism of tissue flattening. However, an alternative hypothesis is that, when all else is equal, the direction in which the tissue buckles may be biased as the result of very small influences from outside of the tissue, such as asymmetries in the experimental setup (as discussed in section 4.5).

Further evidence of tissue mechanical asymmetry was found in the dynamics of flattening in tissues which buckled with shapes other than single arcs. In the case of tissues which buckled as a single apical arc, the contraction of the contour length appeared uniform (Fig. 4.9). In contrast to this, where tissues initially formed a buckle with two arcs, one apical and one basal, the shape changes which followed did not occur at a spatially

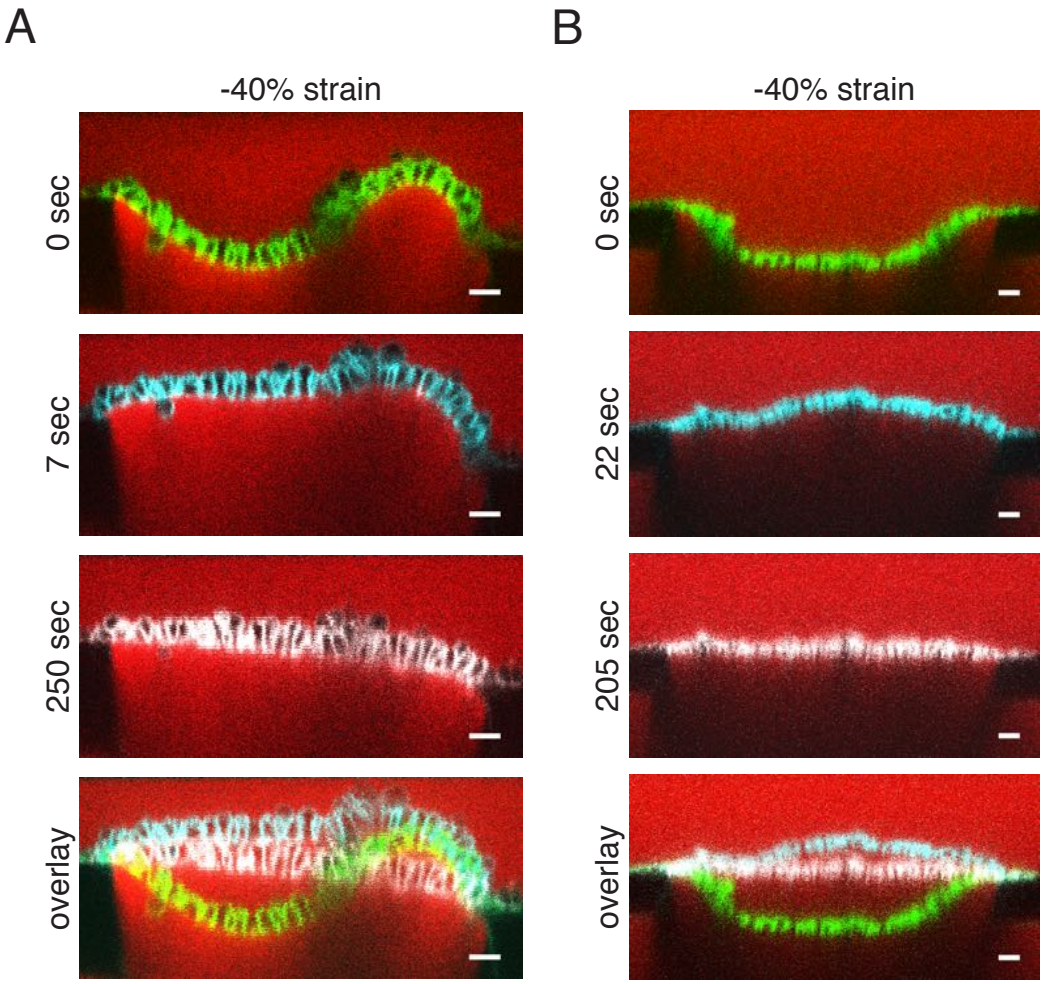

Figure 4.15: Asymmetries in the dynamics of tissue flattening. (A) Cross sectional images of a suspended MDCK monolayer after a 40% compressive strain. A buckle with two arcs forms but the buckles do not flatten symmetrically. Instead the basal buckle moves apically so that a single arc is formed. This arc then flattens at a slower rate. (B) A tissue which buckles with a single basal arc. The arc rapidly transitions to a single apical arc which then flattens at a slower rate. (Scale bars: 20 μm)

uniform rate. (Fig. 4.15A). Instead, the basal arc contracted more rapidly than the apical buckle. This had the effect of moving the basal section of the tissue apically until a single apical arc was formed. This single apical arc then flattened at a slower rate (Fig. 4.15A). This behaviour was seen in all of 8 of the 31% of tissues which buckled with two arcs and the reverse behaviour (i.e. faster contraction of apically buckled sections to produce one basal arc) was never found.

An analagous phenomenon was observed in one of the two tissues which buckled basally. Instead of contracting uniformly until a flat shape was reached, this tissue rapidly overshot the flat shape and became buckled apically. After this the tissue returned at a slower spatially uniform rate until it reached a flat configuration (Fig. 4.15B).

While it is possible to imagine that asymmetries in the experimental setup may provide the small influence necessary to bias buckling direction apically, it is harder to imagine how such influences would have such a strong effect on the dynamics of flattening. A more straightforward explanation is that the basal side of the tissue has a higher bending rigidity, making an apical buckle energetically more favourable than a basal one. However, this behaviour should be reproduced and examined with a mechanical model if it is to be understood clearly.

Given the crucial role of the actomyosin cytoskeleton in tissue flattening which was established in section 4.7, it is possible that asymmetric mechanical properties could be the result of polarised myosin localisation. Isoforms A and B of the heavy chain peptide which forms part of non-muscle myosin II are known to play non-redundant roles in regulating contractility in MDCK monolayers [266]. Therefore, to investigate the localisation of these myosin isoforms in suspended MDCK monolayers, GFP-tagged non-muscle myosin heavy chain IIA (NMHC IIA–GFP) and IIB (NMHC IIB–GFP) was stably expressed in wild-type MDCK cells (see section 4.2.5). These cell lines were grown on the collagen scaffolds of devices using the protocol described in section 3.

Before the removal of the collagen scaffold, NMHC IIA–GFP and IIB–GFP was found

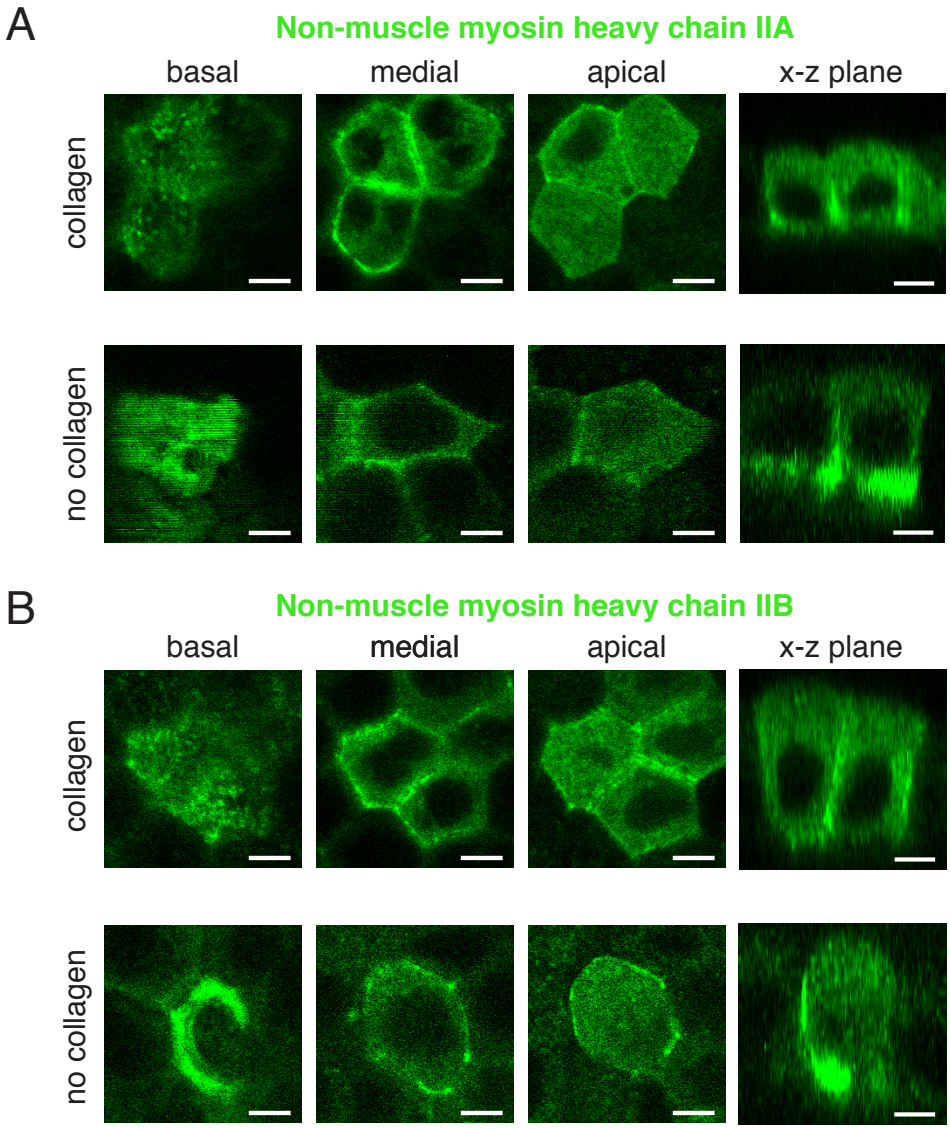

Figure 4.16: Myosin localisation in suspended MDCK monolayers. (A) MDCK monolayers stably expressing non-muscle myosin heavy chain IIA–GFP (NMHC IIA–GFP), grown on stretching devices, before (top) and after (bottom) collagen digestion. NMHC IIA–GFP is localised basally in puncta and at junctions. Localisation at junctions is strongest basally. Localisation is similar before and after collagen digestion but the basal signal is stronger and more uniform after digestion. (B) MDCK monolayers stably expressing non-muscle myosin heavy chain IIB–GFP (NMHC IIB–GFP). NMHC IIB–GFP localisation is similar to that of NMHC IIA–GFP, except that junctional myosin extends further apically. (Scale bars: 5 μm)

basally in puncta (Fig. 4.16A,B top row, left and right) and was enriched at cell-cell junctions (Fig. 4.16A,B top row, middle and right). The junctional localisation of NMHC IIA–GFP was strongest basally, whereas NMHC IIB localised throughout the lateral junctions. Upon the removal of collagen there did not appear to be any significant change in junctional localisation of either NMHC IIA or IIB. However, basal accumulation was clearly visible for both isoforms (Fig. 4.16A,B bottom rows).

Therefore, assuming that the localisation of the GFP-tagged construct reflected that of endogenous myosin, these results suggest that polarised myosin may explain the asymmetric mechanical properties of the suspended epithelia. To investigate this further, however, it would be important to apically localise myosin without affecting overall contractility.

4.9 Epithelial monolayers mechanically adapt to compressive strains

The behaviour described thus far can be captured by a simple mechanical model: a prestretched elastic sheet, would contract without buckling during the slow application of a 'compressive' strain, up until the point at which it reached its rest length. If this compression was applied with a high enough strain rate, however, a transient buckle could form which would rapidly flatten. Just as was observed with suspended epithelia, a strain which reduced the length of the sheet to a point beyond the rest length would result in the formation of a stable buckle in the sheet. Consistent with this conceptual model, measurements from the Charras lab have demonstrated that suspended MDCK monolayers at rest generate an actomyosin dependent contractile stress (data not shown). Therefore, this simple mechanical model would appear to capture the full range of the tissue level behaviours which have been described above.

This simple view of the tissue as a prestretched elastic sheet, however, may be expected to fail upon closer inspection. Indeed, epithelia are known to behave viscoelastically when

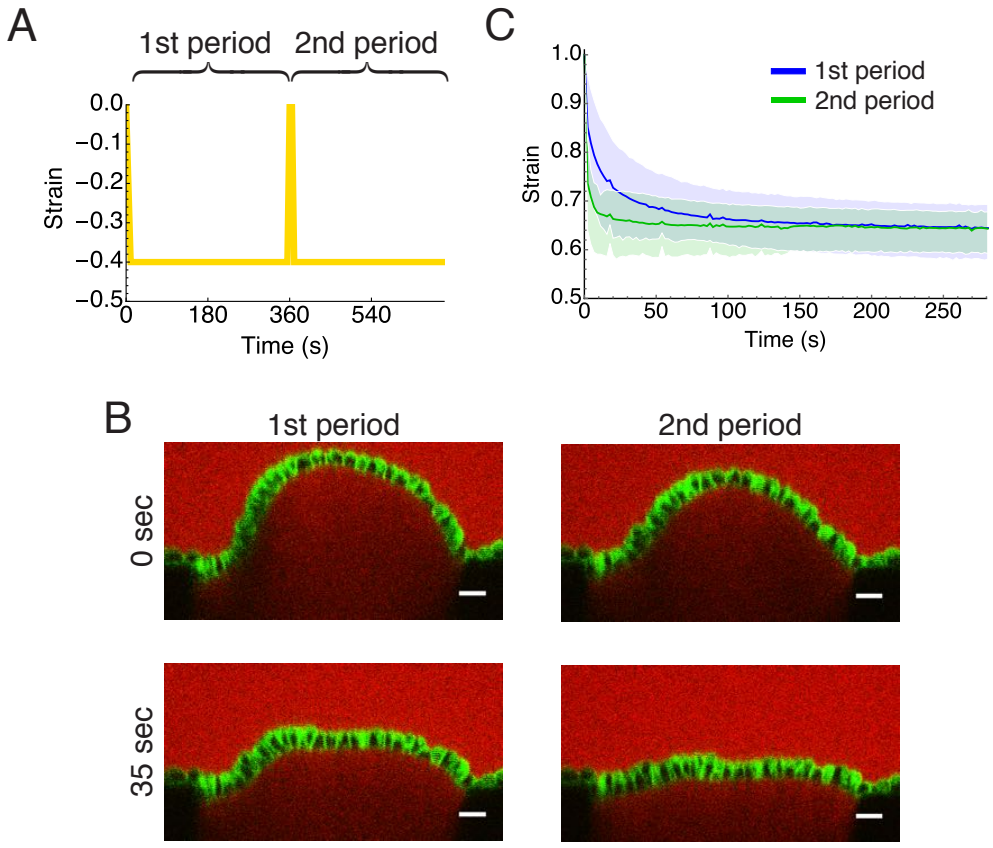

Figure 4.17: MDCK monolayers mechanically adapt to a shorter length after compression. (A) The sequence of strains (yellow line) applied to suspended MDCK monolayers over a 12 minute period. (B) Cross sectional images of the monolayer (green) immediately after application of strain (top) and 35 seconds after the strain (bottom) both for the first compression period (left) and the second compression period (right). In contrast to the first flattening period during which significant arcs are still visible at 35s, in the second period the tissue is almost completely flat within 35 seconds. (Scale bars: 20 μm). (C) The evolution of cross sectional contour length of the tissues after the first compression (blue line) and the second compression (green line). The shaded regions demark the total range in the data. N = 14 monolayers.

stretched [90, 92] and have been shown to exhibit a rich variety of other mechanical behaviours, such as strain stiffening and fluidisation [280, 281], have been reported. Furthermore, the deformations of cell shape measured in section 4.4 necessarily involve changes in structure at the sub-cellular level, such as the elongation of cell-cell junctions in the z-direction and remodelling of the cytoskeleton, which may alter the mechanical properties of the tissue.

To test whether the compressional strain applied here caused any changes in the me-

chanical properties of the tissue, the cycle of compression was applied twice to each tissue. Thus, the suspended MDCK monolayers were compressed by a constant 40% strain for 6 minutes, then returned to their rest length for just 3 seconds and then compressed by 40% once more (see Fig. 4.17A). As before, strains were applied at a fast rate of >100%/s so that buckles were formed and the dynamics of tissue flattening could be observed.

In the ideal prestretched elastic sheet described above, this sequence of strains would produce identical behaviour during the two periods of compression. However, this was not the case is suspended MDCK monolayers. Instead, the tissue flattening during the second period of compression occurred much faster than the first. In the example shown in figure 4.17B, the tissue is almost entirely flat 35 seconds after the second compression (Fig. 4.17B, bottom right), whereas a substantial buckle remained at the same stage after the first compression (Fig. 4.17B, bottom left). The same increased rate of flattening was observed in N = 14 tissues (Fig. 4.17C). Therefore, the changes in tissue and cell shape which occur when the tissue flattens and spends 6 minutes at a shorter length are not superficial - they are accompanied by a measurable change in the mechanical state of the tissue.

Having shown that the tissue quickly adapts to reductions in length, it remained to be tested whether or not these changes were reversible, i.e. whether the tissue could be induced to return to its initial state. To address this, a third cycle of strains were applied to the tissues (Fig. 4.18A). After the second compressive period, the initial length of the tissue was restored and the length was kept constant for 6 minutes before the application of a final 40% compressive strain (Fig. 4.18A). As shown in the example in figure 4.18B, the rate of tissue flattening returned to the original slower rate in the third period. As a result the size of the buckle 35 seconds after the third compression (Fig. 4.18B, bottom right) is similar to that of the first buckle at this time point (Fig. 4.18B, bottom left). The same restored rate of flattening was observed in N = 7 tissues (Fig. 4.18C). Overall there was no significant difference between the initial rate of flattening in the first period of compression

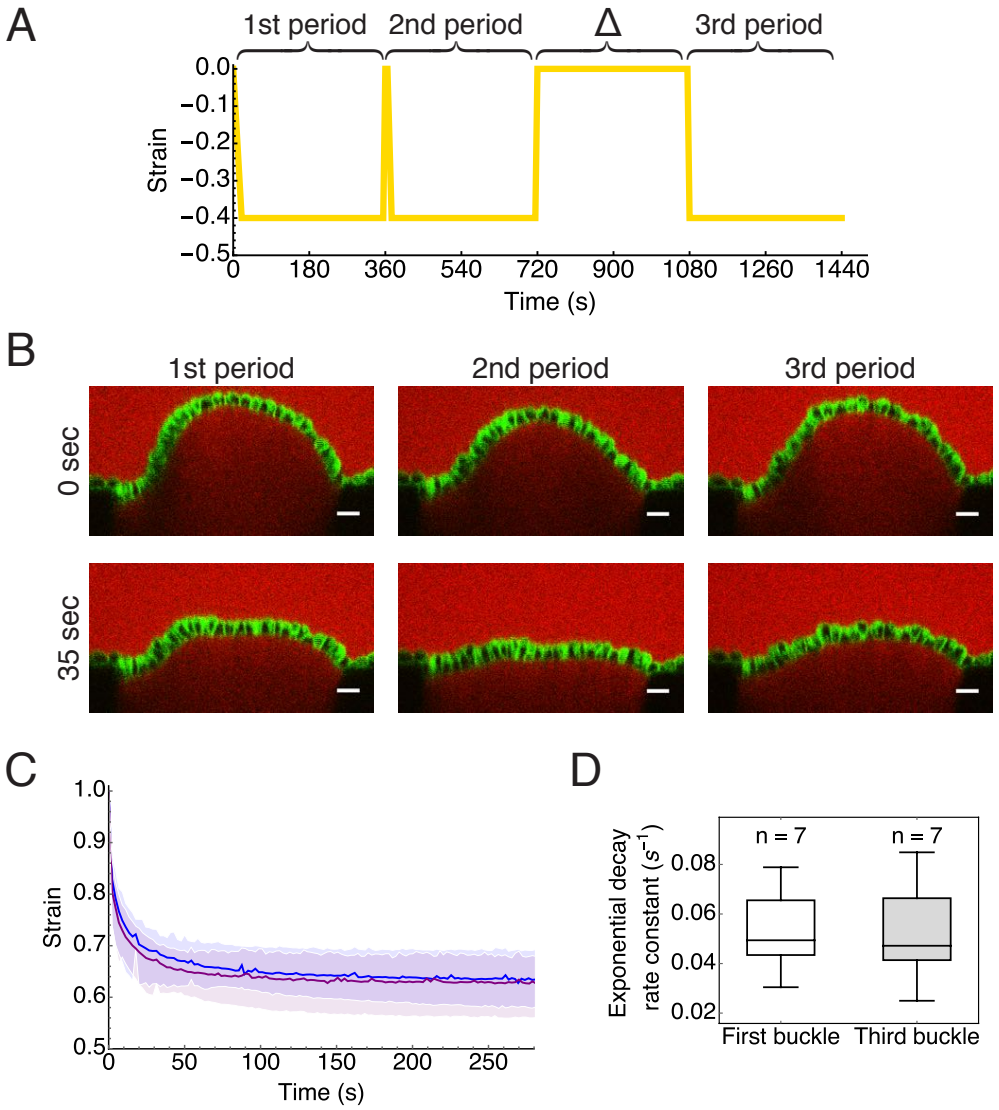

Figure 4.18: Mechanical adaptation to a shorter length is reversible. (A) The sequence of strains applied to suspended MDCK monolayers over a 24 minute period. (B) Cross sectional images of the monolayer (green) immediately after application of strain (top) and 35 seconds after the strain (bottom) both for the first compression (left), the second compression (middle) and the third compression (right) (Scale bars: 20 μm) (C) The evolution of the strain in cross sectional contour length of the tissues after the first compression (blue line) and the third compression (purple line). The shaded regions demark the total range in the data. N = 7 monolayers. (D) The initial rate of tissue flattening during the first compressive period and the third compressive period. The horizontal line and top and bottom of boxes represent the median, 75th percentile, and 25th percentile in all box plots, respectively. The whiskers demark the range.

and in the period following a 6 minute adaption (third period of compression) (Fig. 4.18D).

To determine the time required for this adaption to take place, the final period of 0% strain (Fig. 4.18A, 'Δ') was maintained for different lengths of time. Since 6 minutes was clearly enough time for the tissue to return to its initial state, smaller adaptation times of Δ = 30, 60 and 180 seconds were tested. The initial rate of flattening was measured during the first and third periods of compressions as before (section 4.5) and the ratio of the third rate to the first rate was calculated to show the degree to which the mechanical state of the tissue had returned to its initial state (Fig. 4.18E). For $\Delta = 180$ seconds the ratio was 1.02 ± 0.12 (mean $\pm$ standard deviation), showing that the tissue returns to its original mechanical state after 180 seconds at 0% strain. However, for $\Delta = 30$ and 60 seconds, the ratio was 1.71 ± 0.58 and 1.95 ± 0.48, respectively, showing that the flattening rate was still significantly faster during the third period of compression compared with the first ($p = 0.035$ and $p = 0.003$, respectively, Student's t-test). Therefore, the tissue returns to the original mechanical state when the tissue length is returned to the initial value for approximately 2-3 minutes (Fig. 4.18E).

4.10 Autonomous tissue flattening and mechanical adaptation does not require signalling via stretch activated ion channels

The process of autonomous tissue flattening after compression, described here, as well as the subsequent mechanical adaptation, may be an automatic result of the mechanical properties of the tissue. Upon tissue compression, the resting tension of the tissue (measured by others in the Charras lab, data not shown) is no longer resisted by the coverslip boundaries and could therefore act to automatically direct tissue flattening. At the same time, the arrangement of membrane and adherent molecules at cell-cell junctions may lead to automatic junction growth when it is permitted by the boundary conditions. The ubiquitous

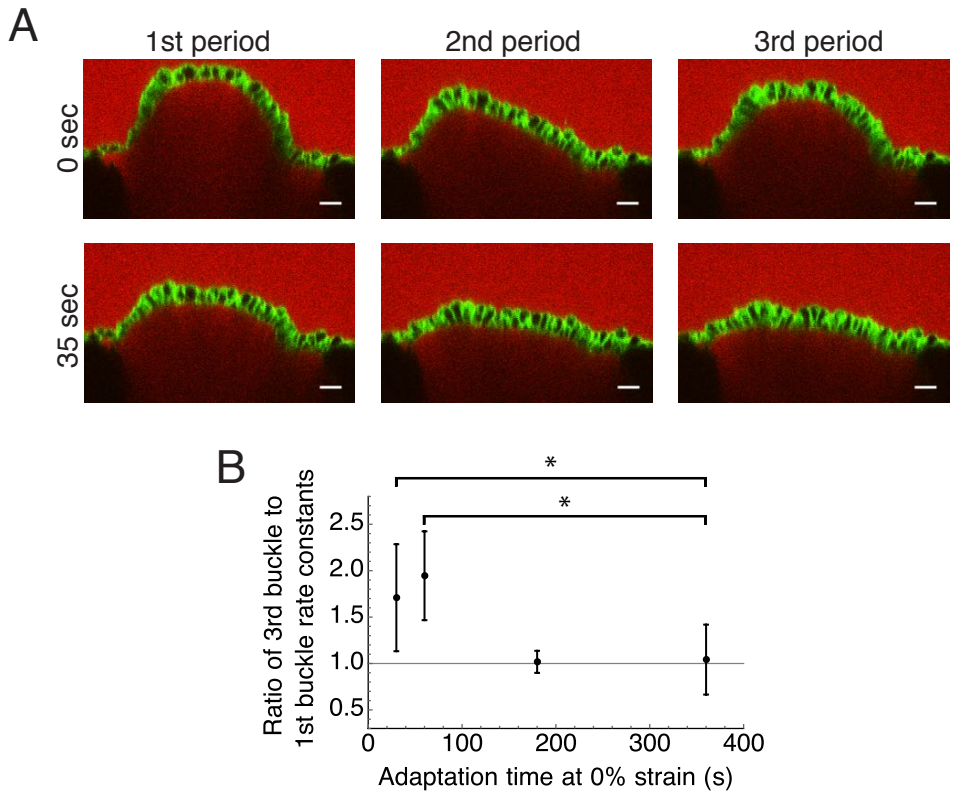

Figure 4.19: Readaptation to the original mechanical state occurs over several minutes. (A) Cross sectional images of the monolayer (green) immediately after application of strain (top) and 35 seconds after the strain (bottom) both for the first compression (left), the second compression (middle) and the third compression (right) for Δ = 30 seconds. (Scale bars: 20 µm). (B) The ratios between the initial rate of flattening in the first and third compressive periods, for a range of different adaptation times Δ. The points demark the means, the error bars demark mean $\pm$ standard deviation.

and continuous turnover and redistribution of molecular structures in the cytoskeleton, cell-cell junctions and plasma membrane could all contribute to the further mechanical adaptation which was measured upon repeated cycles of strain. In this scenario, there is no specific requirement for mechanotransduction to explain the observed behaviour. That is, it is not required that information about the mechanical environment is converted into a chemical signal which then initiates a cascade of signalling that directs adaptation of the cell.

Alternatively, the observed behaviour may be a response which is triggered by the detection of compression via a dedicated mechanotransduction pathway. The compression

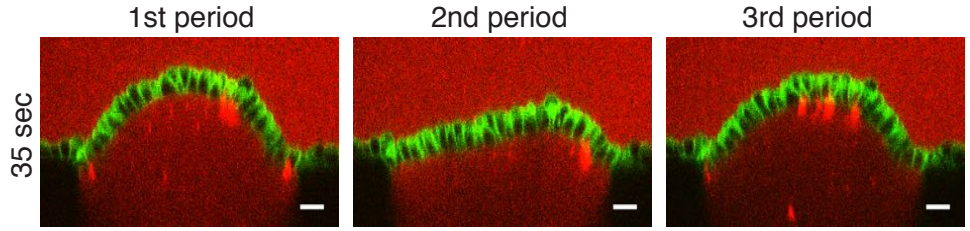

Figure 4.20: Epithelial adaptive response to compression does not require stretch activated ion channels. Cross sectional images of the monolayer (green) treated with $100\,\mathrm{mM}$ Gd^{3+} 30 minutes prior to compression. Images show the tissue 35 seconds after the application of strain both for the first compression (left), the second compression (middle) and the third compression (right) for Δ = 360 seconds. (Scale bars: $20\,\mu\mathrm{m}$)

may cause, for instance, a change in membrane or cytoskeletal tension which leads to the opening of an ion channel or the unfolding of a protein, which then triggers a response mediated via biochemical signalling cascades that direct cell behaviour.

The onset of tissue flattening after compression effectively appeared to be instantaneous, since the tissue contour length was, on average, reduced by an average of 15% within the first 2 seconds after compression (Fig. 4.9). While this indicates that constitutive tissue tension may automatically drive tissue flattening (the first scenario described above), it is hard to rule out a role for biochemical signalling due to the plethora of pathways which could contribute. As a first step towards this, however, suspended epithelia were treated for 30 minutes with $100\,\mathrm{mM}$ gadolinium III chloride (Gd^{3+}), which is known to inhibit stretch activated ion channels and blocks cell extrusion induced by compression in MDCK monolayers [84]. This had no detectable effect on the response of the tissues to compression. The suspended epithelia flattened after buckling just as before (Fig. 4.20 left) and the rate of flattening increased (Fig. 4.20 middle) and decreased (Fig. 4.20 right) as the tissue adapted to different lengths.

4.11 Discussion

A material subjected to compression may deform, buckle and fracture. Much effort is spent by engineers to ensure that manmade structures of all kinds can endure compression

while continuing to function as required. Epithelial tissues likewise experience compression with widely varying characteristics during developmental morphogenesis, as well as during a multitude of everyday processes in adult life. While a great deal of research has focussed on the specific morphogenetic pathways which govern the generation of spatially and temporally regulated patterns of force, the default, developmentally 'nonprogrammed' response of an epithelium to deformation is just as important in determining a tissue's final form. Here, therefore, this was studied by applying a simple uniaxial compression to a developmentally inactive epithelium and studying the response.

A majority of tissues *in vivo* are mechanically connected to surrounding structures such as neighbouring tissues or the extracellular matrix. Under these circumstances, the mechanical properties of one structure may dominate over another when deformation is applied to dictate the final shape, obscuring the separate contributions of individual tissues. To circumvent this, a novel model system is utilised in which epithelia are generated which are devoid of a substrate. This allows the tissue to be studied in relative isolation, specifically revealing the autonomous response of the tissue with greater clarity.

The immediate result of planar uniaxial compression applied to suspended MDCK monolayers was found to depend strongly on strain rate. At relatively slow rates of 0.5%/s, epithelia accommodated strains of up to 40% without buckling (Fig. 4.4A and B), whereas when a 40% strain was applied at a much higher rate (>100%/s), buckles of various shapes were formed (Fig. 4.8). Remarkably, however, the buckles which formed where not static structures. Instead, the tissues actively and autonomously flattened themselves in a matter of minutes (Fig. 4.9). Importantly, this phenomenon was not unique to MDCK cells, since the same behaviour was observed in cultured HaCaT tissues (Fig. 4.12B and C), despite their significantly different structure (Fig. 4.12A).

As with many processes which involve cell shape change in eukaryotes, tissue self-flattening relies on forces produced by the actomyosin cytoskeleton, since tissues treated with blebbistatin, Y27632 (Fig. 4.13) or latrunculin B (Fig. 4.14) were unable to flatten

and instead remained buckled. The constitutive tissue tension, measured by others in the Charras lab (data not shown), was also abolished by these drug treatments. This molecular underpinning of tissue self-flattening was further supported by the observed concordance between polarised myosin localisation and an asymmetry in the dynamics of buckling and flattening. Both NMHCIIA–GFP and NMHCIIB–GFP localised to the base of cells when expressed in suspended MDCK monolayers (Fig. 4.16), as well as to cell-cell junctions, indicating that the basal side may be more contractile than the apical. As would be predicted if this mechanical asymmetry was significant, the overwhelming majority of tissues buckled towards the apical direction (Fig. 4.8). Furthermore, when more complex shapes of buckles were produced, sections of tissue in which curvature was oriented basally changed shape with faster dynamics than sections with apically oriented curvature (Fig. 4.15).

Ultimately there is a limit to the size of buckle which tissue self-flattening can erase - the residual buckles induced by a constant 60% compressive strain remained buckled for over 10 minutes (after an initial period of reduction in contour length) (Fig. 4.4C). Interestingly, the strain at which stable buckles formed appears to coincide with the strain at which constitutive tension falls to zero (as measured by others in the Charras lab, data not shown), further supporting a causal link between the tissue scale constitutive tension and tissue self-flattening. The limit to self-flattening is perhaps not so surprising considering the substantial change in cell shape that is required in order for compressed tissues to flatten. In the short time that tissues took to flatten after a rapid 40% compression, the height of cells and their junctions increased and the length along the axis of compression decreased so that, overall, cells transitioned from an initial roughly isotropic shape to a considerably anisotropic shape (Fig. 4.6). Simple geometric considerations show that this implies an approximately 25% increase in the total surface area of each cell. In addition, cell nuclei which are stiffer and so require more energy to deform underwent an equivalent change in overall shape (Fig. 4.7). It will be important, however, to ascertain whether or not rotation of nuclei may account for any part of this apparent change in shape.

Overall, these remarkably coordinated changes in tissue structure were accompanied by a measurable change in the mechanical properties of the cell-sheet. This was revealed by comparing the speed of tissue flattening after the initial compression (which was maintained for 6 minutes) to the speed once the compression was released and immediately re-applied (Fig. 4.17A). Tissue self-flattening was considerably faster during the second period of compression (Fig. 4.17B and C), indicating that adaptation to the new shorter length during the first period leads to less resistance in returning to the flat shape a second time.

Importantly, this change in tissue mechanical properties induced by a 6 minute period of 40% compression, was not permanent but could be reversed simply by returning the tissue to the initial length for more than a minute (Fig. 4.18). In identifying the approximate timescale of this re-adaptation process (1 to 3 minutes, Fig. 4.19B), the set of possible molecular processes which may be involved is narrowed. While turnover rates of different cell constituents can vary over orders of magnitude depending on the context [93, 282, 283], a timescale of several minutes does not preclude a role for cytoskeletal turnover, turnover of adherens junctions and possibly membrane trafficking. In future work the relative contributions of these processes should be investigated.

Altogether, the conceptual framework which has emerged is one in which a constitutive actomyosin driven tension guides the reshaping of cells, their junctions and nuclei such that global tissue curvature and surface area are minimised. This global tissue tension, however, can only drive shape change up to a point. As this limiting deformation is reached, a balance has in some way been achieved in the tissue such that it makes no further active shape changes and tissue tension tends to zero. Further compressive strain beyond this point therefore forces tissue buckling which is not immediately flattened.

It will now be important to explore where this framework can be applied to inform our understanding of morphogenetic processes involving epithelia. An analogous actomyosin driven constitutive tension is indeed present in a wide range of morphogenetically ac-

tive epithelia [284], perhaps shown most clearly in laser cutting experiments [285, 286]. In medaka fish embryos this constitutive tension is governed by YAP and without it the embryos sag under the influence of gravity and tissues misalign [111]. The experiments presented here support the idea that constitutive tension can help to maintain a defined structure, erasing irregularities if they form.

While it is difficult to know how general this behaviour will be throughout animal epithelia, the counter-examples may be particularly informative. Indeed, the reverse processes of epithelial self-buckling (i.e. invagination or tissue folding) are crucial in gastrulation [72], neurulation [287], leg [86] and eye morphogenesis [288] and many other morphogenetic processes and are likewise driven by the same actomyosin-based machinery. A tissue which can spontaneously unbuckle itself is therefore often the last thing which is called for. More generally speaking, tissues bent on erasing curvature are not useful when building structures requiring detailed shape.

For this reason, in the future it will be particularly interesting to attempt to identify exactly what it is that causes the transition between planar deformation and tissue buckling at the point of $\sim$40% compression (Fig. 4.4B). Is it that the constituent cells have reached, in some sense, a 'preferred shape'? If that is the case can a single parameter be isolated which is being regulated, such as cell height, width, total surface area, planar surface area or junctional perimeter? Can this preferred shape be understood in terms of a balance between adhesion and tension, as it is in the model proposed by Hannezo *et al.* [289] or perhaps it is instead dictated by nuclear packing restrictions? On the other hand, the transition point may be caused by a maximum *change* in shape rather than an absolute value. For instance the limiting factor may be the maximum increase in cell surface area which can be accommodated by membrane unfolding [97] or the maximum change in density of components which can be tolerated. Any model which attempts to address this must also show that global tissue tension disappears at the point of transition. Ultimately, clarifying the role of geometric factors in causing the transition to a state where self-flattening is

inhibited may help explain the decades old observation that in many instances epithelial cells undergo a squamous-to-columnar transition (just as they did here) before commencing invagination [57, 287].

While defining the geometric parameters which characterise the transition point will be informative, it is also clear that the preferred geometry of an epithelial cell can be directly controlled through genetic regulation. In the *Drosophila* wing disc epithelium, for instance, signalling via the morphogen Decapentaplegic initiates a cell-autonomous cuboidal-to-columnar shape transition [290] via Rho1. Therefore, a particularly exciting future use for this system may be to explore the genetically governed mechanisms which define the target shapes of cells and tissues.

Chapter 5

Tissue strain reorients cell divisions via changes in cell shape and not through tissue stress

5.1 Introduction

In contrast to chapter 4, where the short timescale response of epithelia to compressive strain was studied, in this chapter the focus is on a longer timescale response to tissue stretch. As discussed previously, epithelia are subjected to stretch in a great number of scenarios during development and adult life (see section 1.2.1) and therefore their ability to function normally during such deformation is crucial. To this end, epithelial tissues assemble a highly integrated network of cell-to-cell adhesive and cytoskeletal structures in order to create a sturdy mechanical syncitium [26, 291], thereby helping epithelia to maintain a faithful barrier which is robust in the face of deformation. On top of this, epithelia display a repertoire of mechanisms which act in response to stretch to further protect the tissue against damage or malfunction. At short timescales of seconds and minutes, this can involve reorganisations of the cell plasma membrane [88, 96–98] and actin cytoskele-

ton [105, 106, 257, 258].

At longer timescales, of minutes and hours, a host of alternative mechanisms at the cellular level may contribute to stress relaxation, including cell-cell neighbour exchange, cell extrusion and cell division (see section 1.2.2). These processes have the common feature that they reorganise or redistribute cellular material at the length scale of cells and so may affect tissue shape and the distribution of stress. In particular, both the rate and orientation of cell division have been proposed to be responsive to tissue stress and strain [51, 117, 148, 154]. It is the effect of tissue stretch on division orientation which is the focus of this chapter.

Both cell shape and tissue stress are expected to be altered by tissue uniaxial extension. Indeed both parameters have been shown to influence the orientation of cell divisions [129, 167, 220, 221]. Divisions oriented with cell shape, in which the cytokinetic ring bisects the long axis of the cell, have been reported in a variety of systems and so shape-oriented cell division is considered a widely accepted rule (sometimes known as "Hertwig's rule"). In the large cells of early embryos, the mechanisms involved have been studied and models such as those based on cytoplasmic-generated forces acting on astral microtubules have emerged [167] (see section 1.4.2).

In single cells, however, a role for forces in orienting cell division has been uncovered [221]. This suggests that cell shape is not the sole governing parameter. The relative importance of cell shape and stress is difficult to separate in the mechanically complex environment of a tissue, because the natural effect of tissue stress is to elongate the constituent cells causing the stress field and cell shape to align. This section addresses this problem by taking advantage of the suspended monolayer system to overcome these difficulties. Initial experiments showed that a constant 30% uniaxial stretch was found to cause an alignment of cell divisions to the axis of tissue stretch. Tissue-scale stress measurements and cell-scale laser ablations were used to show that stress and cell shape are not always aligned in suspended monolayers. This allowed the relative contributions to

be decoupled. In such cases of shape and stress misalignment, cell divisions were found to orient preferentially with cell shape, showing that the influence of shape dominates over that of stress. Cell shape oriented division was found to require myosin activity, since orientation to cell shape was perturbed in tissues treated with Y27632. Finally, cell divisions were also found to become globally oriented in response to tissue compression (applied as in section 4). Again division orientation appeared to be determined by cell shape rather than a stress signal, demonstrating that the phenomenon is not particular to stretch.

5.2 Methods

5.2.1 Live imaging of cell divisions

The live imaging system described in section 2.5 was used to image cell divisions in suspended epithelial monolayers. After collagenase treatment (section 2.4), monolayers were incubated for one hour at 37 °C and 5% CO in imaging media (section 2.5) or stretched by 30% (section 2.6). After a period of incubation, an area of the suspended monolayer was imaged every 5 minutes for 2.5 hours. A motorised stage allowed the acquisition of a large area of the tissue via montaging. Approximately 25 slices of thickness 1 µm were acquired. The videos were processed as described in section 3.3. During data analysis, a division was not used if a neighbouring cell divided with overlap in time because of the complex interactions of forces and shapes between the neighbouring divisions..

5.2.2 Determining the direction of division

The orientation of division was measured for each imaged division. At the end of furrow ingression, in the time point where the new junction between the daughter cells is first apparent, a straight line was drawn along the junction in FIJI [261]. The angle of this line was measured and the division orientation defined as the angle perpendicular to this angle. Angles were measured relative to the horizontal which corresponded to the direction of

stretch. Angles therefore lie in a range of -90° to 90°.

5.2.3 Determining cell shape orientation

Cell shapes were measured from the E-cadherin–GFP signal at cell junctions. This signal was segmented using the Tissue Analyzer, v2.0 plugin in FIJI [245] or by hand using the polygon tool in FIJI [261]. To define a measure of the aspect ratio of the irregular cell shape, the best fit ellipse of the output of the segmentation was calculated. The aspect ratio was then defined as the ratio of the major to minor axis lengths.

For the measurement of interphase cell shape, the time point 5 minutes before the first signs cell rounding was chosen. This was found to occur ∼35 minutes before the initiation of furrow ingression. Cell rounding was rapid, usually completing within 10 minutes, so this time point was clearly defined. For the rounded cell, shape was measured 10 minutes before furrow ingression, since anaphase elongation which occurred 5 minutes before furrow ingression affected cell shape significantly.

5.2.4 Laser perturbation

Monolayers expressing E-cadherin–GFP (to visualise cell shape changes) were prepared and stretched precisely as described in previous experiments. The scanning laser confocal set-up described in section 2.5 was used. Monolayers were incubated with Hoechst 34332 ($5\,\mu g/ml$; Merck-Biosciences) for 10 minutes before laser perturbation to allow identification of individual cell nuclei. Interphase cells with a significant long axis (aspect ratio >1.4) were chosen such that there were similar numbers with the long axis oriented approximately with the direction of stretch as there were with the long axis oriented approximately orthogonal to the direction of stretch. A confocal stack of the E-cadherin signal was acquired and then a small region of the nucleus of the chosen cell was exposed to a pulsed 405-nm laser (PicoQuant) and a 405-nm laser (Olympus) for 30 seconds. This was found to induce movement (‘recoil’) in the surrounding tissue. A second confocal stack

was therefore acquired 5 minutes later in order to measure this shape change. This time interval was chosen as it was the characteristic time over which a significant recoil was observable.

5.2.5 Determining the direction of recoil after laser perturbation

In order to ascertain the principal direction of recoil after laser perturbation, a custom script was written in Mathematica (Wolfram Research) which applied stretch transformations to the initial image of the perturbed region in order to find which transformation best matched the change observed in experiments. First, a confocal slice was chosen from both the confocal stack obtained before laser perturbation and that taken 5 minutes after perturbation. The slices corresponded to each other as closely as possible in regard to location through the thickness of the tissue. The outline of the patch of tissue which included the chosen cell and its neighbours was manually segmented in FIJI (Fig. 5.1A) and converted into binary mask A (before perturbation) and binary mask B (after perturbation). The masks were translated so that the centroid of each mask was at the centre of each image. The shape change associated with the mechanical recoil after perturbation was modelled as a stretch of scale factor m along axis x' and scale factor n along axis y', where the axes x' and y' made an angle θ with the direction of stretch (Fig. 5.1B, bottom left). Therefore, overall the transformation $T(\theta, m, n)$ was applied to the mask which was formed of a rotation transform $R(\theta)$ given by:

$$R(\theta) = \begin{pmatrix} \cos(\theta) & \sin(\theta) \\ -\sin(\theta) & \cos(\theta) \end{pmatrix},$$

combined with a stretch transformation $S(m, n)$ given by:

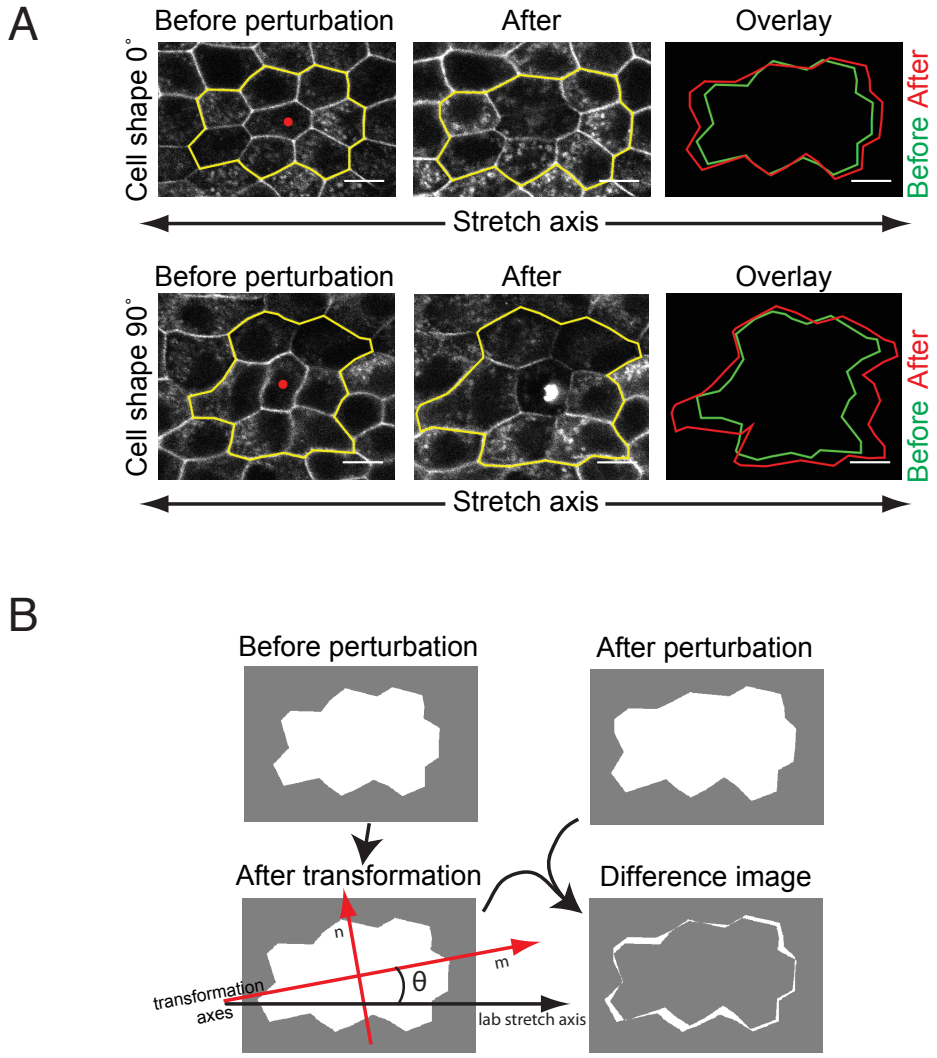

Figure 5.1: Determining the direction of recoil after laser perturbation. (A) The outline of the cell in question (red dots) along with its nearest neighbours was traced manually (yellow outline). (B) The outlines were converted into binary image masks and transformations (stretches of different magnitudes at varying angles) were applied to these masks (bottom left). The transformed masks were then compared to the masks of images taken after laser perturbation (top right). The closeness of the fit was quantified via computation of a difference image (bottom right). (Scale bars: 10 µm)

$$S(m,n) = \begin{pmatrix} m & 0 \\ 0 & n \end{pmatrix},$$

in the combination:

$$T(\theta,m,n) = R(\theta)S(m,n)R(-\theta),$$

such that:

$$T(\theta,m,n) = \begin{pmatrix} m\cos^2(\theta) + n\sin^2(\theta) & m\cos(\theta)\sin(\theta) - n\cos(\theta)\sin(\theta) \\ m\cos(\theta)\sin(\theta) - n\cos(\theta)\sin(\theta) & n\cos^2(\theta) + m\sin^2(\theta) \end{pmatrix}.$$

The transformed binary mask A was then compared to mask B by overlaying the two masks and summing the total number of pixels in the overlay which were part of the mask in both images (the central section in the difference image (Fig. 5.1B). This number was then normalised by the number of pixels which were part of the mask in either image. This was systematically repeated over a range of θ, m and n in order to find the transformation which best matched the observed recoil. The value of θ from the highest scoring transformation was then taken to be the principal direction of stress in the monolayer at the location of the perturbed cell, on the condition that m and n were significantly different (i.e. a well defined direction existed as opposed to isotropic expansion) and that transformations with very different θ did not match similarly well.

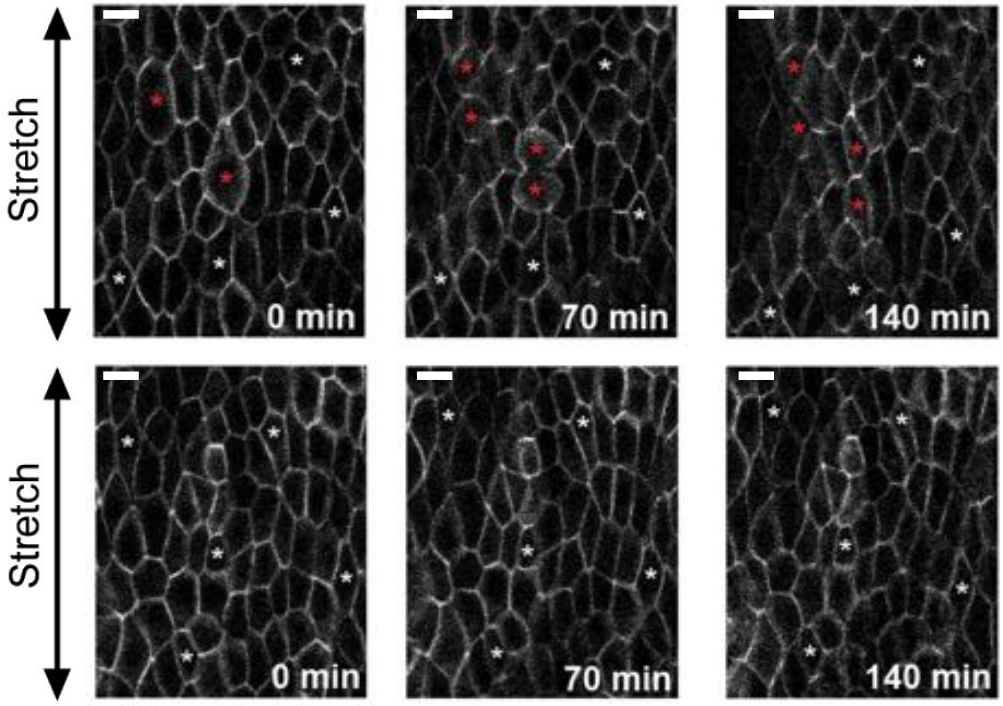

Figure 5.2: No T1s occur in stretched suspended monolayers. Junctions are visualised using E-cadherin–GFP. An area which contained divisions (top) and an area with no divisions (bottom) are shown. Red asterisks show the corresponding dividing cells in sequential time points. White asterisks show corresponding non-dividing cells. (Scale bars: 10 μm)

5.2.6 Immunostains

Immunostaining was used to investigate the presence (or otherwise) of any ECM components which may remain attached to the suspended tissues after collagenase treatment. Such remnant matrix components may exist either due to incomplete action of the collagenase or as a result of collagenase resistant ECM components which may be secreted by the MDCK cells during growth. Monolayers were stained both before and after collagenase treatment. Neither fixation nor permeabilisation were required since only extracellular components were of interest. Monolayers were attached to glass-bottomed Petri dishes with hot glue and washed in PBS. They were then incubated at 37 °C in 5% CO_2 for 30 min with the primary antibody diluted in unsupplemented DMEM (either monoclonal mouse anti-collagen antibody (1:100 dilution; Sigma-Aldrich), polyclonal rabbit anti-fibronectin

antibody (1:200 dilution; Abcam), or polyclonal rabbit anti-laminin (1:25 dilution; Sigma-Aldrich)). Monolayers then were incubated for 30 min with either Alexa Fluor 647 goat anti-mouse (1:100 dilution; Invitrogen) or Alexa Fluor 568 goat anti-rabbit (1:100 dilution; Life Technologies) in DMEM which was supplemented with 10% FCS. Monolayers were then washed in supplemented DMEM and imaged immediately.

5.3 Cell shape in stretched suspended monolayers

Given an imposed constant uniaxial strain of 30%, the cells which make up the tissue are expected to deform by an equal amount and therefore become elongated. However, an alternative is that cells may undergo cell-cell rearrangements via neighbour exchange events which could counteract the effect of tissue strain on cell shape [292]. To investigate whether neighbour exchange events occurred in stretched suspended monolayers, cell junctions were carefully followed during videos of suspended monolayers (Fig. 5.2). No neighbour exchange events were found during these searches (Fig. 5.2) thus indicating that cell-cell rearrangements were either very rare in the tissue or not present at all.

As found in most metazoan epithelial tissues [141], the non-stretched suspended monolayers exhibited a wide variety of interphase cell shapes (Fig. 5.3). The distribution of the aspect ratio of cells peaked at 1.25, with a long tail and a mean of 1.32 (Fig. 5.3B). The orientation of the cell long axis was randomly distributed (Fig. 5.3A). Upon application of a constant 30% stretch, the mean aspect ratio of interphase cells rose to 1.49 and cells became strongly oriented towards the direction of the stretch (Fig. 5.3A and B). Importantly, however, $\sim$5% of cells remained with a significant aspect ratio ($>$1.4) which was oriented $>35^{\circ}$ from the direction of stretch (Fig. 5.3C). This is consistent with a model in which the stretch imposes a uniform deformation to the tissue and the subset of 'misoriented' cells are those which, prior to stretch, had a large aspect ratio which was not aligned with the stretch axis.

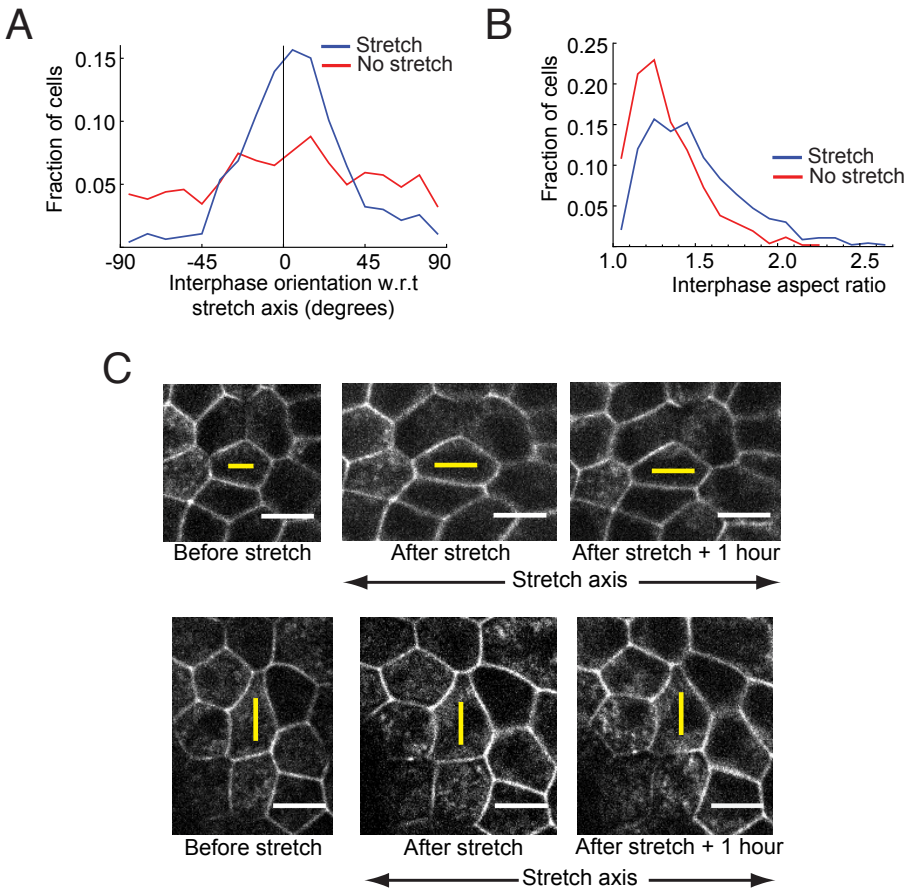

Figure 5.3: Cell shape in non-stretched and stretched suspended monolayers. (A) The orientation of the interphase long cell axis relative to the stretch direction (or relative to the test rods in the non-stretched case), in non-stretched (red) and stretched (blue) monolayers. The orientation of each cell is defined as the orientation of the major axis of the best fit ellipse of the cell shape. (B) The aspect ratio of interphase cells as defined by the ratio of the major and minor axes of the best fit ellipse. (C) Cells in suspended monolayers before and after stretch with cell-cell junctions visualised with E-cadherin–GFP. An example of both a cell which was initially oriented (top) and misoriented (bottom) with the direction of stretch is shown. The yellow bars indicate the orientation of the long cell axis. (Scale bars in white: 10 μm).

5.4 Global and local tissue stress in stretched suspended monolayers

The viscoelastic nature of suspended monolayers was established by Harris *et al.* in [90]. Implementing similar techniques, Andrew Harris demonstrated that despite rapid stress dissipation in the first minutes following a 30% stretch, a residual stress of $\sim 40\,\mathrm{nN/cell}$ was maintained in the suspended monolayers for at least 200 minutes (Fig. 5.4A). While

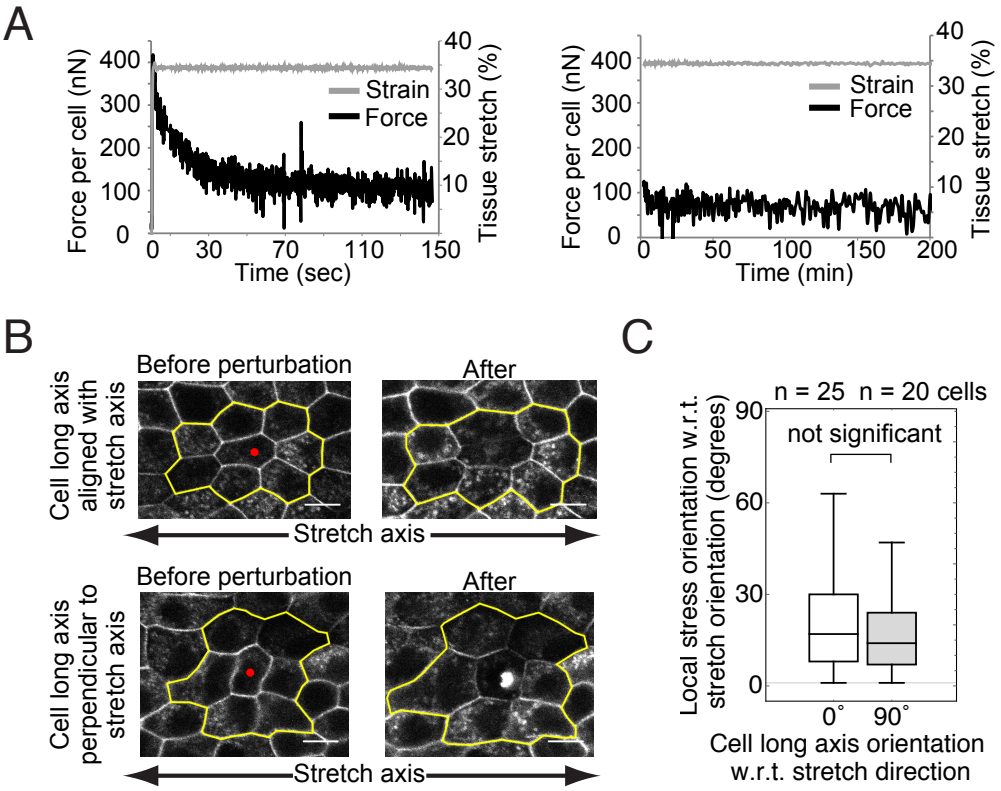

Figure 5.4: Cell stress in stretched monolayers. (A) A plot showing the evolution of stress (black) and strain (grey) in stretched monolayers over short (left) and long (right) timescales. This data was obtained by Andrew Harris. (B) Confocal images of cells in stretched monolayers expressing E-cadherin–GFP. Images show the cells before (left) and 5 minutes after (right) perturbation by a pulsed UV laser. Both a cell with an interphase shape oriented (top) and misoriented (bottom) with the direction of stretch are shown. Red dots indicate the point which was perturbed by the laser. The yellow outline highlights the region containing the perturbed cell and its neighbours. (Scale bars: 10 µm.) (C) A box-whisker plot showing the orientation of the recoil measured after cells were perturbed by a UV laser.

this measurement was important to establish the magnitude of tissue level tension which remained several hours after stretch, this measure could not provide insight into the distribution of stress at the cellular level.

At the cellular scale, the magnitude and orientation of the local stress field could conceivably vary between regions in the tissue or even correlate with cell shape as it does in foams [293]. To test this, the mechanical integrity of cells was perturbed with a pulsed 405 nm laser. This induced a mechanical recoil in the local cell patch that was complete within 5 minutes following perturbation (Fig. 5.4B). By comparing images of the perturbed

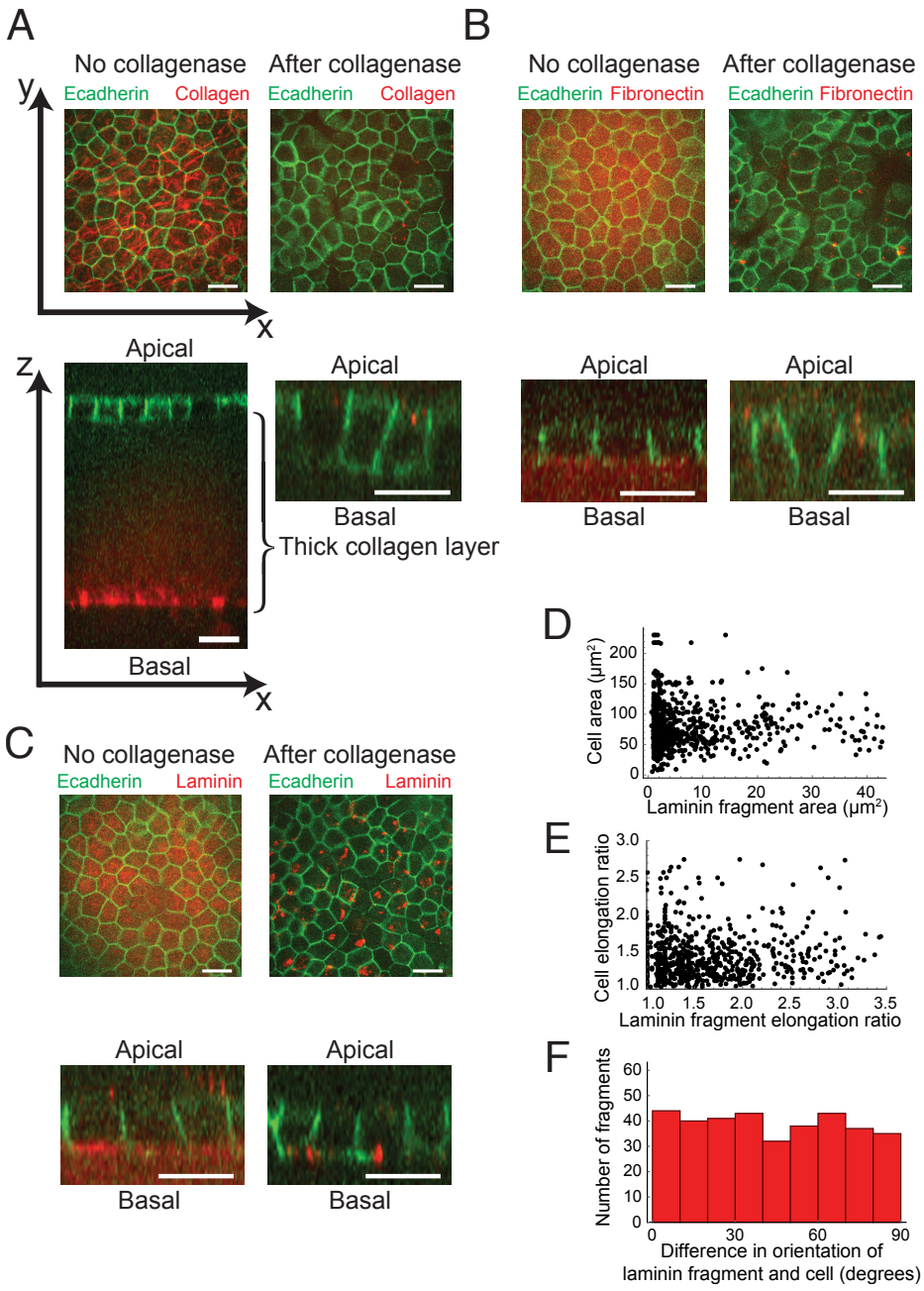

Figure 5.5: No continuous ECM network remains after collagenase treatment. (A-C) X-Y (above) and X-Z (below) projections of monolayers made from MDCK cells expressing E-cadherin–GFP (green) stained for collagen (red; (A)), fibronectin (red; (B)) or laminin (red; (C)), before and after collagenase treatment. Images show a representative example from n = 27 images taken from N = 3 monolayers in each of A,B and C. (Scale bars: 15 μm). (D) Scatter plot showing the area of the laminin fragments found on the basal side of monolayers vs. the area of the cells to which they are attached. Fragments analysed are from n = 6 images taken from N = 3 monolayers. (E) Scatter plot showing the elongation of the laminin fragments found on the basal side of monolayers vs. the elongation of the cells to which they are attached. (F) Histogram showing the difference in orientation of each laminin fragment compared with the cell to which it is attached.

cell and its neighbours before and after the exposure to the laser, the principal direction of recoil was deduced and used as a readout of the local orientation of the stress field (Fig. 5.4B, see methods section 5.2.5). Importantly, the orientation of stress was in this way found to lie close to the direction of stretch in all cases, irrespective of the orientation of cell shape (Fig. 5.4C). Thus, cell shape and local tissue stress were not aligned in the small subpopulation of cells which retained a significant aspect ratio oriented perpendicular to the stretch direction.

Due to the digestion of the collagen substrate, it was likely that the tissue stresses measured here were transmitted solely through the cells themselves via the cortex, membrane, cytoplasm and cell-cell junctions. It is possible, however, that the cells may secrete ECM components during growth of the monolayer and that these may remain after the collagen digestion and bear part of the stress. Given the known role of cell-ECM interactions in orienting cell divisions it was crucial to establish whether or not this might be the case. Therefore, to test for the presence of ECM components, monolayers were stained for collagen, fibronectin and laminin, both before and after collagenase treatment (Fig. 5.5). Reassuringly, the thick collagen scaffold which the cells grew on was detected before the collagenase treatment (Fig. 5.5A). Interestingly, a weak laminin signal at the basal side of the monolayer was also detected (Fig. 5.5C). No corresponding fibronectin signal could be found (Fig. 5.5B). Upon incubation with collagenase, the collagen signal, as expected, disappeared as did the majority of the laminin staining (Fig. 5.5A and C). Small fragments of laminin could be detected but a lack of a continuous laminin network confirmed that the tissue stress was transmitted solely through the cells themselves. It is also worth noting that the shape of the residual laminin fragments did not correlate with the size or orientation of the cells to which they were attached (Fig. 5.5D-F). Therefore, the fragments would not be able to play a role in any cell shape detection mechanism.

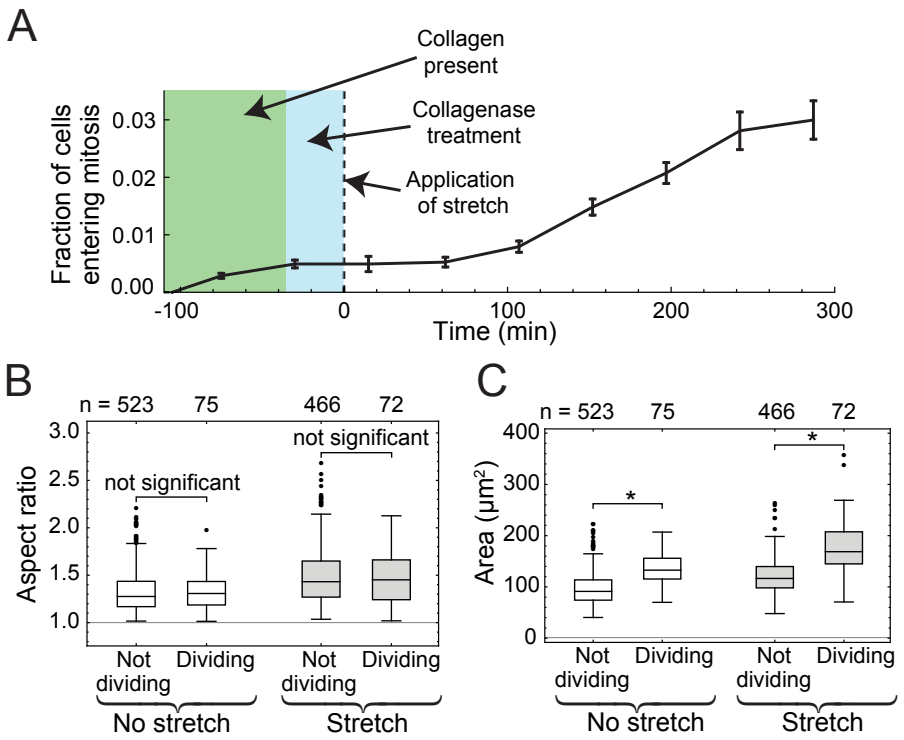

Figure 5.6: Characterisation of divisions which occurred in suspended monolayers. (A) Using STLC, cells were arrested in mitosis and could be identified via their rounded morphology. The cumulative frequency graph shows quantification of the amount of cells entering mitosis based on this method. Errors bars show the SD based on N=5 monolayers. (B) Box whisker plots showing the aspect ratio of cells which divided during the experiment or did not divide, in stretched and non-stretched monolayers. The horizontal line and top and bottom of boxes represent the median, 75th percentile, and 25th percentile in all box plots, respectively. The whiskers demarcate the range, and the dots are outliers. "not significant" indicates that $p > 0.6$. (C) Box whisker plots showing the cell apical area of cells which divided during the experiment or did not divide, in stretched and non-stretched monolayers. * indicates a p-value of $p < 0.01$.

5.5 Characterisation of cell division in suspended monolayers

The rate of entry into mitosis in stretched suspended monolayers was measured by adding 50 μM S-trityl-L-cysteine (STLC) to the media to induce mitotic arrest. Cells which had entered mitosis could then be identified by their rounded morphology and mitotic cell number was then assessed over a 5 hour experiment. This revealed a transient inhibition of mitotic entry directly after collagenase treatment and the application of stretch, consistent with other reports of inhibition of G1/S progression following deformation [294, 295] (Fig.

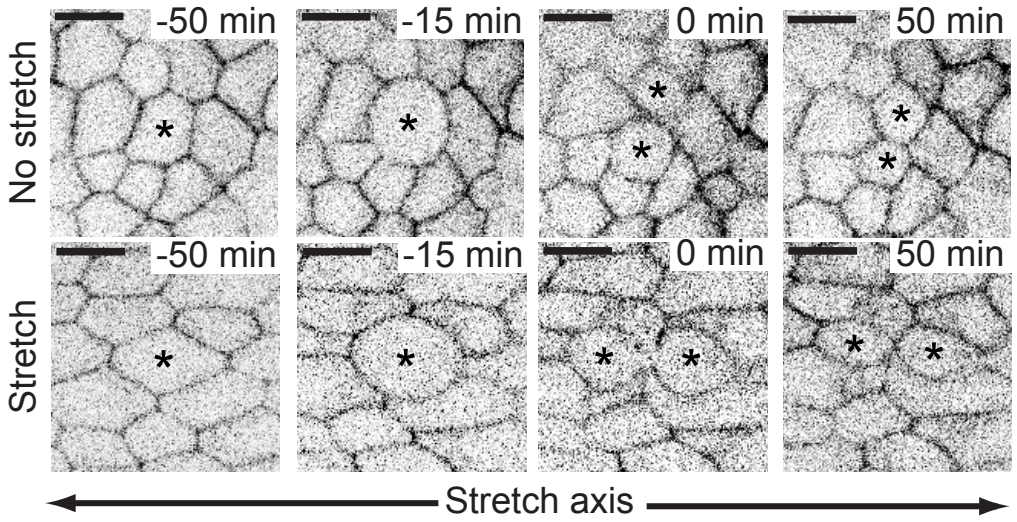

Figure 5.7: An example cell division in a non-stretched suspended monolayer and a stretched suspended monolayer. Cell junctions are visualised using E-cadherin–GFP. Cells are in interphase at -50 minutes, have rounded up by -15 minutes, divide at 0 minutes and the daughters have reintegrated into the monolayer by 50 minutes. (Scale bars: 10 μm)

5.6A). After ∼90 minutes, cells began to enter mitosis again at a rate which appeared similar to the rate before the application of stretch (Fig. 5.6A).

The cells which divided were not the most elongated, so an increase of aspect ratio did not appear to trigger cell cycle progression in these experimental conditions (Fig. 5.6B). The cells which divided, however, tended to be those which had the largest interphase area, suggesting that these were cells which were already in G2 and simply had resumed normal cell cycle progression following a transient arrest (Fig. 5.6C).

Live imaging revealed that cells, both in stretched and non-stretched suspended monolayers, rounded up and divided within the plane of the epithelium, just as is observed in MDCK cells attached to collagen or glass substrates [43] (Fig. 5.7).

5.6 Cell divisions align to cell shape, rather than stress

Next the orientation of divisions in stretched and non-stretched suspended monolayers was measured to assess how this was affected by stretch. Whereas division orientation was

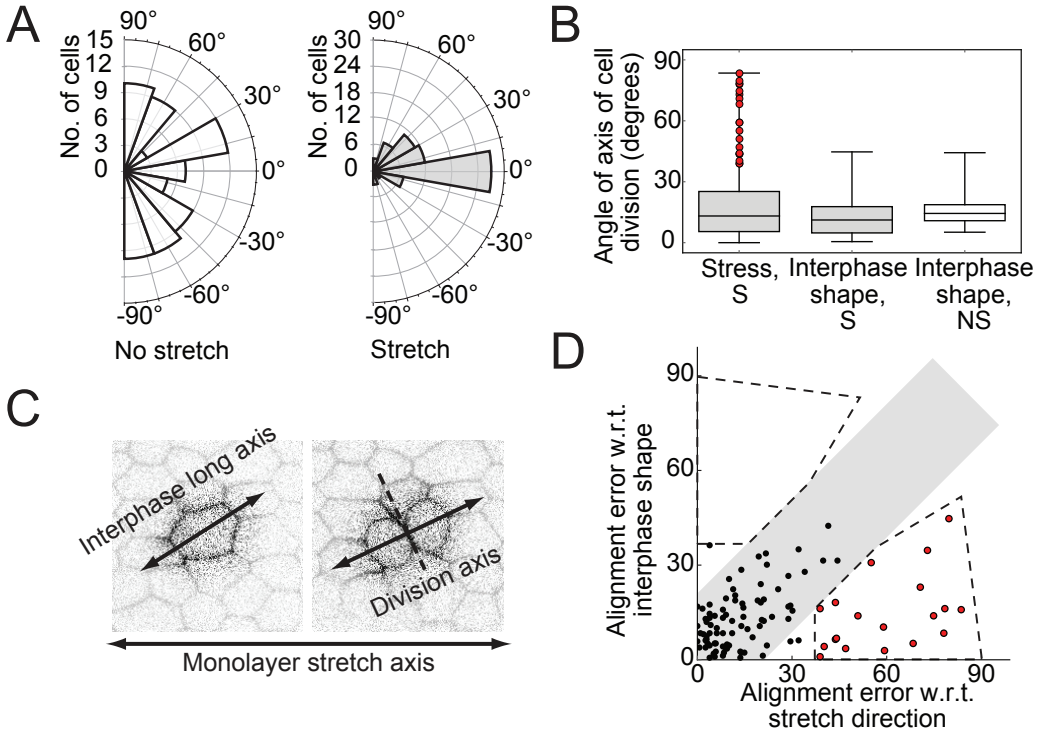

Figure 5.8: Cell divisions align with cell shape in stretched and non-stretched suspended monolayers. (A) Rose plots giving the orientation of cell divisions in non-stretched and stretched suspended monolayers. Orientations given are relative to the direction of stretch (or of the test rods in the non-stretched case). $n \geq 72$ divisions and $N = 3$ monolayers for each condition. (B) Box-whisker plots showing, for elongated cells (r > 1.4), the orientation of division with respect to the axis of stretch (stress, left), to the interphase shape orientation in stretched monolayers (middle), and to the interphase orientation in non-stretched monolayers (right). Red points correspond to cells which also appear in red in E. NS, non-stretched; S, stretched. (C) An example of a cell in a stretched monolayer dividing along the axis of its interphase shape, rather than the stretch direction. (D) Scatter plot showing the error in alignment of divisions with the monolayer stress direction, plotted against the error in alignment with interphase shape orientation. Data points are for elongated (r > 1.4) cells in stretched monolayers. The grey shading delimits the region in which divisions align with monolayer stress and interphase shape equally well. Dotted lines delimit regions where divisions align better with interphase shape than stress, or vice versa.

indistinguishable from a random distribution in non-stretched layers (Fig. 5.8A), divisions in stretched layers were found to globally orient with a strong bias to the direction of stretch (Fig. 5.8A). Indeed, in stretched monolayers, 57% of cell divisions were oriented within 20° of the stretch axis.

While previous studies have suggested a role for both stress and cell shape in orienting cell division [167, 221], decoupling the effects of both within the mechanically complex environment of a living tissue can be challenging, not least due to the fact that cell shape

will usually be deformed by a stress such that the long axis aligns with the local stress field. To address this difficulty here, the division orientation of cells with a significant aspect ratio ($>$1.4) were chosen and their division orientation was compared to both their interphase shape orientation and the orientation of local tissue stress (which, as established in section 5.4, is always aligned with the axis of stretch). See figure 5.8C for a diagram depicting the measurements taken.

Although most divisions aligned equally well to stress and shape in stretched monolayers (since in most cases these two axes were roughly parallel), a significant subset of cells were found to divide with a large angle from the stress axis, as shown by the long tail in the distribution (Fig. 5.8B, red dots). There was, however, no equivalent group of cells which divided far from the shape axis (Fig. 5.8B). The subset of cells which did not divide in the orientation of the stress axis were found to be the subset, described in section 5.3 (Fig. 5.3C, bottom row), which had a long axis which was misoriented with the stress direction, despite the application of stretch (Fig. 5.8C and D, red dots). The conclusion therefore is clear. Cells in stretched monolayers divide in line with the local cell shape, not stress (Fig. 5.8B-D). The global alignment of cell division in response to tissue stretch is therefore regulated by a local signal, cell shape, which happens to have been globally aligned by stretch.

In addition, cells in non-stretched monolayers which happened to have a large aspect ratio aligned their division to their long axis just as well as cells in stretched monolayers (Fig. 5.8B). This further supports the notion that a tissue stress signal is not required for orienting cell divisions in these tissues.

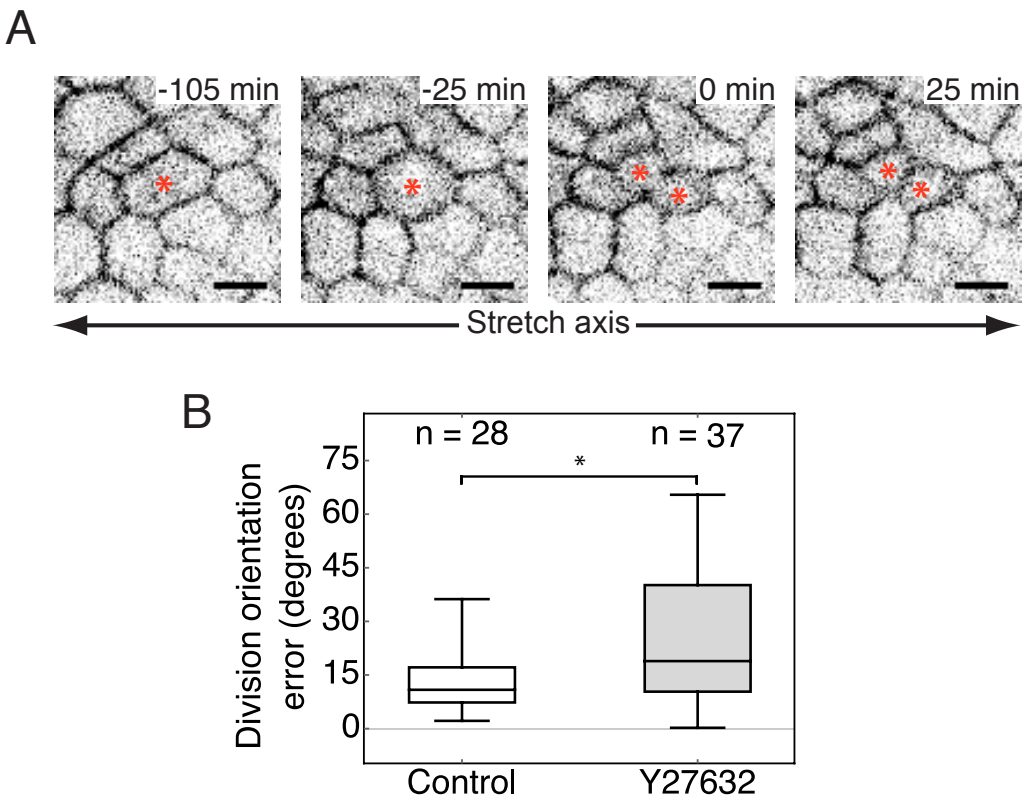

Figure 5.9: Alignment with the cell long axis requires myosin activity. (A) A cell division in a suspended MDCK monolayer stretched by 30% treated with 60 µM Y27632. Cells stably expressing E-cadherin–GFP were used in order to visualise cell junctions (black). Red asterisks mark the dividing cell and its corresponding daughter cells. (Scale bars: 10 µm) (B) Box-whisker plot showing the difference in orientation of the cell interphase long axis orientation and the orientation of cell division, for cells treated with DMSO or 60 µM Y27632. The horizontal line and top and bottom of boxes represent the median, 75th percentile, and 25th percentile in all box plots, respectively. The whiskers demarcate the range. * signifies a significant difference with $p < 0.05$. The number of cell divisions measured is indicated above the plots. $N \geq 3$ monolayers were tested in each case.

5.7 Division orientation with the long axis requires active myosin

A long list of molecular players, many of which were discussed in section 1.4.1, are known to be essential in orchestrating spindle orientation in a range of systems. In many cases the underlying physical mechanisms and molecular pathways through which they are regulated are at least partially understood. A recent study of cell divisions which were found to align to a stretch axis in a zebrafish embryo epithelium, however, found that myosin II

was required for this orientation [51]. While actin is known to be required to anchor the Gαi/LGN/NuMA complex and may act to mechanically resist the pulling forces which are required to move the spindle [187], the role that myosin could play in this process is less clear and remains unknown.

As a first step towards investigating this question, the effect of myosin II activity inhibition on division orientation was tested in stretched suspended monolayers. In the zebrafish experiments of Campinho *et al.* [51], inhibition of myosin activity also caused a reduction in the average aspect ratio of cells, leaving open the possibility that myosin may play an indirect role via its control of cell shape. In stretched suspended monolayers, however, cell shape is globally imposed by the applied strain and so cannot be altered by myosin activity. In this case, the effect of myosin II activity inhibited via treatment of the monolayers with $60\,\mu\mathrm{M}$ Y27632 was the same - division orientation to the cell long axis was significantly perturbed (Fig. 5.9A and B). It will be important to investigate this finding further in order to clarify why myosin is required. A key next step will be to assess the role which myosin II inhibition has on the dynamics of spindle movements.

5.8 Cell divisions align to the cell long axis in compressed monolayers

The results presented up to now in this chapter have demonstrated that uniaxial tissue stretch causes global alignment of cell division simply by deforming cell shape such that cell long axes are globally aligned in the stretch direction. Within this framework, a uniaxial compressive strain may also be expected to cause cell division alignment via the effect it has on cell shape. Indeed, as shown in figure 4.6, a uniaxial compressive strain of 30% produces cells with long axes globally aligned - not to the axis of compression but to the axis perpendicular to the direction of compression.

As before, live imaging was used to follow cells as they progressed through mitosis,

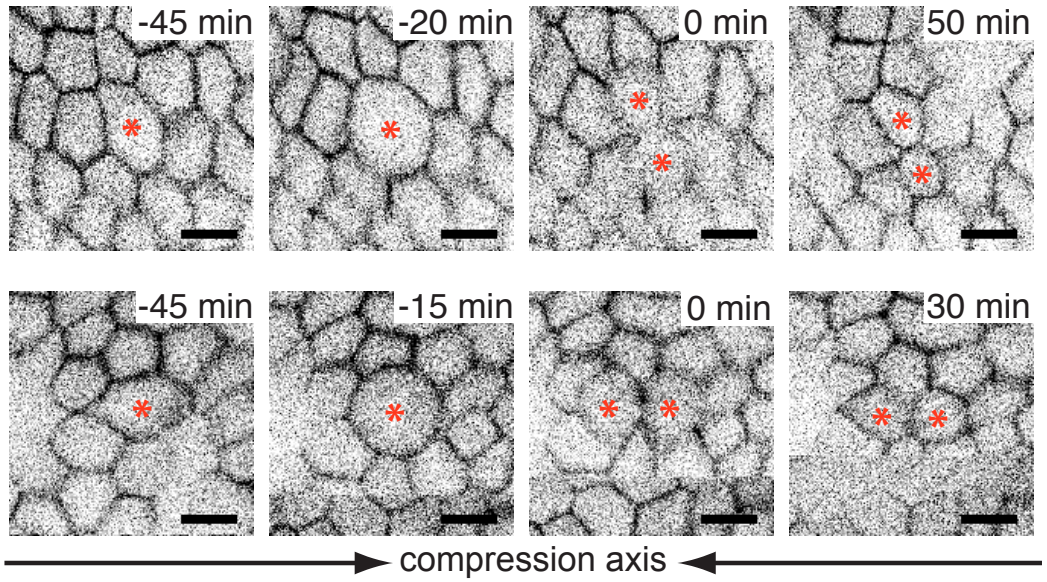

Figure 5.10: Example cell divisions in compressed suspended monolayers. Two examples of cell division in a suspended MDCK monolayer compressed by 30%. In the top row the cell initially has a shape oriented perpendicular to the direction of compression. In the bottom row the cell initially has a shape oriented parallel to the direction of compression. Cells stably expressing E-cadherin–GFP were used in order to visualise cell junctions (black). Red asterisks mark the dividing cell and its corresponding daughter cells. (Scale bars: 10 μm)

now in tissues deformed by a 30% uniaxial compressive strain (Fig. 5.10). Despite the increase in cell height accompanying compression (Fig. 4.6C), which caused the true cell long axis to lie in the apical to basal direction, cells continued to divide oriented within the plane of the monolayer (Fig. 5.10). Overall, as predicted by the results discussed thus far, cell divisions were strongly biased towards the axis perpendicular to the axis of compression (Fig. 5.11A). That is, ignoring the cell shape in the z-dimension, cell divisions globally aligned to the most frequent direction of the cell shape long axis in the xy plane.

To assess whether cell shape was really the parameter which locally controlled orientation, the alignment of division orientation to the interphase cell shape long axis was compared with the alignment of division to an experimental axis. Previously the experimental axis chosen for comparison was the axis of uniaxial strain, since this was known to coincide with the stress axis. Here, however, divisions aligned with the axis perpendicular to the axis of strain (the y axis), therefore this is the axis against which alignment was

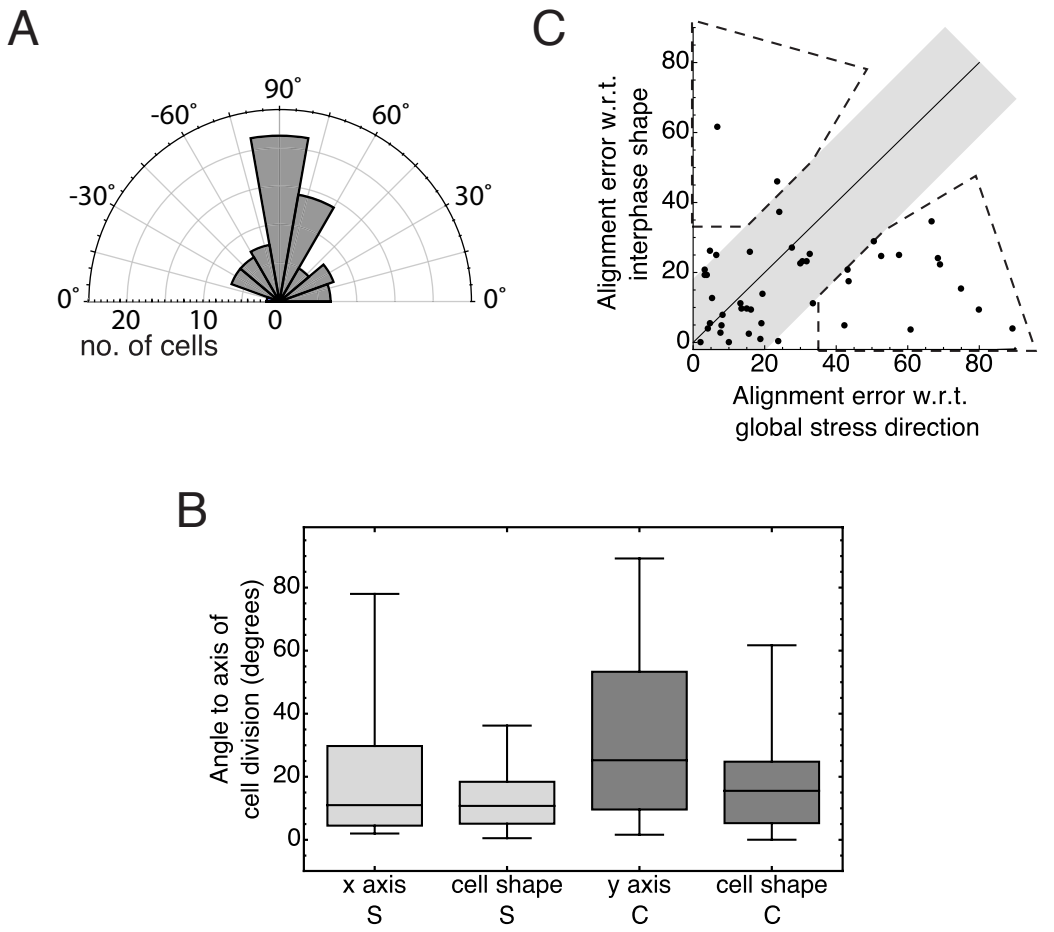

Figure 5.11: Cell divisions orient to the cell long axis in compressed epithelia. (A) Rose plot giving the orientation of cell divisions in compressed suspended monolayers. Orientations given are relative to the direction of compression. $n = 93$ divisions and $N = 4$ monolayers. (B) Box-whisker plots showing, for elongated cells (r > 1.4), the orientation of division with respect to the axis of stretch (x axis) in a 30% stretched monolayer (left), to the interphase cell shape axis in stretched monolayers (middle left), to the axis perpendicular to the compression axis (y axis) in compressed monolayers (middle right) and to the interphase cell shape axis in compressed monolayers (right). S, stretched; C, compressed. n $\geq$ 43 cells. (C) Scatter plot showing the error in alignment of divisions with the axis perpendicular to the compression axis, plotted against the error in alignment with interphase shape orientation. Data points are for elongated (r > 1.4) cells in compressed monolayers. The grey shading delimits the region in which divisions align with y axis and interphase shape equally well (or equally badly). Dotted lines delimit regions where divisions align better with interphase shape than the y axis, or vice versa.

tested. These measurements clearly showed, just as in the case of tissue stretch, that in the small subpopulation of cells with shape misaligned to the y axis, the divisions oriented with cell shape and not with the y axis (Fig. 5.11B and C).

It is worth noting that while compressed tissues were shown to be in a state of low global stress at short timescales (shown by other members of the Charras lab, data not shown), the long timescale behaviour of tissue stress under these conditions remains unknown.

Chapter 6

Epithelial cell shape homeostasis and cell mass redistribution via oriented cell division

The work presented in this study was carried out in collaboration with Maxine Lam. I obtained the experimental data. Measurements and analysis of cell shape was carried out by both Maxine Lam and me. I have written the text and generated the plots.

6.1 Introduction

As described in the introduction of this thesis, oriented cell division has been demonstrated to influence a wide variety of morphogenetic and homeostatic epithelial processes. Indeed, cell division broadly determines cell packing distributions in epithelia [141] and oriented divisions have been shown to relieve tissue stress during epiboly in zebrafish embryos [51] and can contribute to anisotropic tissue growth in a variety of systems [147–149]. How-

ever, isolating the precise contribution of oriented cell divisions to morphogenetic processes in these *in vivo* systems is challenging. A major problem is that a number of processes, such as oriented division, neighbour exchange and cell extrusion, typically occur in parallel. Long range mechanical coupling throughout developing embryos [87] can further complicate interpretation by causing one section of a tissue to be influenced by morphological events in tissues which are not necessarily close. On top of this, developmental patterning of gene expression can regulate complex and specific cell behaviours [80] which can be difficult to separate from generic behaviours resulting from cell mechanical properties.

Therefore, the oriented divisions which were studied in the previous chapter, which occurred in the highly simplified environment of a suspended monolayer, provide an ideal system in which to examine the effects of individual oriented divisions on tissue shape and organisation, in relative isolation. Developmental patterning, mechanical coupling between neighbouring tissues and parallel processes such as neighbour exchange are all absent in suspended monolayers. Thus, to better understand the contribution of individual oriented divisions to epithelial packing and cell and tissue shape changes, the shapes of cells progressing through mitosis in deformed suspended monolayers were analysed. Individual oriented cell divisions were found to redistribute the mother cell mass along the axis of division and to contribute to the homeostasis of cell packing by producing daughter cells with more isotropic cell shapes. Combining these results with computational modelling, the sequence of shape changes which occur are found to result from an interplay between cell and tissue mechanics and cell-autonomous changes in mechanical properties which occur through mitosis.

6.2 Methods

6.2.1 Measurements of cell shape

As before, cells were segmented either automatically in Tissue Analyzer [245] or by hand in using the polygon tool in FIJI [261]. Here, however, shape changes relative to the orientation of division were required. Therefore, segmentations were rotated so that they were in line with the orientation of division. The bounding rectangle of the rotated segmentation was then calculated which defined the cell length (along direction of division) and width (perpendicular to the axis of division). The ratio of length to width was used as a measure of aspect ratio. See figure 6.1A for a diagram depicting these measurements. After the division, the measurements were taken of both individual daughter cells and of the combined shape of both daughter cells. These measurements were taken at ± 60, ± 50, -10 and 0 minutes before/after furrow onset. This choice of time frame was the maximum span which did not reduce the number of eligible divisions to an unacceptable level. For a randomly selected subset of cells these measurements were obtained at 5 minute intervals throughout mitosis so that shape changes could be analysed at greater time resolution. The previous measures of cell shape which calculated the major and minor axis lengths of the best fit ellipse were also recorded and used when alignment to the orientation of division was not required (in measurements of cell rounding, Fig. 6.2, for instance).

6.2.2 Image overlays

To visualise small shifts in junctions which were difficult to quantify reliably, before/after overlays were created which allowed direct comparison of junction positions. To create these images, manual positioning of the before and after images was performed using the TrackEM2 plugin in FIJI.

6.2.3 Implementation of oriented cell division with a vertex model

Oriented division was implemented within a version of Farhadifar's [286] vertex model, the basis of which was replicated in MatLab by Aida Mehonic [53]. Briefly, cells are represented as two dimensional polygons consisting of a set of vertices and a set of edges joining the vertices. The cell is arranged in a continuous two dimensional space and an epithelium is then represented as a space filling tiling of such polygonal cells. The mechanics of the objects within the system is defined via an energy function, E, which is essentially equivalent to that of the cellular Potts model, used by Graner *et al.* [296, 297], which is given by:

$$E = \sum_{\langle i,j \rangle} \Lambda_{ij} l_{ij} + \sum_{\alpha} \frac{K_\alpha}{2}(A_\alpha - A_\alpha^{(0)})^2 + \sum_{\alpha} \frac{\Gamma_\alpha}{2} L_\alpha^2. \tag{6.2.1}$$

The first term represents the energy due to the length of each cell-cell junction. The sum over $\langle ij \rangle$ is a sum over all junctions and l_{ij} is the length of junction ij. The coefficient of line tension, Λ_{ij} can be positive or negative, since, for instance, cell adhesion would generally contribute negatively to this term whereas tension created by actomyosin contractility would contribute positively. The second term represents a notion of area elasticity. The sum is over all cells α and K_α is the elastic modulus of the cell α which has an area A_α and a preferred area $A_\alpha^{(0)}$. The final term defines an energy which is associated with cell perimeter. Cell α has perimeter L_α with energy coefficient Γ_α.

The implementation of the Farhadifar vertex model used here is stochastic and movements of vertices $\sigma(i,j) \rightarrow \sigma'(i,j)$ are randomly generated and accepted or rejected with probability P according to the Boltzmann distribution of E, as in the Monte Carlo algorithm [298]:

$$P(\sigma(i,j) \rightarrow \sigma'(i,j)) = \begin{cases} e^{-\Delta E/T}, & \text{if } \Delta E > 0 \\ 1, & \text{if } \Delta E \leq 0 \end{cases}, \tag{6.2.2}$$

where the number T is an 'effective temperature'.

The initial parameters (Λ = 56.8, $K = 160$ and $\Gamma = 49.9$) chosen for these simulations were those established by Aida Mehonic [53] to best represent the *Drosophila* pupal notum epithelium. These parameters, however, were found to not well represent MDCK cells subjected to stretch. As described in the main text, cells with a larger preferred area became less isotropic when stretch was applied, compared with their smaller neighbours. To counter this, cell junctional contractility was varied according to cell size (i.e. target area, see main text). While this succeeded in producing the correct cell aspect ratios, the cell areas significantly grew or decreased when contractility was decreased or increased, respectively. To counter this, a larger value of $K = 1600$ was used in all simulations.

Cell division is implemented within the model simply by introducing a new edge into the system and halving the preferred area of the two daughter cells which are produced. The new edge can be positioned to create a division which is oriented with cell shape, or otherwise. Stretch was modelled via simple transformations of the coordinate system. The cell preferred areas were also increased by the scale factor of the strain, so that plastic deformation is in some way accounted for [90]. Cell shapes therefore are naturally transformed as they are in a stretched tissue, however, the precise state of stress in the tissue is probably not well captured. For instance, the dynamics of the viscoelastic stress relaxation response [90] is clearly not be represented. Note, however, that an effective stress is indeed present in the stretched tissue since cells are not in the preferred isotropic configuration. A short period of equilibration was required after applying stretch as cells made the small shape changes to reach the energy minimum of the stretched tissue. Further behaviours implemented in the model are discussed in the main text.

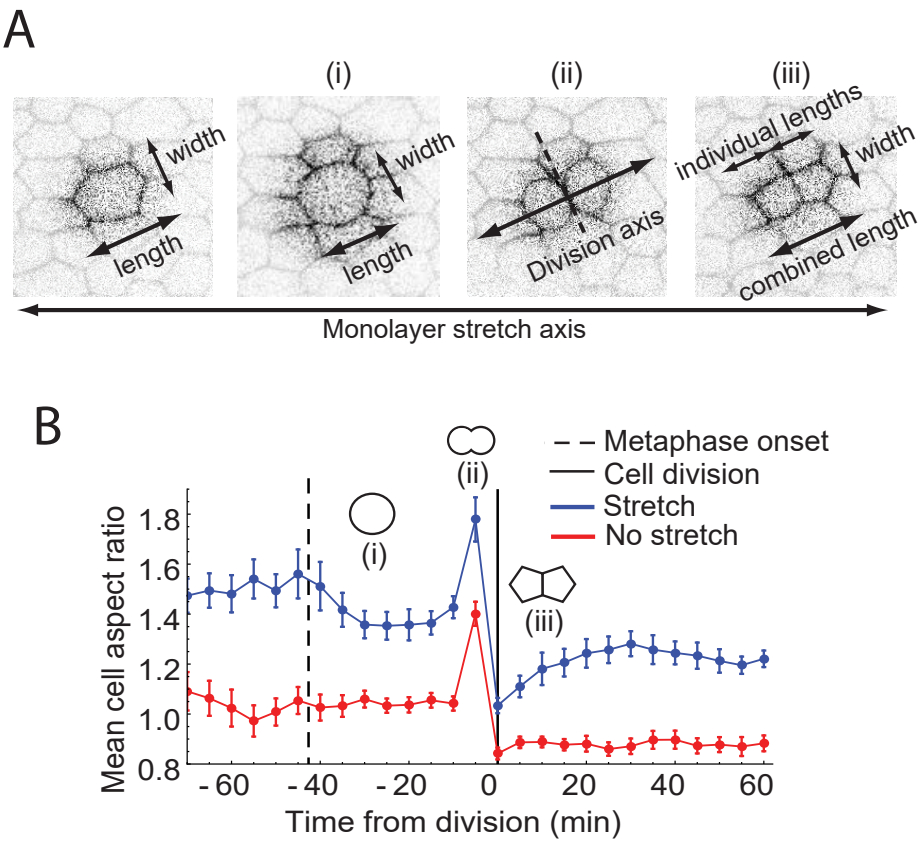

Figure 6.1: Cell shape changes during mitosis in suspended monolayers. (A) Diagrams depicting a cell in a stretched monolayer at different stages through the cell cycle, along with the measurements of cell shape which were taken. For each cell division, the measurements of length and width were oriented along the axis of division for all time points. (B) A plot showing the evolution of the aspect ratio (length/width) of cells through mitosis. Key points during the evolution are marked which are (i) cell rounding, (ii) anaphase elongation and (iii) daughter cell reintegration (these correspond to the marked time-points in (A)) and are accompanied by illustrative pictograms. The dashed vertical line demarks rounding onset and the solid vertical line demarks division. Error bars indicate SE.

6.3 Cell shape changes throughout mitosis in stretched suspended monolayers

The shape of cells in stretched and non-stretched suspended monolayers was measured at 5 minute intervals as cells progressed through mitosis. Measurements of cell dimensions were taken with respect to axes which were aligned with the direction of division, since these were the axes along which reproducible patterns of shape change were driven.

The length of cells along the axis of division is referred to the cell 'length', whereas the length of the cells along the axis perpendicular to this is referred to as cell 'width'. These measurements are depicted in figure 6.1A.

Figure 6.1B shows the progression of the aspect ratio (length/width) of cell shape in stretched (blue) and non-stretched (red) suspended monolayers from before mitotic entry through to after exit. Changes in shape at key time points are marked on the graph. At (i) the onset of cell rounding is reflected in the reduction of aspect ratio in the cells of stretched monolayers. While morphological changes are clear at this point in non-stretched monolayers (see Fig. 5.7, top row), this is not reflected in changes in aspect ratio since the majority of cell shapes are roughly isotropic already. At (ii) the aspect ratio of cells in stretched and non-stretched monolayers rapidly increases during anaphase elongation, which is a common feature across many mammalian cells types [299]. Immediately after this, the cell aspect ratio is reduced by the creation of two daughter cells (which are here measured separately). In the period following division (iii), there is no discernible change in the aspect ratio of non-stretched cells, however, the daughter cells in stretched tissues elongate over a period of 20-30 minutes. Interestingly, no previous mention of this post-division elongation could be found in the literature. These time points are discussed further in the following sections.

6.4 Tissue stretch limits the extent of cell rounding during mitosis

In suspended MDCK monolayers, cells rounded-up in early mitosis as is observed in many mammalian cell types (Fig. 6.1A (i) and 6.2A). Cell rounding occurred $\sim$30 minutes before furrow ingression and this timing was not affected by the application of stretch. The shape changes accompanying rounding occurred over a duration of $\sim$5 minutes meaning that any possible effect of stretch on rounding rate was not measurable due to the time

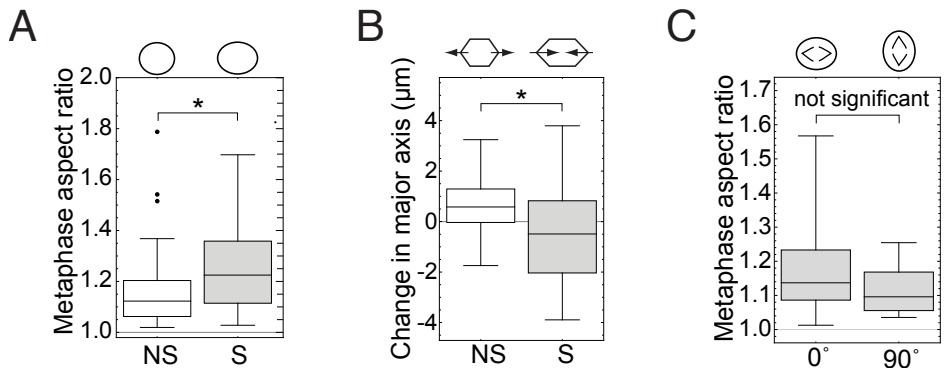

Figure 6.2: Mitotic cell rounding in stretched and non-stretched suspended monolayers. (A) Box-whisker plots of the aspect ratio of mitotic cells 10 minutes prior to furrow onset. The pictograms above the plots show the median shape of rounded cells in each condition. NS is non-stretched and S is stretched. (* denotes a significant difference, $p < 0.002$) (B) Box-whisker plots showing the change in major axis length undergone during rounding, in non-stretched (NS) and stretched (S) monolayers. The pictograms above the plots show the most frequent direction of shape change. ($n \geq 48$ cells and $N = 3$ monolayers for each condition; * denotes a significant difference, $p < 0.001$) (C) Box-whisker plots showing the aspect ratio of metaphase cells in stretched monolayers. The plot compares cells with an interphase shape aligned with the direction of stretch (0°) with those that are misaligned (90°), ($n \geq 12$ cells for each condition; P > 0.05).

resolution of the live imaging (5 minutes).

In non-stretched monolayers, cell shape became more isotropic via expansion along the cell short axis by an average of $2.4(1)\,\mu\mathrm{m}$ [1]. On average, non-stretched cells expanded along their long axis but by a lesser amount of $0.7(1)\,\mu\mathrm{m}$ (Fig. 6.2B). These shape changes resulted in a near isotropic shape prior to anaphase elongation of mean aspect ratio of just $1.16(2)$ (Fig. 6.2B).

Interestingly, the route taken towards a more isotropic shape during rounding was different in stretched monolayers. Dividing cells in stretched monolayers expanded by a similar average of $2.4(2)\,\mu\mathrm{m}$ along their short axis. However, in contrast to non-stretched cells, the long axis of stretched cells contracted during rounding (in addition to the expansion of the short axis) (Fig. 6.2B). Despite an average reduction in long axis of -$0.6(3)\,\mu\mathrm{m}$ (Fig. 6.2B), these cells did not reach the near isotropic state of their non-stretched equivalents, instead maintaining a residual aspect ratio of $1.25(2)$ (Fig. 6.2A). Extreme mitotic flat-

[1] the numbers in parentheses indicate the uncertainty associated with the final digit of the corresponding mean, measured as the standard error of the mean

tening has been shown to perturb spindle morphogenesis and chromosome capture [235], however, the cells which failed to completely round here never failed to complete division.

The $\sim 40\,\mathrm{nN/cell}$ stress measured in suspended monolayers stretched by 30% is comparable in magnitude to the $\sim 80\,\mathrm{nN}$ force measured as the maximum force generated by isolated cells during rounding [233]. This raises the possibility that the tissue tension prevents cells in stretched monolayers from completing rounding. On the other hand, cells in stretched monolayers are more elongated in interphase, so this elongation and the additional stresses which may be required to round an elongated cell may be the cause of the difference. To test this, two groups of cells in stretched tissues were chosen: those with an interphase shape aligned with stretch and those with and interphase shape perpendicular to it. It was hypothesised that cells oriented away from the stretch axis may have to do less work against the tissue tension and so would be able to round more easily. However, no significant difference in the rounded shapes of these two groups was found (Fig. 6.2C), suggesting that both cell elongation and tissue tension play a role in preventing complete cell rounding.

6.5 Cell divisions redistribute the mother cell mass along the axis of division

As discussed in the introduction to this thesis and the introduction to this chapter, oriented cell division has been linked in a number of systems with oriented tissue growth [147–149]. In an attempt to better define the morphological contribution that oriented cell divisions could have, the overall change in the shape of individual dividing cells and the tissue surrounding them was examined. Therefore, cell shape was measured significantly before and significantly after division, in order to assess the final result of the division on shape. Time points at 50 and 60 minutes before division, at division, and 50 and 60 minutes after division were chosen. It was clear that division was associated with a substantial rear-

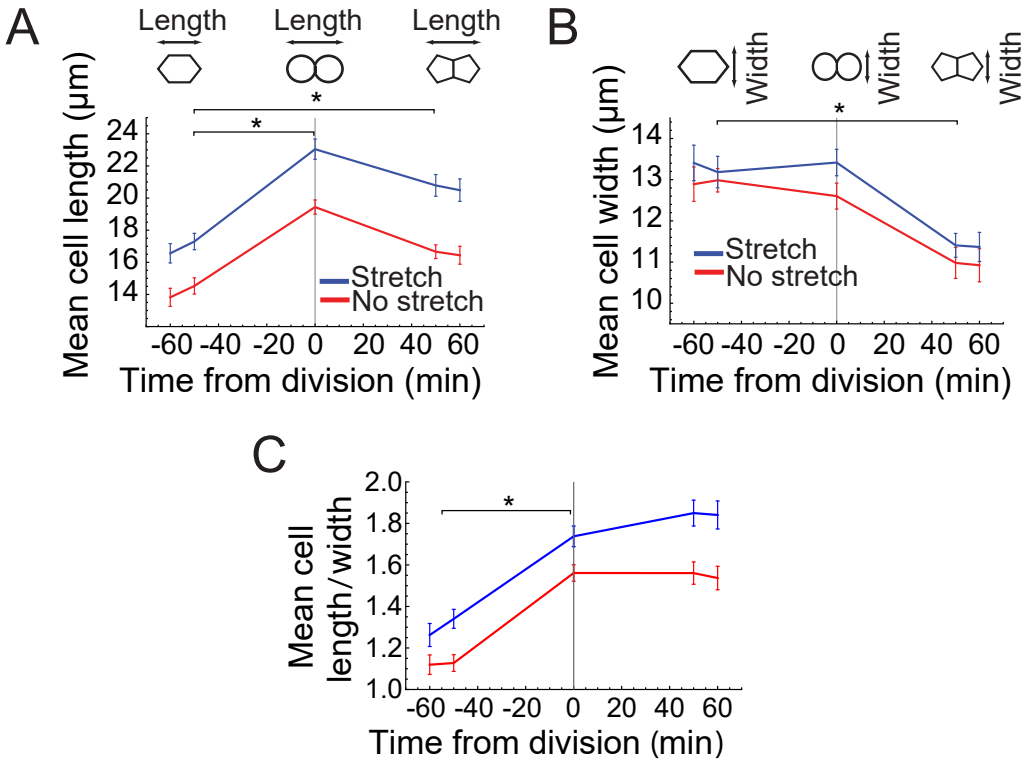

Figure 6.3: Oriented division redistributes the mother cell mass along the axis of division. (A) The length of the mother cell (before division) or the combined spatial envelope of the daughter cells (after division) as cells progress through mitosis in stretched (blue) and non-stretched (red) monolayers. (* signifies $P < 0.01$; $n \geq 38$ cells from n = 3 monolayers for each condition). The pictograms above the graph describe the measurements taken. (B) The same as in (A) but for cell width. (C) The same as in (A) and (B) but for the cell aspect ratio, as given by cell length/width.

rangement and reshaping of the mother cell mass. To measure this, rather than measuring the shapes of individual daughter cells, the combined spatial envelope of the daughter cells (at 50 and 60 minutes) was segmented, and the shape of this envelope was compared to the shape of the mother cell. Once again, these shapes were measured relative to the orientation of division (Fig. 6.1A).

Interestingly, the changes in shape measured overall were similar in stretched and non-stretched tissues. In both, the length of the cell increased from -50 minutes to 0 minutes (at division), and then decreased a little from 0 minutes to 50 minutes (Fig. 6.3A). Overall, however, the length over which the cell mass was spread was larger after division than before division, elongating from $13.8(6)\,\mu\mathrm{m}$ to $16.4(6)\,\mu\mathrm{m}$ in non-stretched

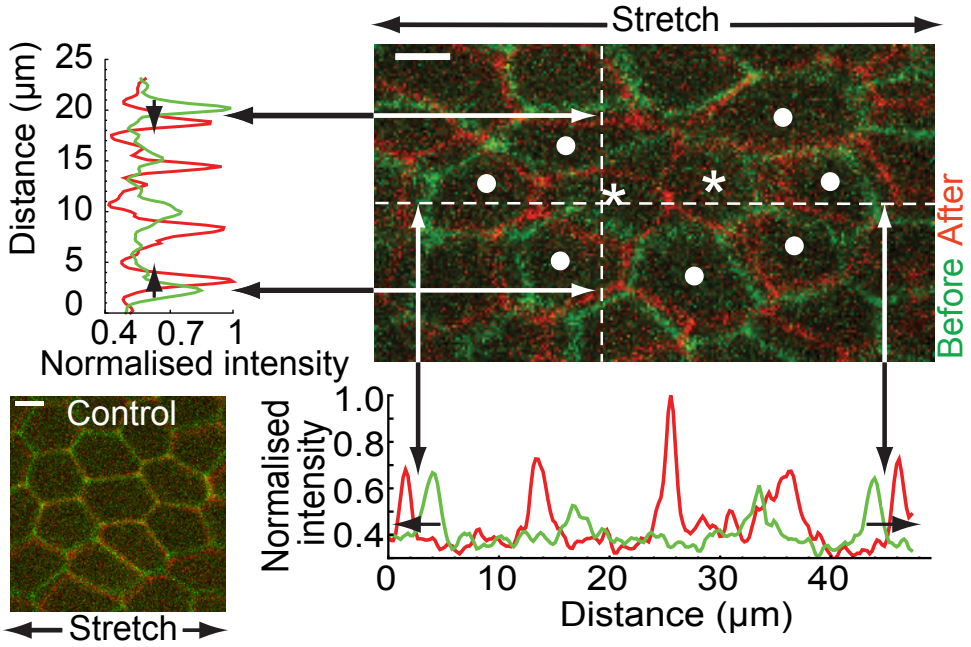

Figure 6.4: Oriented division reshapes the tissue local neighbourhood. An overlay of cells 10 minutes before (green) and 30 minutes after (red) furrowing onset in an oriented division. Line profile intensity plots along the dotted lines show a shifting of junctions which is not seen in the control (inset). (Scale bars: 10 μm).

monolayers and from $17.3(5)$ μm to $20.5(7)$ μm in stretched monolayers (Fig. 6.3A). Concomitantly, the width of the cell spatial envelope narrowed from $13.0(3)$ μm to $11.0(4)$ μm in non-stretched monolayers and from $13.2(4)$ μm to $11.4(3)$ μm in stretched monolayers (Fig. 6.3B). Overall the aspect ratio of the cell envelope strongly increased from $1.17(5)$ to $1.54(6)$ in non-stretched monolayers and from $1.26(6)$ to $1.84(7)$ in stretched monolayers (Fig. 6.3C). This clearly showed the reorganisation of cell matter induced by cell divisions: cell mass is redistributed along the division axis to create a longer and narrower structure. It is interesting to note that while the effect of an individual division is similar in both stretched and non-stretched monolayers, the alignment of many divisions in stretched tissue will cause a net, directional flow of mass, whereas the random orientation in non-stretched tissue will have no directional outcome.

Given that divisions had an appreciable effect on the organisation of mother cell mass,

it was natural to ask if the surrounding tissue was affected in a similar way. The junctions of cells neighbouring the dividing cell were therefore examined. The effects of the division at this distance were more subtle and difficult to measure quantitatively. However, the pattern of their effect could be seen when images before and after division were directly compared by overlaying them and creating line intensity profiles (Fig. 6.4). This revealed that in both stretched and non-stretched monolayers, a small shape change was induced in the neighbouring cells by the division, which was equivalent to the shape change of the mother cell mass. Thus, it was clear that junctions belonging to cells that were positioned along the axis of division were shifted away from the dividing cell (Fig. 6.4). At the same time, junctions belonging to cells that were positioned along the axis perpendicular to the division orientation behaved differently - these were shifted towards the dividing cell (Fig. 6.4). It was clear, therefore, that the cell division had morphological effects not just on the mass of the dividing cell itself, but also on the neighbouring cells.

6.6 Oriented cell division in stretched monolayers produces daughters of reduced anisotropy

The region marked (iii) in figure 6.1B shows that in non-stretched monolayers, the shape of daughter cells is established at division, with little change in aspect ratio occurring from that point onwards. Indeed, the mean change in aspect ratio between division and 25 minutes later is $0.02(3)$ (Fig. 6.5A). For cells in stretched monolayers, however, region (iii) in figure 6.1B looks quite different after division. Here, the aspect ratio of daughter cells rises substantially in the 20 - 30 minutes following division, so that after 25 minutes the aspect ratio was $0.22(4)$ greater than it was at 0 minutes (Fig. 6.5A). To test the role of tissue tension in driving this elongation, cells in stretched monolayers which divided along the direction of stretch (i.e. oriented with tissue tension) were compared with those in the same monolayers which divided perpendicular to the stretch direction (i.e. oriented

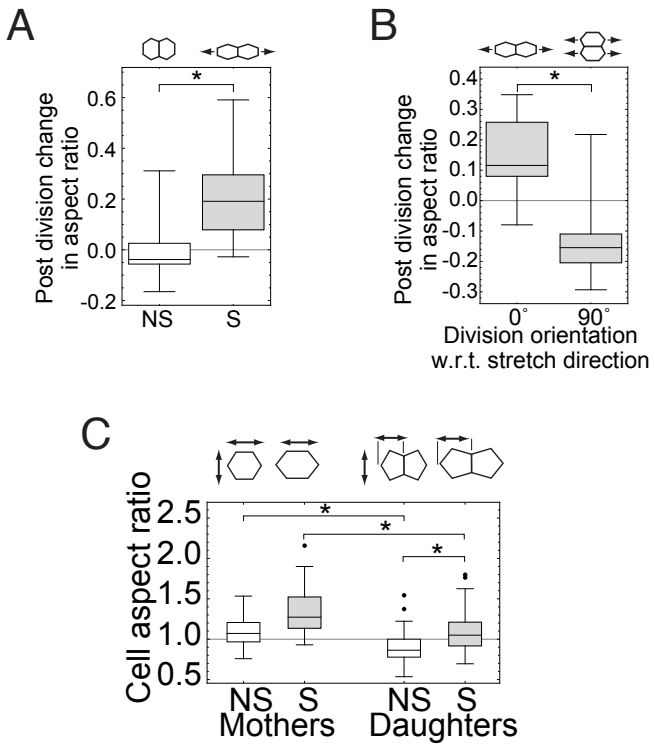

Figure 6.5: Elongation of daughter cells post-division in stretched suspended monolayers. (A and B) Box-whisker plots showing the change in aspect ratio (measured with respect to the direction of division) between division (t = 0) and t = 25 min (n = 20 cells for each condition; * denotes a significant difference, $p < 0.001$).(A) compares divisions in non-stretched and stretched tissues whereas (B) compares divisions in stretched tissues which were oriented either in the direction of stretch or perpendicular to stretch. (C) Box whisker plots showing the aspect ratio of cells immediately before the onset of rounding (mothers) and 50 minutes after (daughters) oriented division. The pictograms above the box plots describe the measurements taken.

perpendicular to tissue tension). Interestingly, these measurements showed that, after division, daughter cells elongated in the direction of the tissue tension, irrespective of the orientation of the division (Fig. 6.5B). This strongly suggests that the tissue tension is driving the shape changes observed in daughter cells after abscission.

The resultant shape of daughter cells is therefore determined by a complex interplay of mother cell shape, division orientation and cell-intrinsic and -extrinsic tension. This final shape is influential, since the results in chapter 5 suggest that it will dictate the orientation of the next round of division. The final shapes of the individual daughter cells were therefore measured 50 minutes after division, in order to assess the overall effect of oriented

division on cell shape. Aspect ratios were once again measured with respect to the orientation of the division. Mother cells in non-stretched monolayers, measured just before the onset of rounding, were slightly elongated in the direction of division, with an aspect ratio of $1.09(3)$ (Fig. 6.5C). This slight elongation is ultimately a mark of their ability to divide along their long axis in the cases where a well defined long axis happens to exist (Fig. 6.5C). After division, however, the daughter cells in non-stretched monolayers had an aspect ratio of $0.91(2)$ showing that they remained anisotropic and now had a long axis perpendicular to the mother cell long axis (Fig. 6.5C). This predicts that these cells would divide in an orientation perpendicular to the first division, reminiscent of the alternating orientations of divisions in early embryos [182].

In contrast to non-stretched divisions, mother cells in stretched monolayers had an aspect ratio of $1.34(5)$ (Fig. 6.5C). After division, the daughter cells have a resultant aspect ratio of $1.10(3)$, showing the division has reduced the anisotropy of the mother cell but that the next round of divisions would be predicted to orient in the same direction as the first (Fig. 6.5C).

6.7 Oriented divisions in compressed monolayers redistributes the mother cell mass and restores isotropic cell packing

This chapter has thus far explored the sequence of cell shape changes which accompanies the passage through mitosis of cells in stretched and non-stretched monolayers. The overall changes in form appear to be the result of an interplay between cell-autonomous processes and the mechanical state of the surrounding tissue. The divisions oriented by a uniaxial compressive strain, which were explored in section 5.8, provide an interesting third setting in which to explore this interplay further. While the state of tissue tension in compressed suspended monolayers is still not known at long timescales, at short timescales tissue tension is very low (measured by others in the Charras lab, data not

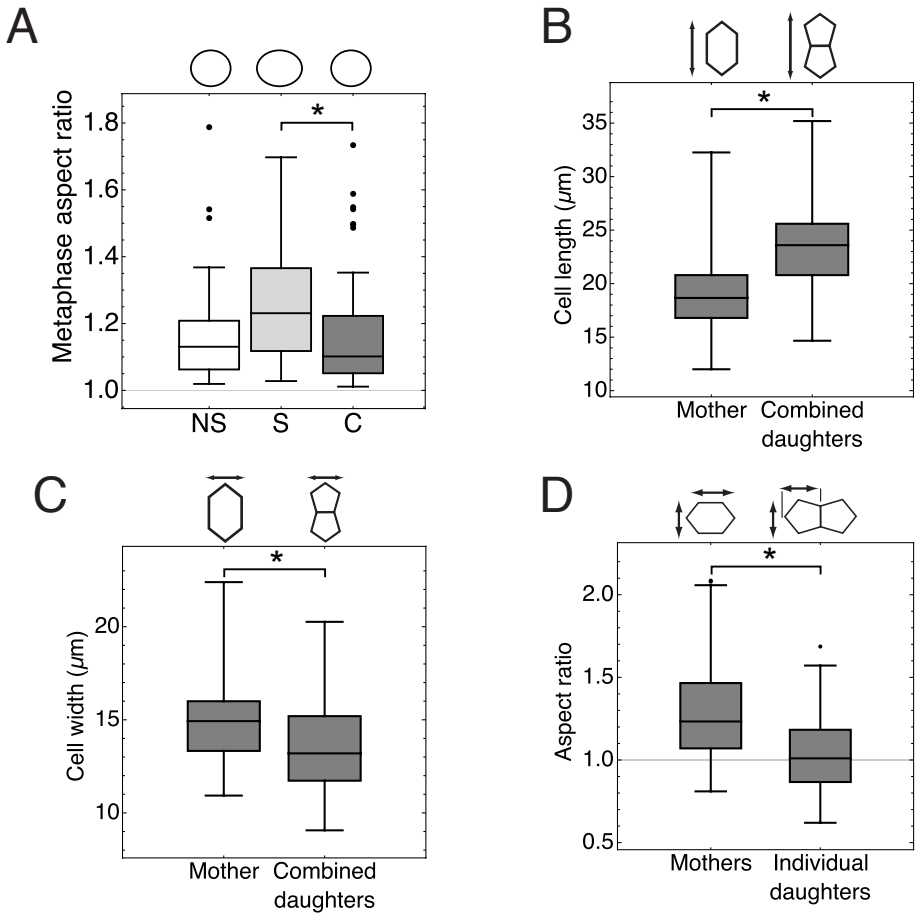

Figure 6.6: The cell shape changes during mitosis in compressed tissues. (A) Box-whisker plots of the aspect ratio of mitotic cells 10 minutes prior to furrow onset in non-stretched (NS), stretched (S) and compressed (C) tissues. The pictograms above the plots show the median shape of rounded cells in each condition. (* denotes a significant difference, $p < 0.002$) (B) Box-whisker plots of the length of the mother cell (before division) or the combined spatial envelope of the daughter cells (after division) in compressed tissues. (* signifies p< 0.01; $n \geq 66$ cells from $n = 4$ monolayers for each condition). The pictograms above the graph describe the measurements taken. (C) The same as in (B) but for cell width instead of cell length (see pictograms). (D) The same as (B) and (C) but for the aspect ration of the mother or individual daughter cells.

shown). Therefore it is likely that these oriented divisions occur in an environment which is low in tension but with similar levels of cell shape anisotropy. Furthermore, while the tissue height is reduced by stretch, it is increased by compression so that cells are longer in the apical-basal axis than in any other axis (Fig. 4.6).

To test whether these differences have an effect on the sequence of cell shape changes which occur through mitosis, the same measurements of cell shape were recorded for dividing cells in compressed tissues. Interestingly, despite the similar level of shape anisotropy, cells in compressed tissues could round up much better than their equivalents in stretched tissues (Fig. 6.6A). Overall they reached an average aspect ratio which was indistinguishable from that of cells in non-stretched tissues (Fig. 6.6A). This further suggests that tissue tension induced by stretch can limit the extent of cell rounding. While this feature of cell shape change was markedly different, the ability for cell divisions to redistribute the mother cell mass was not altered (Fig. 6.6B and C). Indeed, the combined spatial envelope of the daughter cells was significantly longer than the mother cell along the direction of division (Fig. 6.6B) and significantly narrower in the perpendicular direction (Fig. 6.6C). Similarly, just as in stretched tissues, oriented cell division contributed to restoring pre-deformation cell shapes by converting the elongated mother cell into two daughter cells which were more likely to be isotropic (Fig. 6.6C).

6.8 A simple computational model of epithelial cell mechanics reproduces shape changes

The observed differences between mitotic cell shape changes in stretched and non-stretched tissues may result from identical cell behaviours taking place within differing mechanical environments. Indeed, the overall cell behaviour may only consist of mitotic behaviours which have been well studied previously, such as the up-regulation of cortical contractility during cell rounding [233]. On the other hand, the observed differences may result

from differences in signalling that would lead to the dividing cells behaving differently in stretched and non-stretched tissues. That is, tissue stretch may be detected by the dividing cell via mechanotransduction which may subsequently elicit a behaviour which is different to that in the non-stretched tissue. Furthermore, it is possible that novel behaviours which have not yet been studied play a role in the observed evolution of shape.

To test whether or not the first of these two scenarios is possible, a computational model is employed. The general approach is to model known cell behaviours within a model which meaningfully reproduces physical characteristics of the shapes of cells in living epithelia. For this purpose an adaptation of the vertex model of Farhadifar *et al.* [286] is used, which has previously been successful in modelling a variety of epithelial processes, such as proliferation-determined cell-packing [286], crowding-induced cell delamination [53] and division-driven oriented tissue growth [148, 154], amongst others [74, 300, 301]. The vertex model reduces the entire molecular complexity of an epithelial tissue to a network of cell-cell 'junctions' which enclose mechanically uniform areas ('cells'). However, overall it is a mesoscopic representation of a tissue since the tissue is not further reduced to a continuum - the cellular basis of the tissue is coarsely retained. The mechanical properties of these junctions and enclosed areas are captured by an energy function (equation 6.2.1) which is stochastically minimised via the Monte Carlo algorithm [298] (equation 6.2.2). For further details of the model and its implementation see the methods section 6.2.3.

The topology and geometry of the local tissue environment (that is, the cell polygon types of neighbouring cells, along with their shapes and sizes), likely plays some role in the specifics of the shape changes which were observed experimentally in each cell division [142]. However, the number of possible topological environments is combinatorially large and so any possible effects are difficult to study systematically and would not be supported with enough experimental data. In these simulations, therefore, cell divisions were simulated within a uniform hexagonally packed tissue and it is assumed that the effects of

the shapes of neighbouring cells cause variations which are of second order magnitude.

As a first step, the most basic features of oriented cell division were modelled. A cell in a stretched or non-stretched tissue was simply converted into two cells by the introduction of one additional junction (Fig. 6.7A and B) and the halving of the preferred area of the daughter cells ($A_0 \rightarrow A_0/2$, see methods section 6.2.3). No other mechanical changes were included, therefore it was not expected that the full range of shape changes would be captured. Despite this, the basic patterns of mother cell mass redistribution and restoration of isotropic shape were reproduced in these simple simulations. Indeed, upon division the length of the combined spatial envelope of daughter cells increased (Fig. 6.7C) and the width decreased (Fig. 6.7D). Altogether the aspect ratio of the spatial envelope was dramatically increased (Fig. 6.7E), just as was found in experiments. In further agreement with experiment, the overall behaviours here were similar in stretched and non-stretched tissues. The final aspect ratio of individual daughters was also well reproduced by the model. In non-stretched tissues, daughter cells were less isotropically shaped after division (Fig. 6.7F), whereas oriented division in the stretched tissue produced roughly isotropic daughters (Fig. 6.7F).

While it was difficult to experimentally test the effect of mis-oriented cell divisions, it was simple to implement in simulations. As shown in figure 6.7F, the orientation of division has no effect on shape changes in non-stretched tissues (as expected) but mis-orientated divisions are predicted to produce highly anisotropic cells in stretched tissues, thus highlighting the importance of oriented divisions in regulating daughter cell shape. Note that in figure 6.7F a different measure of aspect ratio is used compared with figure 6.7D. The aspect ratio of the best fit ellipse is used instead of the length divided by width (see methods section 6.2.1 and figure 6.1 for definitions of length and width) as this allows for more direct comparison between the oriented and mis-oriented cases.

As a next step, a number of additional features were added to the model in an attempt to match the experimental behaviour more closely. One important difference between sim-

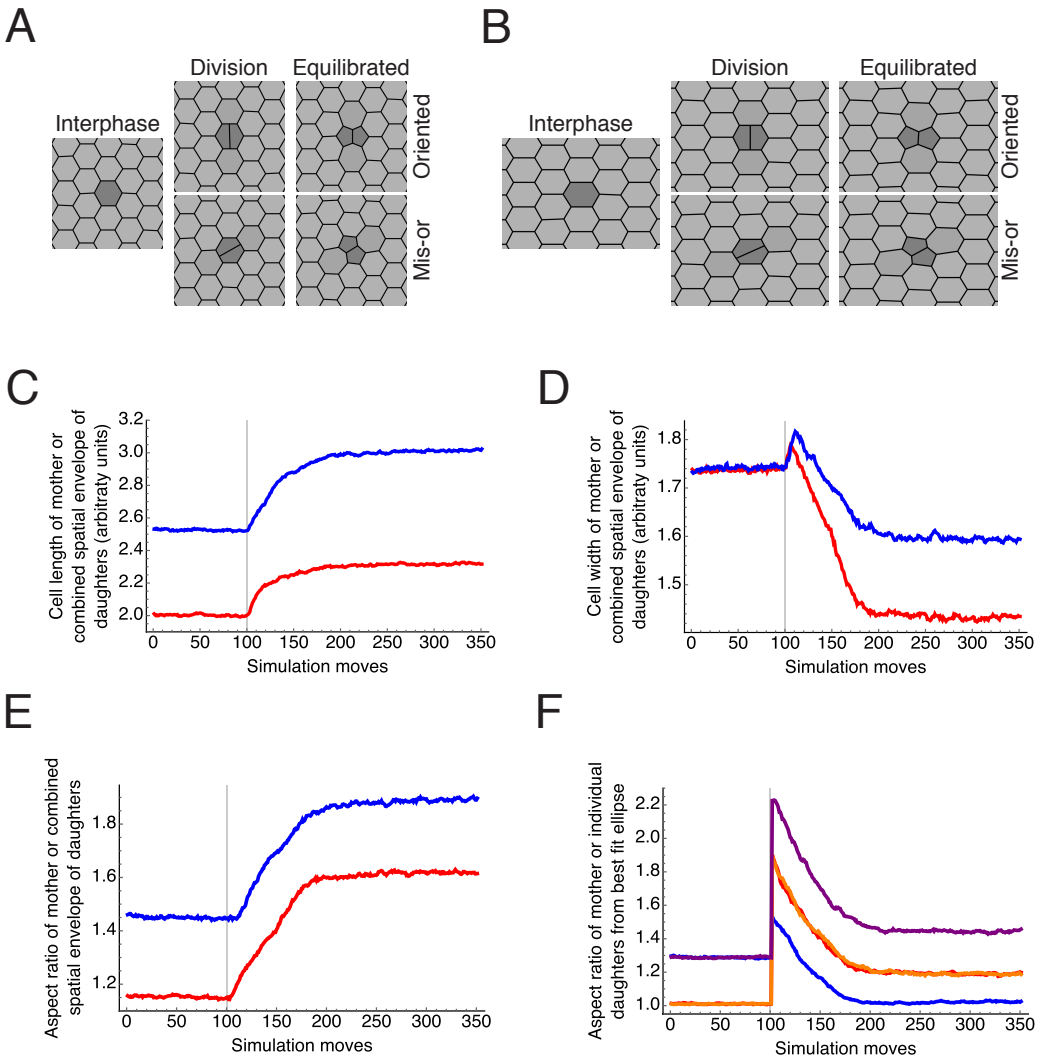

Figure 6.7: Mother cell mass redistribution in a simple vertex model. (A and B) Images of a cell division (grey cell) as modelled with a vertex model in non-stretched (A) and stretched (B) tissues. Both shape oriented (top rows) and mis-oriented (bottom rows) divisions are simulated. (C) The length of the mother cell before division and the length of the combined spatial envelope of the daughter cells after division in non-stretched (red) and stretched (blue) tissues. The mean of 8 simulations is plotted. The variance is too small to plot. The grey vertical line marks the time point where division occurred. (D and E) The same as in (C) but for cell width and aspect ratio, respectively. (F) The aspect ratio of the best fit ellipse to cell shape. The measurements after division are for individual daughters. The measurements shown are for oriented divisions in non-stretched tissues (red) and stretched tissues (blue) and misoriented divisions in non-stretched (orange) and stretched (purple) tissues.

ulation and experiment thus far is that the dividing cells in suspended monolayers were on average ∼40% larger than non-dividing cells before they entered mitosis (Fig. 5.6C). Therefore, the size of the dividing cell was initially increased by increasing the target preferred area (Fig. 6.8A). The target area of all other cells in the simulated tissue was kept constant. While this succeeded in producing cells which grew to the required size (Fig. 6.8A), the larger cells were surprisingly found to resist stretch more than their smaller neighbours, such that they ended up with a lower aspect ratio (Fig. 6.8B). This pattern was found to apply over a wide range of cell sizes and the reverse effect was found in cells whose area was decreased via reduction of the target area parameter (Fig. 6.8B). This effect did not appear to reflect the true behaviour of MDCK cells since no correlation was found between aspect ratio and cell area in stretched suspended monolayers (Fig. 6.8C). Therefore, to counter this effect, the junctional stiffness of large cells was lowered by scaling the values of Λ and Γ. For a range of cell sizes, parameter searches were conducted to determine the stiffness scaling factor which was required to produce cells which maintained the same aspect ratio as neighbours when stretched by 30% (Fig. 6.8D). The relationship between the cell area and the stiffness factor which was required to give an aspect ratio which matched global strain, was well fitted by an exponential decay function (Fig. 6.8D, orange line) which was subsequently used to provide the stiffness factor for any required cell area. It may be interesting to further investigate whether there is any real biological analogy here, however, it may just be a quirk of the vertex model.

In addition to matching the average relative size of dividing cells, the final feature which was added was an imposed sequence of cell stiffness changes aimed at modelling the changes in mechanical properties which occur in cells as they progress through mitosis. Firstly, the cell stiffness was abruptly increased in an attempt to reproduce the cell rounding observed in experiments. Stewart *et al.* [233] previously combined atomic force microscopy of mitotic HeLa cells with pharmacological treatments to reveal that cell rounding is driven by an increase in intracellular pressure and actomyosin contractility.

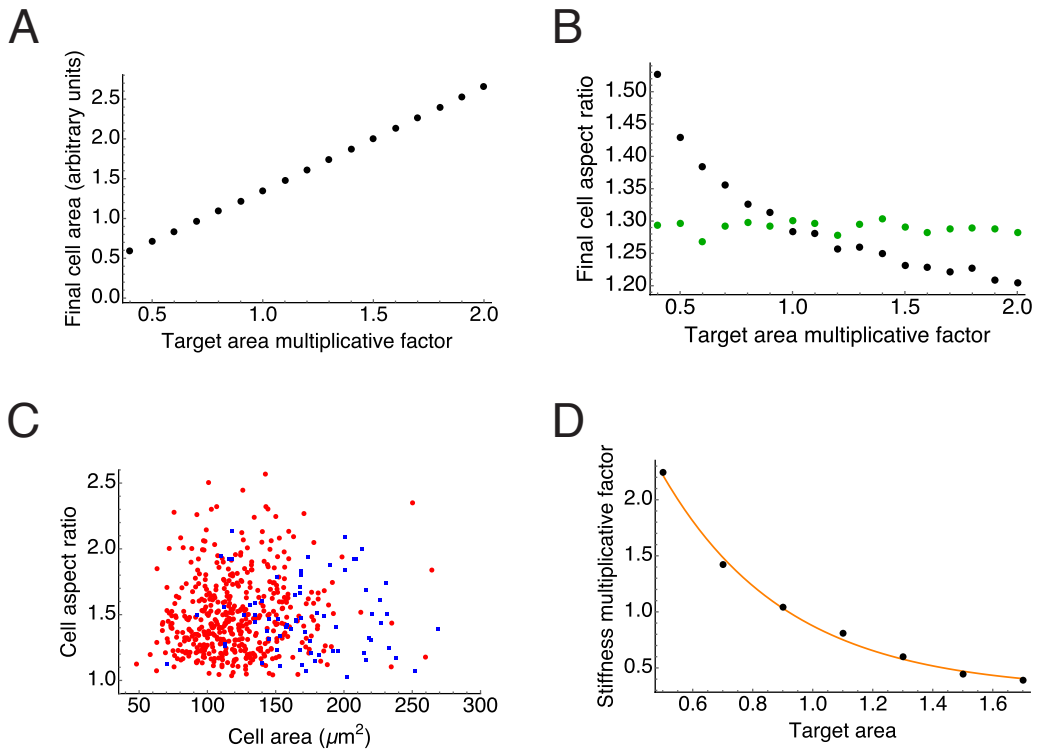

Figure 6.8: Cell contractility must be scaled according to cell area in vertex models. (A) A plot showing the final cell area of cells in which the target area was increased by a given factor. The high value of K used in these simulations (see methods section 6.2.3) leads to the target area being followed very closely. (B) The final aspect ratio of a cell, whose size has been altered by a target area multiplicative factor (black dots), after an imposed 30% stretch. The green dots show the aspect ratios of cells in the same tissues whose target area was not altered. (C) The cell area and aspect ratio of cells in stretched suspended monolayers for cells which did not divide during experiments (red circles) and cells which did divide (blue squares). N = 3 tissues. (D) The cell stiffness multiplicative factor that was required to produce the correct aspect ratio in cells whose target area had been altered (black dots). The orange line shows the best fit exponential decay function.

To replicate this in the vertex model, the parameters controlling cell junctional stiffness, Λ and Γ were increased by a multiplicative factor. This indeed produced a reduction in the aspect ratio of cells in stretched simulated tissues (Fig. 6.9A) and a parameter search revealed that the change of aspect ratio observed in stretched suspended monolayers could be matched by a 1.2-fold increase in stiffness (Fig. 6.9B).

While the increase in cell contractility as cells enter mitosis is well documented, changes in mechanical properties as cells exit mitosis have not been accurately measured. In the study by Stewart *et al.* [233], for instance, rapid cell shape changes during anaphase caused

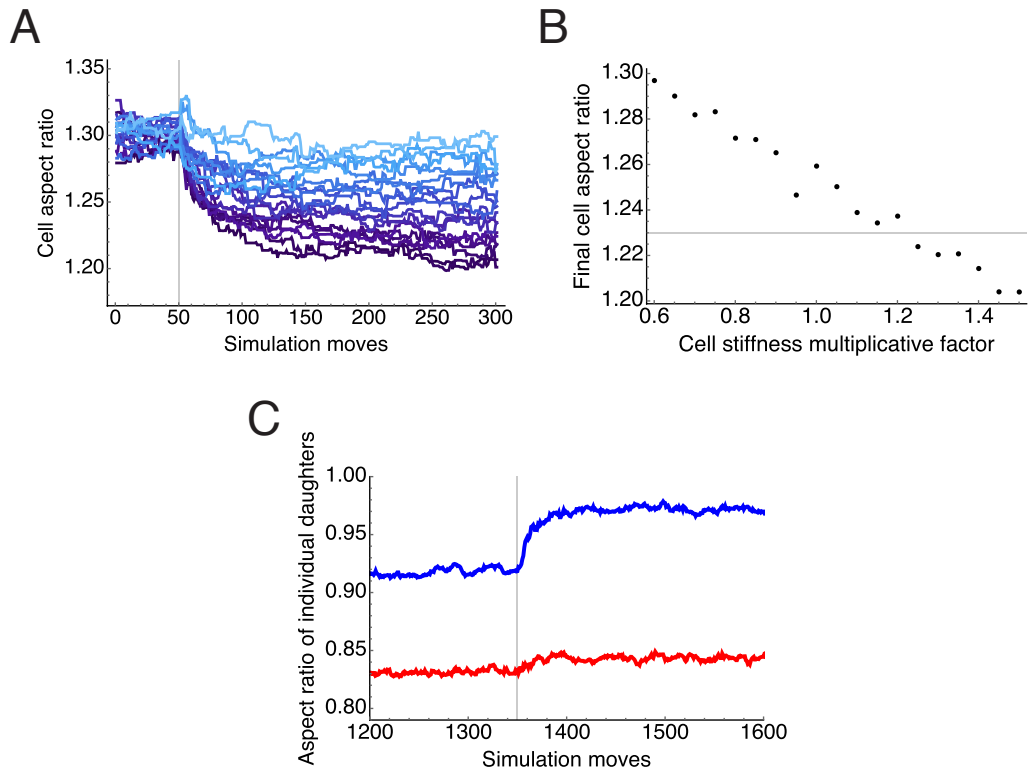

Figure 6.9: Mitotic changes in cell mechanics replicate cell rounding and post-division elongation. (A) Plots showing the change in cell aspect ratio of cells which is induced by an increase in cell stiffness in a 30% stretched simulated tissue. Increasing darkness of blue represents increasing change in stiffness. The grey line marks the time point at which the stiffness change is made. (B) The final aspect ratio of cells in stretched simulated monolayers for a given change in cell stiffness. The grey line marks the average aspect ratio reached by MDCK during mitosis in stretched suspended monolayers. (C) The aspect ratio (length/width) of post-division cells in stretched (blue) and non-stretched (red) simulated tissues. The mean of 8 simulations is plotted. The grey line marks the time point at which the mechanical properties of the daughter cells are returned to the interphase levels.

the readings of mechanical properties to be unreliable. Here, therefore, the assumption had to be made that the mechanical properties of cells exiting mitosis must return eventually to those of normal interphase cells. Therefore the cell stiffness increase which drove cell rounding was removed after division and the daughter cells were given the stiffness appropriate for their size, according to the exponential decay function of figure 6.8D. Interestingly, this change in daughter cell stiffness prompted an elongation of the daughter cells in stretched tissues but not in non-stretched tissues (Fig. 6.9C), just as was observed in experiments (Fig. 6.5A). However, the magnitude of change in aspect ratio was signifi-

cantly smaller in simulations.

The agreement between model and experiment could perhaps be made more quantitatively accurate through more detailed parameter searches. For instance, Λ and Γ were always changed by equal factors, whereas changing them independently may provide the extra freedom required to find a better fit. However, for now this was not the aim of the model. Indeed, the experimental measurements generally contained much variation, which is not surprising given the broad distribution of starting shapes of cells [141]. Therefore fitting the model data, obtained in a uniform hexagonally packed tissue, to the mean of broadly spread experimental data is not likely to be useful. As discussed above, increasing the topological and geometric complexity of the simulated tissues may improve the model likeness but will also not be immediately informative.

Instead, the model has altogether qualitatively reproduced the full range of shape changes which were observed during oriented division within stretched and non-stretched tissues, all within a relatively simple framework. Mother cell mass redistribution and the approximate final shapes of daughter cells were matched in the simplest implementation of the model, supporting the idea that both can be brought about by little more than the mechanical consequences of introducing an additional junction. Cell rounding and post-division elongation of daughter cells were reproduced through implementing a simple sequence of cell stiffness changes with just one fit parameter. Importantly, the shape changes in the model qualitatively matched experimental observations in both stretched and non-stretched tissues, using precisely the same mitotic cell behaviour. This supports the notion that the experimentally observed evolutions in shape are the consequence of identical cell-autonomous mitotic changes in mechanical properties occurring within the differing mechanical environments of stretched and non-stretched tissues.

6.9 Discussion of chapters 5 and 6

Understanding the parameters which influence division orientation, the mechanisms by which orientation is achieved, and the impact that division orientation has at the cell and tissue level is an important but dauntingly complex task for the biological community. Cell shape and local stress fields are intimately linked but appear to be separate and competing signals. Decoupling these effects is further complicated by the fact that cell shape and local stress can change rapidly during cell rounding at mitosis. On top of this, cell-cell adhesions, cell-ECM adhesions and cell and tissue polarity are also all able to feed into the spindle orientation signal.

To explain how the cell achieves the desired orientation, a menagerie of molecules and mechanisms have been investigated. Astral microtubules can be stably linked to the membrane via Khc-73, they can push through polymerisation, pull through depolymerisation and be pulled by dynein which is either in the cytoplasm or linked to the actin cortex. In order to guide the spindle, the location of force generators can be regulated through coupling with cell polarity, cell adhesion or via spindle pole or chromosome derived signals. Alternatively, even homogenous distributions of dynein can lead to specific spindle orientation, such as alignment with cell shape, via forces which depend on astral microtubule length.

Ultimately, the effort exerted by the cell to orient the spindle is likely to be to some purpose. Division orientation has been proposed to help maintain epithelial structure; help generate cell diversity during asymmetric division; to aid monolayer spreading through relaxation of stress, control of monolayer volume and control of monolayer cell number and to drive tissue elongation in order to generate shape during morphogenesis. In an embryo, however, the possibility that processes such as cell intercalation and apoptosis may act in parallel to cell division and the likelihood that simultaneous morphogenetic events may affect one-another make the effects of oriented cell division difficult to isolate.

To make these problems tractable, a system which is stripped of much of this com-

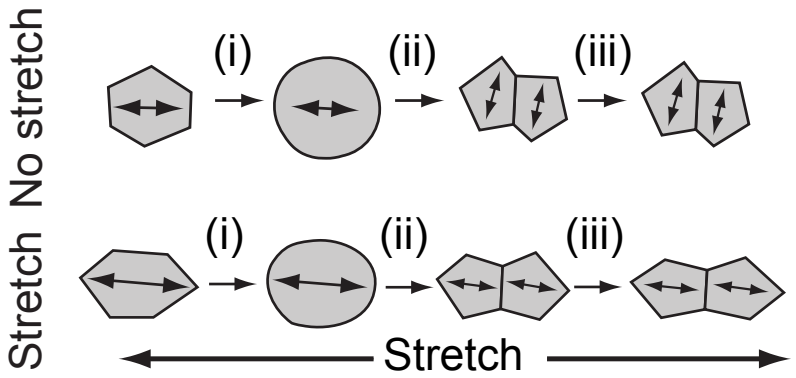

Figure 6.10: Simple cell-autonomous behaviours characterise cell division in stretched and non-stretched epithelial monolayers. In both stretched and non-stretched monolayers, cells round up and then divide in the orientation of their long cell-axis. Stretch, however, inhibits complete cell rounding either through tension or elongation of cell shape (or both), leaving significant cell anisotropy. After division, tissue tension causes the elongation of daughter cells as their stiffness returns to interphase levels.

plexity was utilised. As a cell culture system, the suspended monolayers used here were naturally devoid of developmental patterning. Neighbour exchange did not occur in the tissue, so the effect of cell division could be studied in isolation (Fig. 5.2). Cell-ECM interactions could not play a role since the ECM was removed. Furthermore, the mechanical state of the tissue which was induced by strain was also straightforward - a constant, uniaxial strain was imposed which resulted in the elongation of cell shape and a steady stress of $\sim 40\,\mathrm{nN/cell}$ (Fig. 5.3 and 5.4). Importantly, stress was uniformly oriented in the direction of stretch, irrespective of cell shape (Fig. 5.4). This allowed for the decoupling of shape and stress signals via a small subset of cells whose shape was misoriented with the stretch axis. By tracking divisions in such cells, it was shown that elongated cells always divide along their long cell axis, clearly showing that shape is the dominant cue over force. This is an important result since it reinforces the notion that cell shape is a strong cue and it shows that it can dictate the spindle orientation in a tissue context, even in the presence of significant stress along a conflicting axis.

Interestingly, cell divisions were also able to globally align in response to tissue compression. This is significant, not least because the overall 3-dimensional cell shape was very different in compressed tissues compared with stretched tissues (Fig. 4.6). While the

state of tissue tension is still not certain in compressed tissues at long timescales, preliminary data shows that it is very low at short timescales (data not shown). Whether or not an axis of tissue tension is eventually established in the compressed tissues, it is clear that the long cell axis remains as the dominant orienting signal in this setting, since once again divisions aligned better with the local cell shape axis than with any global axis of deformation.

Since adherens junctions are known to participate in mechanotransduction [28], as well as in orienting the mitotic spindle [138, 193], it is significant that the above results rule out the possibility of a dominant adherens junction-based stress signal for spindle orientation in this system. Overall, the ability of the cell to orient the spindle to stress may have been lost due to the removal of a basal substrate [221], so it will be important to find a system which can be tested in a similar manner without the removal of the ECM. Searching for any stress oriented signal in monolayers under greater tension or in cells which are less elongated (thereby reducing the shape signal) would also be valuable. In addition, it is noteworthy that cells in non-stretched and compressed monolayers, which became roughly isotropic during mitosis (Fig. 6.6A), were able to align their spindles with the interphase cell shape despite the loss of the shape signal throughout most of mitosis. This demonstrates a 'memory' of the interphase shape which persists during the 30-35 minutes during which the cell is round. Investigating the nature of this memory constitutes important future work. As noted in section 5.7, it will also be important to investigate the role which myosin seems to play in this process, given the misalignment of divisions in the presence of Y28632 (Fig. 5.9).

Measurements of cell shape changes throughout oriented division were taken to better understand the mechanical changes undergone by the cell and to understand how these changes could contribute to the monolayer organisation. The first changes in shape were cell rounding. Whereas cells in non-stretched and compressed monolayers became almost isotropic during cell rounding, dividing cells in stretched monolayers retained a signifi-

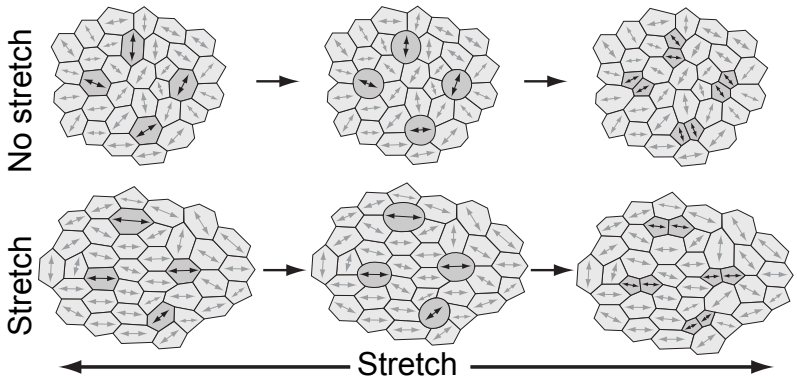

Figure 6.11: Identical, cell-autonomous behaviour at the cell-level lead to differing emergent, tissue-level behaviour in stretched and non-stretched monolayers. The stretch imposes alignment of cell long axes leading to alignment of division orientation. Mass redistribution during mitosis therefore sums to produce a net flow in the orientation of stretch. The random orientation of cell long axes in non-stretched monolayers, however, causes a uniform distribution of division orientation which leads to no net, oriented effect.

cant anisotropy right up to furrowing onset (Fig. 6.6A). Forcing single cells to remain flat throughout mitosis has been shown to induce errors in spindle morphogenesis and chromosome segregation [235], however, cells in stretched monolayers never failed mitosis. Cell rounding is known to produce considerable force [233] and can even contribute to tissue buckling [59] during morphogenesis. Here, however, the force required to deform the surrounding tissue enough to completely round the cell was clearly more than the cells could generate. The experimental system may therefore provide an opportunity to study the limits and dynamics of the osmotic and actomyosin based forces generated by the cell, which have been examined in detail in single cells [233] but not in tissues.

During anaphase, cells in stretched and non-stretched monolayers elongated dramatically (Fig. 6.1B (ii) and 6.3A). The lack of dependence of this feature on tissue stretch suggests it is robustly controlled in a cell-autonomous manner. This is in agreement with previous studies which demonstrated that equatorial recruitment of Rho-kinase and myosin II promotes anaphase elongation prior to and partly independently from furrowing onset [302]. Polar relaxation also contributes to shape changes in *Drosophila* cells at this time point, via inactivation of ezrin/radixin/moesin proteins at cell poles by kinetochore-

localised PP1-Sds22 [299]. The lack of effect of tissue tension on the shape changes controlled by these cell-autonomous process may be due to the high cell stiffness at this point [303, 304]. Indeed, after division, when cells would be expected to return to normal interphase levels of stiffness, a difference between the non-stretched and stretched tissues became clear: daughter cells in stretched tissues elongate in the orientation of stretch whereas cells in non-stretched tissues remained unchanged (Fig. 6.1A (iii) and 6.5A).

The overall increase in length and decrease in width of the cell mass envelope, between 50 minutes before and 50 minutes after division, in stretched, non-stretched and compressed tissues (6.3A and B and 6.6B and C), resulted in a significant redistribution of the mother cell mass in the direction of the division. This induced a small but nevertheless equivalent deformation on the surrounding tissue (Fig. 6.4). Although the overall effect of a single oriented division on the tissue was modest, in many developing tissues cells may undergo many rounds of division during morphogenesis, so altogether a large effect could be produced if the deformations measured here are additive. Indeed, a subsequent round of divisions in the stretched tissue is predicted to orient in the same direction since the interphase shape of daughter cells in stretched monolayers remained slightly elongated in the orientation of stretch (Fig. 6.5C). In contrast, the daughter cells in non-stretched tissues had an aspect ratio oriented 90° to the mother cell shape, meaning that a second division would be predicted to orient perpendicular to the first, as is commonly seen in the first few divisions of early embryos. Overall, the initial random orientation of the cell shapes in non-stretched cells means that the mass redistribution caused by the divisions can have no net directional effect. However, cell divisions are aligned by the application of stretch and so the redistribution of mass is also aligned giving the possibility of tissue-scale elongation. It is tempting, therefore, to draw comparisons between this and the elongated clones caused by oriented divisions in the fly wing [148]. Technical limitations restricted the length of our experiments, meaning that larger scale deformations that may be caused by the sum effect of a large number of divisions were not attainable in the current setup.

Overcoming these limitations should be a key target for future developments.

Computational simulations which modelled the monolayers using a validated mechanical framework were able to reproduce the pattern of experimentally measured shape changes in both stretched and non-stretched monolayers without requiring differences in cell behaviour (section 6.8). Altogether, therefore, this draws a simple picture in which cells in both stretched and non-stretched tissues generate similar rounding forces, orient their spindle to their interphase long axis, redistribute the mother cell's mass upon division and then return to their original interphase stiffness (Fig. 6.10). Despite this identical behaviour at the local cell level, the alignment of cell long axes in stretched monolayers causes a net flow of cell mass in the direction of stretch, whereas no net change is produced in non-stretched monolayers (Fig. 6.11).

Chapter 7

Discussion and future directions

This thesis has sought to better understand the response of epithelial tissues to extrinsically imposed deformation. Such deformations are ubiquitous at every stage of metazoan life, whether it is during the gastrulation of every eumetazoan embryo or during a peristaltic contraction in a labrador. Epithelia are a natural choice of tissue class to focus on. While many epithelia are structurally simple, they take a leading role during embryonic morphogenesis and perform a remarkable range of crucial functions during adult life. Unlike much of an animal's nervous tissue, for instance, which lives shielded from deformation by a skull or vertebra, epithelia are often found at locations that experience the most extreme mechanical activity, such as the skin, lungs, blood vessels and the digestive system. How is it that epithelia, in so many disparate settings, can so robustly maintain structure and function in the face of extrinsically applied deformations of such varied natures?

Throughout this thesis, this question has been tackled via a reductionist approach: the highly simplified model system of suspended epithelial monolayers has been the central tool. By taking the epithelium out of the context of the mechanically and biochemically complex environment of an organism, the response of the tissue to deformation could be studied in a relatively isolated setting which provided a uniquely clear picture. With this

tool, the above question has led to the study of two phenomena which were observed in suspended epithelia upon deformation. In the first, epithelia were unexpectedly found to possess the ability to rapidly and autonomously adjust their length to flatten buckles in the tissue, which were formed by tissue compression. As they flattened, tissues underwent a reversible change in mechanical properties which was suggestive of adaptation to the new length. In the second process, cell division was found to be globally oriented by the application of either compression or stretch. Each cell division was found to redistribute the mother cell mass along the axis of division, regardless of tissue context, both in stretched and compressed tissues. Where global deformation had created highly anisotropic cells, the oriented cell divisions homeostatically restored cells to a more isotropic shape. Chapters 4, 5 and 6, which present these studies, contain their own detailed discussions relating to the findings. Here, some final remarks are made on the most important unresolved questions which have arisen and some specific suggestions are made as to how they could be addressed.

7.1 Tissue self-flattening after compression

Tissue self-flattening in response to compression-induced buckling was an unexpected phenomenon and as such, has given rise to many more questions than could be addressed here. Indeed, while the results have linked the process to a constitutive actomyosin tension, the results presented here are mainly descriptive. It remains to be determined how the tissue can undergo such a drastic change in shape and structure so rapidly and how this could be choreographed at the sub-cellular scale. Here, two avenues which may be particularly productive are briefly described.

Firstly, it is noted that, during the application of strain at a low strain rate, the change in behaviour between the monolayer remaining flat and buckling is quite abrupt (Fig. 4.4B). There appears to be something about the state of the tissue after $\sim$40% compression which causes it to suddenly stop being able to reduce its own length - so that further strain results

in buckling, rather than shortening. It would be interesting to investigate whether this transition can be linked to a geometric property of the constituent cells. For instance, cells may have reached a height, width or apical area which is in some way the preferred value. On the other hand, it may be the magnitude of change which is the limiting factor. To test this, monolayers can be grown to different cell densities and the experiment can be repeated. It may be found that the point at which the transition occurs will shift according to the initial shape of cells. In that case the shape of the cells at the different transition points can be compared to see if they share anything in common. It may also be useful to consider cell nuclei in regard to this question, since the transition point may occur when the nuclei (which are known to be particularly stiff) have been deformed by a maximal amount. It may be possible to genetically perturb the nuclear lamina, in order to soften the nucleus, to see if this allows flattening at greater compressive strains.

Secondly, now that the timescale of length adaptation has been approximately determined (Fig. 4.19), it will be important to establish what physical processes lead to adaptation. What is it that causes the tissue to flatten much faster during the second compression? And what changes in the tissue during the 60-180 seconds in which the adaptation is reversed? Cell-cell junctions, the cytoskeleton and the nuclei are all good candidates for initial investigations. It may be possible to slow the rate at which cell-cell junctions can change in size by treatment of the tissues with factors such as calcium chelators at an appropriate concentration. Similarly, it would be interesting to test whether cytoskeletal drugs which inhibit turnover of the actin or microtubule cytoskeleton have any affect on the rate of length adaptation. The challenge will be to find perturbations which alter adaptation without affecting tissue self-flattening. They cannot be precisely the same process but they may be intimately linked.

7.2 Oriented division induced by tissue strain

Perhaps the most interesting question which arose from chapters 5 and 6 was how cells could remember their interphase shape throughout mitosis. While many cells in stretched tissues maintained some degree of a long cell axis throughout metaphase and so would not require such a memory, many cells appeared entirely isotropic at metaphase without their capacity to orient division along their interphase long axis being perturbed (Fig. 6.6A). This was particularly clear in tissues subjected to a compressive strain, which clearly yielded shapes with aspect ratios very close to 1 but which still managed to align division to the original interphase long axis (Fig. 5.11B and C).

A recent study in the *Drosophila* notum [305] has demonstrated one mechanism which can act as just such a memory. Here, the protein Mud (the *Drosophila* homologue of NuMA), localises to tri-cellular junctions during G2 interphase and throughout mitosis and allows for the generation of pulling forces on the spindle from these locations. In elongated cells, the vertices tend to be arranged such that there are more vertices at either end of the cell long axis than in the mid region. Since this pattern is not entirely lost upon rounding, a torque is produced on the spindle when it is not aligned to the interphase long axis.

It will be important to determine whether such a mechanism may work in mammalian cells such as MDCK. However, a direct comparison cannot be made immediately since NuMA localisation throughout the cell cycle is significantly different in mammalian cells. In MDCK, NuMA is maintained within the nucleus throughout interphase and is only released into the cytoplasm at nuclear envelope breakdown [127]. Once released, in MDCK NuMA localises to entire cell-cell junctions rather than just the tri-cellular junctions. While NuMA does appear to be polarised in elongated cells [306], how this polarisation is established is unknown. This does not preclude a tri-cellular junction based mechanism for interphase shape memory. NuMA could, for instance, only become activated at tri-cellular junctions. However, the cell-polarised localisation across entire junctions

suggests a different mechanism may be at play. A crucial next step, therefore, will be to characterise the precise timings of the relocalisation of NuMA and the establishment of polarity. Characterising the same for NuMA's binding partners Gα_i and LGN will also be informative. From this point, the route to investigating how shape is measured and remembered will depend strongly on which proteins go where and when. Once again, the simplified system of suspended monolayers represents a particularly good system in which to explore this, since the localisation of these proteins can be observed while imposing cell shape changes in real time. It is likely that compressed tissues would be an easier environment in which to explore the question of interphase shape memory, since cells are able to round up more completely.

A second, quite different direction which could be productive would be to use the suspended monolayers to explore in more detail the changes in stiffness which occur during mitosis. Chapter 6 highlighted the importance of understanding such mechanical changes, since the recapitulation of shape evolution within the computational model required several assumptions which haven't been tested experimentally. While these mechanical changes have been well characterised in single cells [233], the tissue environment is much more relevant. Indeed, it is likely that the purpose of the rounding force is at least in part to shield against forces from the surrounding tissue, so that a mechanically insulated environment is created in which to execute orderly division.

To this end, as a final unfinished part of this study, the experimental system was modified so that a single dividing cell could be imaged during the application of an oscillatory strain to the host tissue. By tracking the strain of the dividing cell throughout the cycle, the relative stiffness of the dividing strain could be determined via comparison to the strain in cells of the surrounding tissue. Preliminary results showed an approximately six-fold increase in stiffness which was, as expected, myosin dependent. This technique would be particularly useful if it can be used continuously through mitosis to reveal the dynamics of stiffness changes.

Bibliography

[1] Frederik Ruysch. *Thesaurus anatomicus tertius [...].* apud J. Wolters, 1703.

[2] David R. Burgess. Morphogenesis of intestinal villi: Ii. mechanism of formation of previllous ridges. *Journal of Embryology and Experimental Morphology*, 34(3):723–740, 1975.

[3] Amanda M. Marchiando, W. Vallen Graham, and Jerrold R. Turner. Epithelial barriers in homeostasis and disease. *Annual Review of Pathology: Mechanisms of Disease*, 5(1):119–144, 2010. PMID: 20078218.

[4] Scott A. Nichols, William Dirks, John S. Pearse, and Nicole King. Early evolution of animal cell signaling and adhesion genes. *Proceedings of the National Academy of Sciences*, 103(33):12451–12456, 2006.

[5] Daniel J. Dickinson, W. James Nelson, and William I. Weis. A polarized epithelium organized by Îš- and Îś-catenin predates cadherin and metazoan origins. *Science*, 331(6022):1336–1339, 2011.

[6] Monika Abedin and Nicole King. The premetazoan ancestry of cadherins. *Science*, 319(5865):946–948, 2008.

[7] Albert B. Reynolds. Epithelial organization: New perspective on Îś-catenin from an ancient source. *Current Biology*, 21(11):R430 – R432, 2011.

[8] Enrique Rodriguez-Boulan and Ian G. Macara. Organization and execution of the epithelial polarity programme. *Nat Rev Mol Cell Biol*, 15(4):225–242, 04 2014.

[9] Chris Q. Doe. Cell polarity: the party expands. *Nat Cell Biol*, 3(1):E7–E9, 01 2001.

[10] David Bilder, Min Li, and Norbert Perrimon. Cooperative regulation of cell polarity and growth by drosophila tumor suppressors. *Science*, 289(5476):113–116, 2000.

[11] Yang Hong, Beth Stronach, Norbert Perrimon, Lily Yeh Jan, and Yuh Nung Jan. Drosophila stardust interacts with crumbs to control polarity of epithelia but not neuroblasts. *Nature*, 414(6864):634–638, 12 2001.

[12] Patrick Laprise, Kimberly M. Lau, Kathryn P. Harris, Nancy F. Silva-Gagliardi, Sarah M. Paul, Slobodan Beronja, Greg J. Beitel, C. Jane McGlade, and Ulrich Tepass. Yurt, coracle, neurexin iv and the na+,k+-atpase form a novel group of epithelial polarity proteins. *Nature*, 459(7250):1141–1145, 06 2009.

[13] Aron B. Jaffe and Alan Hall. Rho gtpases: Biochemistry and biology. *Annual Review of Cell and Devel-*

opmental Biology, 21(1):247–269, 2005. PMID: 16212495.

[14] Tomoyuki Yamanaka, Yosuke Horikoshi, Yuki Sugiyama, Chikako Ishiyama, Atsushi Suzuki, Tomonori Hirose, Akihiro Iwamatsu, Azusa Shinohara, and Shigeo Ohno. Mammalian lgl forms a protein complex with par-6 and apkc independently of par-3 to regulate epithelial cell polarity. *Current Biology*, 13(9):734 – 743, 2003.

[15] Toby W. Hurd, Lin Gao, Michael H. Roh, Ian G. Macara, and Ben Margolis. Direct interaction of two polarity complexes implicated in epithelial tight junction assembly. *Nat Cell Biol*, 5(2):137–142, 02 2003.

[16] Ama Gassama-Diagne, Wei Yu, Martin ter Beest, Fernando Martin-Belmonte, Arlinet Kierbel, Joanne Engel, and Keith Mostov. Phosphatidylinositol-3,4,5-trisphosphate regulates the formation of the basolateral plasma membrane in epithelial cells. *Nat Cell Biol*, 8(9):963–970, 09 2006.

[17] Fernando Martin-Belmonte, Ama Gassama, Anirban Datta, Wei Yu, Ursula Rescher, Volker Gerke, and Keith Mostov. Pten-mediated apical segregation of phosphoinositides controls epithelial morphogenesis through cdc42. *Cell*, 128(2):383 – 397, 2007.

[18] W James Nelson. Remodeling epithelial cell organization: Transitions between front–rear and apical–basal polarity. *Cold Spring Harbor Perspectives in Biology*, 1(1):a000513, 07 2009.

[19] Akihiko Saito, Hiroyoshi Sato, Noriaki Iino, and Tetsuro Takeda. Molecular mechanisms of receptor-mediated endocytosis in the renal proximal tubular epithelium. *J Biomed Biotechnol*, 2010:403272, 2010.

[20] Marios Georgiou, Eliana Marinari, Jemima Burden, and Buzz Baum. Cdc42, par6, and apkc regulate arp2/3-mediated endocytosis to control local adherens junction stability. *Current Biology*, 18(21):1631 – 1638, 2008.

[21] Ravi A. Desai, Lin Gao, Srivatsan Raghavan, Wendy F. Liu, and Christopher S. Chen. Cell polarity triggered by cell-cell adhesion via e-cadherin. *Journal of Cell Science*, 122(7):905–911, 2009.

[22] Ceniz Zihni, Maria S. Balda, and Karl Matter. Signalling at tight junctions during epithelial differentiation and microbial pathogenesis. *Journal of Cell Science*, 127(16):3401–3413, 2014.

[23] Kunyoo Shin, Vanessa C. Fogg, and Ben Margolis. Tight junctions and cell polarity. *Annual Review of Cell and Developmental Biology*, 22(1):207–235, 2006. PMID: 16771626.

[24] Masatoshi Takeichi. Dynamic contacts: rearranging adherens junctions to drive epithelial remodelling. *Nat Rev Mol Cell Biol*, 15(6):397–410, 06 2014.

[25] Nicolas Borghi, Maria Sorokina, Olga G. Shcherbakova, William I. Weis, Beth L. Pruitt, W. James Nelson, and Alexander R. Dunn. E-cadherin is under constitutive actomyosin-generated tension that is increased at cell–cell contacts upon externally applied stretch. *Proceedings of the National Academy of Sciences*, 109(31):12568–12573, 2012.

[26] Andrew R. Harris, Alicia Daeden, and Guillaume T. Charras. Formation of adherens junctions leads to

the emergence of a tissue-level tension in epithelial monolayers. *Journal of Cell Science*, 127(11):2507–2517, 2014.

[27] Shigenobu Yonemura, Yuko Wada, Toshiyuki Watanabe, Akira Nagafuchi, and Mai Shibata. a-catenin as a tension transducer that induces adherens junction development. *Nat Cell Biol*, 12(6):533–542, 06 2010.

[28] Quint le Duc, Quanming Shi, Iris Blonk, Arnoud Sonnenberg, Ning Wang, Deborah Leckband, and Johan de Rooij. Vinculin potentiates e-cadherin mechanosensing and is recruited to actin-anchored sites within adherens junctions in a myosin ii–dependent manner. *The Journal of cell biology*, 189(7):1107–1115, 2010.

[29] Noboru Ishiyama, Nobutoshi Tanaka, Kentaro Abe, Yoo Jeong Yang, Yazan M. Abbas, Masataka Umitsu, Bhushan Nagar, Stephanie A. Bueler, John L. Rubinstein, Masatoshi Takeichi, and Mitsuhiko Ikura. An autoinhibited structure of Îś-catenin and its implications for vinculin recruitment to adherens junctions. *Journal of Biological Chemistry*, 288(22):15913–15925, 2013.

[30] Jodi L. Johnson, Nicole A. Najor, and Kathleen J. Green. Desmosomes: Regulators of cellular signaling and adhesion in epidermal health and disease. *Cold Spring Harbor Perspectives in Medicine*, 4(11), 2014.

[31] Emmanuella Delva, Dana K. Tucker, and Andrew P. Kowalczyk. The desmosome. *Cold Spring Harbor Perspectives in Biology*, 1(2), 2009.

[32] Nargess Khalilgharibi, Jonathan Fouchard, Pierre Recho, Guillaume Charras, and Alexandre Kabla. The dynamic mechanical properties of cellularised aggregates. *Current Opinion in Cell Biology*, 42:113 – 120, 2016. Cell dynamics.

[33] Joshua A. Broussard, Spiro Getsios, and Kathleen J. Green. Desmosome regulation and signaling in disease. *Cell and Tissue Research*, 360(3):501–512, 2015.

[34] W. Howard Evans and Patricia E. M. Martin. Gap junctions: structure and function (review). *Molecular Membrane Biology*, 19(2):121–136, 2002.

[35] Cell Culture Collection Committee., American Type Culture Collection., United States., and Public Health Service. Registry of animal cell lines certified by the cell culture collection committee. *Registry of animal cell lines*, 1964.

[36] S. H. Madin and N. B. Darby. Established kidney cell lines of normal adult bovine and ovine origin. *Experimental Biology and Medicine*, 98(3):574–576, 1958.

[37] David D Sabatini. In awe of subcellular complexity: 50 years of trespassing boundaries within the cell. *Annu. Rev. Cell Dev. Biol.*, 21:1–33, 2005.

[38] M Cereijido, ES Robbins, WJ Dolan, CA Rotunno, and DD Sabatini. Polarized monolayers formed by epithelial cells on a permeable and translucent support. *The Journal of cell biology*, 77(3):853–880, 1978.

[39] D Louvard. Apical membrane aminopeptidase appears at site of cell-cell contact in cultured kidney epithelial cells. *Proceedings of the National Academy of Sciences*, 77(7):4132–4136, 1980.

[40] Joseph Leighton, Larry W. Estes, Sunder Mansukhani, and Zbynek Brada. A cell line derived from normal dog kidney (mdck) exhibiting qualities of papillary adenocarcinoma and of renal tubular epithelium. *Cancer*, 26(5):1022–1028, 1970.

[41] Q. Bao and R.C. Hughes. Galectin-3 expression and effects on cyst enlargement and tubulogenesis in kidney epithelial mdck cells cultured in three-dimensional matrices in vitro. *Journal of Cell Science*, 108(8):2791–2800, 1995.

[42] James A. McAteer, Andrew P. Evan, and Kenneth D. Gardner. Morphogenetic clonal growth of kidney epithelial cell line mdck. *The Anatomical Record*, 217(3):229–239, 1987.

[43] S Reinsch and E Karsenti. Orientation of spindle axis and distribution of plasma membrane proteins during cell division in polarized mdckii cells. *The Journal of Cell Biology*, 126(6):1509–1526, 1994.

[44] P Boukamp, R T Petrussevska, D Breitkreutz, J Hornung, A Markham, and N E Fusenig. Normal keratinization in a spontaneously immortalized aneuploid human keratinocyte cell line. *The Journal of Cell Biology*, 106(3):761–771, 1988.

[45] Adeline F. Deyrieux and V. G. Wilson. In vitro culture conditions to study keratinocyte differentiation using the hacat cell line. *Cytotechnology*, 54(2):77–83, 2007.

[46] Dawn Walker, Tao Sun, Sheila MacNeil, and Rod Smallwood. Modeling the effect of exogenous calcium on keratinocyte and hacat cell proliferation and differentiation using an agent-based computational paradigm. *Tissue Eng*, 12(8):2301–2309, Aug 2006.

[47] Daniel D Bikle, Zhongjian Xie, and Chia-Ling Tu. Calcium regulation of keratinocyte differentiation. *Expert review of endocrinology & metabolism*, 7(4):461–472, 07 2012.

[48] V M Schoop, N Mirancea, and N E Fusenig. Epidermal organization and differentiation of hacat keratinocytes in organotypic coculture with human dermal fibroblasts. *J Invest Dermatol*, 112(3):343–353, Mar 1999.

[49] K Araki-Sasaki, Y Ohashi, T Sasabe, K Hayashi, H Watanabe, Y Tano, and H Handa. An sv40-immortalized human corneal epithelial cell line and its characterization. *Invest Ophthalmol Vis Sci*, 36(3):614–621, Mar 1995.

[50] Herbert D. Soule, Terry M. Maloney, Sandra R. Wolman, Ward D. Peterson, Richard Brenz, Charles M. McGrath, Jose Russo, Robert J. Pauley, Richard F. Jones, and S. C. Brooks. Isolation and characterization of a spontaneously immortalized human breast epithelial cell line, mcf-10. *Cancer Research*, 50(18):6075–6086, 1990.

[51] Pedro Campinho, Martin Behrndt, Jonas Ranft, Thomas Risler, Nicolas Minc, and Carl-Philipp Heisen-

berg. Tension-oriented cell divisions limit anisotropic tissue tension in epithelial spreading during zebrafish epiboly. *Nat Cell Biol*, 15(12):1405–1414, 12 2013.

[52] Ginger L. Hunter, Janice M. Crawford, Julian Z. Genkins, and Daniel P. Kiehart. Ion channels contribute to the regulation of cell sheet forces during drosophila dorsal closure. *Development*, 141(2):325–334, 2014.

[53] Eliana Marinari, Aida Mehonic, Scott Curran, Jonathan Gale, Thomas Duke, and Buzz Baum. Live-cell delamination counterbalances epithelial growth to limit tissue overcrowding. *Nature*, 484(7395):542–545, 04 2012.

[54] Mette Christine Jørgensen, Jonas Ahnfelt-Rønne, Jacob Hald, Ole D. Madsen, Palle Serup, and Jacob Hecksher-Sørensen. An illustrated review of early pancreas development in the mouse. *Endocrine Reviews*, 28(6):685–705, 2007. PMID: 17881611.

[55] Madeleine Durbeej and Peter Ekblom. Dystroglycan and laminins: Glycoconjugates involved in branching epithelial morphogenesis. *Experimental Lung Research*, 23(2):109–118, 1997.

[56] Irma Thesleff. Epithelial-mesenchymal signalling regulating tooth morphogenesis. *Journal of Cell Science*, 116(9):1647–1648, 2003.

[57] Stephen Meier. Development of the embryonic chick otic placode. i. light microscopic analysis. *The Anatomical Record*, 191(4):447–458, 1978.

[58] Luis M. Escudero, Marcus Bischoff, and Matthew Freeman. Myosin ii regulates complex cellular arrangement and epithelial architecture in drosophila. *Developmental Cell*, 13(5):717 – 729, 2007.

[59] Takefumi Kondo and Shigeo Hayashi. Mitotic cell rounding accelerates epithelial invagination. *Nature*, 494(7435):125–129, 02 2013.

[60] Daryl D. Hurd and Kenneth J. Kemphues. Par-1 is required for morphogenesis of the caenorhabditis elegans vulva. *Developmental Biology*, 253(1):54 – 65, 2003.

[61] Bharesh K. Chauhan, Ming Lou, Yi Zheng, and Richard A. Lang. Balanced rac1 and rhoa activities regulate cell shape and drive invagination morphogenesis in epithelia. *Proceedings of the National Academy of Sciences*, 108(45):18289–18294, 2011.

[62] Yanmei Qi, Xiaoxiang Tian, Jie Liu, Yaling Han, Alan M. Graham, M. Celeste Simon, Josef M. Penninger, Peter Carmeliet, and Shaohua Li. Bnip3 and aif cooperate to induce apoptosis and cavitation during epithelial morphogenesis. *The Journal of Cell Biology*, 198(1):103–114, 2012.

[63] Amy E. Shyer, Tuomas Tallinen, Nandan L. Nerurkar, Zhiyan Wei, Eun Seok Gil, David L. Kaplan, Clifford J. Tabin, and L. Mahadevan. Villification: How the gut gets its villi. *Science*, 342(6155):212–218, 2013.

[64] Silvia Aldaz, Luis M. Escudero, and Matthew Freeman. Live imaging of drosophila imaginal disc devel-

opment. *Proceedings of the National Academy of Sciences*, 107(32):14217–14222, 2010.

[65] James W. Fristrom, Dianne K. Fristrom, Eva Fekete, and Andrew H. Kuniyuki. The mechanism of evagination of imaginal discs of drosophila melanogaster. *American Zoologist*, 17(3):671–684, 1977.

[66] Jose Carlos Pastor-Pareja, Ferdinand Grawe, Enrique Martin-Blanco, and Antonio Garcia-Bellido. Invasive cell behavior during drosophila imaginal disc eversion is mediated by the jnk signaling cascade signaling cascade. *Developmental Cell*, 7(3):387 – 399, 2004.

[67] Raphaël Etournay, Marko Popović, Matthias Merkel, Amitabha Nandi, Corinna Blasse, Benoît Aigouy, Holger Brandl, Gene Myers, Guillaume Salbreux, Frank Jülicher, and Suzanne Eaton. Interplay of cell dynamics and epithelial tension during morphogenesis of the drosophila pupal wing. *eLife*, 4, 2015.

[68] Robert P. Ray, Alexis Matamoro-Vidal, Paulo S. Ribeiro, Nic Tapon, David Houle, Isaac Salazar-Ciudad, and Barry J. Thompson. Patterned anchorage to the apical extracellular matrix defines tissue shape in the developing appendages of drosophila. *Developmental Cell*, 34(3):310 – 322, 2015.

[69] Claudio Collinet, Matteo Rauzi, Pierre-Francois Lenne, and Thomas Lecuit. Local and tissue-scale forces drive oriented junction growth during tissue extension. *Nat Cell Biol*, 17(10):1247–1258, 10 2015.

[70] Stephanie Höhn, Aurelia R. Honerkamp-Smith, Pierre A. Haas, Philipp Khuc Trong, and Raymond E. Goldstein. Dynamics of a *Volvox* embryo turning itself inside out. *Phys. Rev. Lett.*, 114:178101, Apr 2015.

[71] Iain R Aitchison. The holiverse: holistic eversion of the 2-sphere in r3. *arXiv preprint arXiv:1008.0916*, 2010.

[72] Adam C. Martin, Matthias Kaschube, and Eric F. Wieschaus. Pulsed contractions of an actin-myosin network drive apical constriction. *Nature*, 457(7228):495–499, 01 2009.

[73] G. Wayne Brodland, Vito Conte, P. Graham Cranston, Jim Veldhuis, Sriram Narasimhan, M. Shane Hutson, Antonio Jacinto, Florian Ulrich, Buzz Baum, and Mark Miodownik. Video force microscopy reveals the mechanics of ventral furrow invagination in drosophila. *Proceedings of the National Academy of Sciences*, 107(51):22111–22116, 2010.

[74] Oleg Polyakov, Bing He, Michael Swan, Joshua W. Shaevitz, Matthias Kaschube, and Eric Wieschaus. Passive mechanical forces control cell-shape change during drosophila ventral furrow formation. *Biophysical Journal*, 107(4):998 – 1010, 2014.

[75] Sergio de Matos Simoes, Avantika Mainieri, and Jennifer A. Zallen. Rho gtpase and shroom direct planar polarized actomyosin contractility during convergent extension. *The Journal of Cell Biology*, 204(4):575–589, 2014.

[76] Matteo Rauzi, Pascale Verant, Thomas Lecuit, and Pierre-Francois Lenne. Nature and anisotropy of cortical forces orienting drosophila tissue morphogenesis. *Nat Cell Biol*, 10(12):1401–1410, 12 2008.

[77] Karen E. Kasza, Dene L. Farrell, and Jennifer A. Zallen. Spatiotemporal control of epithelial remodeling

by regulated myosin phosphorylation. *Proceedings of the National Academy of Sciences*, 111(32):11732–11737, 2014.

[78] Masako Tamada, Dene L. Farrell, and Jennifer A. Zallen. Abl regulates planar polarized junctional dynamics through Îš-catenin tyrosine phosphorylation. *Developmental Cell*, 22(2):309 – 319, 2012.

[79] Jennifer A Zallen and Eric Wieschaus. Patterned gene expression directs bipolar planar polarity in drosophila. *Developmental Cell*, 6(3):343 – 355, 2004.

[80] Adam C. Pare, Athea Vichas, Christopher T. Fincher, Zachary Mirman, Dene L. Farrell, Avantika Mainieri, and Jennifer A. Zallen. A positional toll receptor code directs convergent extension in drosophila. *Nature*, 515(7528):523–527, 11 2014.

[81] Thomas P Neufeld, Aida Flor A de la Cruz, Laura A Johnston, and Bruce A Edgar. Coordination of growth and cell division in the drosophila wing why did you even bother looking. *Cell*, 93(7):1183 – 1193, 1998.

[82] Ortrud Wartlick, Peer Mumcu, Frank Jülicher, and Marcos Gonzalez-Gaitan. Understanding morphogenetic growth control —lessons from flies. *Nat Rev Mol Cell Biol*, 12(9):594–604, 09 2011.

[83] Yun Fan and Andreas Bergmann. Distinct mechanisms of apoptosis-induced compensatory proliferation in proliferating and differentiating tissues in the drosophila eye. *Developmental Cell*, 14(3):399 – 410, 2008.

[84] George T. Eisenhoffer, Patrick D. Loftus, Masaaki Yoshigi, Hideo Otsuna, Chi-Bin Chien, Paul A. Morcos, and Jody Rosenblatt. Crowding induces live cell extrusion to maintain homeostatic cell numbers in epithelia. *Nature*, 484(7395):546–549, 04 2012.

[85] Laure Saias, Jim Swoger, Arturo D'Angelo, Peran Hayes, Julien Colombelli, James Sharpe, Guillaume Salbreux, and Jérôme Solon. Decrease in cell volume generates contractile forces driving dorsal closure. *Developmental Cell*, 33(5):611 – 621, 2015.

[86] Bruno Monier, Melanie Gettings, Guillaume Gay, Thomas Mangeat, Sonia Schott, Ana Guarner, and Magali Suzanne. Apico-basal forces exerted by apoptotic cells drive epithelium folding. *Nature*, 518(7538):245–248, 02 2015.

[87] Claire M. Lye, Guy B. Blanchard, Huw W. Naylor, Leila Muresan, Jan Huisken, Richard J. Adams, and Bénédicte Sanson. Mechanical coupling between endoderm invagination and axis extension in <italic>drosophila</italic>. *PLoS Biol*, 13(11):e1002292, 11 2015.

[88] Jacob L Fisher, Irena Levitan, and Susan S Margulies. Plasma membrane surface increases with tonic stretch of alveolar epithelial cells. *American journal of respiratory cell and molecular biology*, 31(2):200–208, 2004.

[89] Esra Roan and Christopher M Waters. What do we know about mechanical strain in lung alveoli?

American Journal of Physiology - Lung Cellular and Molecular Physiology, 301(5):L625–L635, 11 2011.

[90] Andrew R. Harris, Loic Peter, Julien Bellis, Buzz Baum, Alexandre J. Kabla, and Guillaume T. Charras. Characterizing the mechanics of cultured cell monolayers. *Proceedings of the National Academy of Sciences*, 2012.

[91] Laura Casares, Romaric Vincent, Dobryna Zalvidea, Noelia Campillo, Daniel Navajas, Marino Arroyo, and Xavier Trepat. Hydraulic fracture during epithelial stretching. *Nat Mater*, 14(3):343–351, 03 2015.

[92] Xavier Trepat, Mireia Grabulosa, Ferranda Puig, Geoffrey N. Maksym, Daniel Navajas, and Ramon Farré. Viscoelasticity of human alveolar epithelial cells subjected to stretch. *American Journal of Physiology - Lung Cellular and Molecular Physiology*, 287(5):L1025–L1034, 2004.

[93] Marco Fritzsche, Alexandre Lewalle, Tom Duke, Karsten Kruse, and Guillaume Charras. Analysis of turnover dynamics of the submembranous actin cortex. *Molecular Biology of the Cell*, 24(6):757–767, 2013.

[94] Jakub Sedzinski, Mate Biro, Annelie Oswald, Jean-Yves Tinevez, Guillaume Salbreux, and Ewa Paluch. Polar actomyosin contractility destabilizes the position of the cytokinetic furrow. *Nature*, 476(7361):462–466, 08 2011.

[95] P. F. Machado, G. B. Blanchard, J. Duque, and N. Gorfinkiel. Cytoskeletal turnover and myosin contractility drive cell autonomous oscillations in a model of drosophila dorsal closure. *The European Physical Journal Special Topics*, 223(7):1391–1402, 2014.

[96] R. M. Hicks. The fine structure of the transitional epithelium of rat ureter. *The Journal of Cell Biology*, 26(1):25–48, 1965.

[97] Simon A. Lewis. Everything you wanted to know about the bladder epithelium but were afraid to ask. *American Journal of Physiology - Renal Physiology*, 278(6):F867–F874, 2000.

[98] BD Minsky and FJ Chlapowski. Morphometric analysis of the translocation of lumenal membrane between cytoplasm and cell surface of transitional epithelial cells during the expansion-contraction cycles of mammalian urinary bladder. *The Journal of Cell Biology*, 77(3):685–697, 1978.

[99] Stephen N. Sarikas and Francis J. Chlapowski. Effect of atp inhibitors on the translocation of luminal membrane between cytoplasm and cell surface of transitional epithelial cells during the expansion-contraction cycle of the rat urinary bladder. *Cell and Tissue Research*, 246(1):109–117, 1986.

[100] Mingxi Yao, Benjamin T. Goult, Hu Chen, Peiwen Cong, Michael P. Sheetz, and Jie Yan. Mechanical activation of vinculin binding to talin locks talin in an unfolded conformation. *Scientific Reports*, 4:4610 EP –, 04 2014.

[101] Sergei Sukharev and Frederick Sachs. Molecular force transduction by ion channels: diversity and unifying principles. *J Cell Sci*, 125(Pt 13):3075–3083, Jul 2012.

[102] Akiko Mammoto, Tadanori Mammoto, and Donald E. Ingber. Mechanosensitive mechanisms in transcriptional regulation. *Journal of Cell Science*, 125(13):3061–3073, 2012.

[103] Viola Vogel and Michael Sheetz. Local force and geometry sensing regulate cell functions. *Nat Rev Mol Cell Biol*, 7(4):265–275, 04 2006.

[104] Michele A. Wozniak and Christopher S. Chen. Mechanotransduction in development: a growing role for contractility. *Nat Rev Mol Cell Biol*, 10(1):34–43, 01 2009.

[105] Craig D. Buckley, Jiongyi Tan, Karen L. Anderson, Dorit Hanein, Niels Volkmann, William I. Weis, W. James Nelson, and Alexander R. Dunn. The minimal cadherin-catenin complex binds to actin filaments under force. *Science*, 346(6209), 2014.

[106] Brian C. DiPaolo and Susan S. Margulies. Rho kinase signaling pathways during stretch in primary alveolar epithelia. *American Journal of Physiology - Lung Cellular and Molecular Physiology*, 302(10):L992–L1002, 2012.

[107] Rodrigo Fernandez-Gonzalez, Sergio de Matos Simoes, Jens-Christian Roper, Suzanne Eaton, and Jennifer A. Zallen. Myosin ii dynamics are regulated by tension in intercalating cells. *Developmental Cell*, 17(5):736 – 743, 2009.

[108] Jocelyn Etienne, Jonathan Fouchard, Demosthene Mitrossilis, Nathalie Bufi, Pauline Durand-Smet, and Atef Asnacios. Cells as liquid motors: Mechanosensitivity emerges from collective dynamics of actomyosin cortex. *Proceedings of the National Academy of Sciences*, 112(9):2740–2745, 2015.

[109] Fengzhu Xiong, Wenzhe Ma, Tom W. Hiscock, Kishore R. Mosaliganti, Andrea R. Tentner, Kenneth A. Brakke, Nicolas Rannou, Arnaud Gelas, Lydie Souhait, Ian A. Swinburne, Nikolaus D. Obholzer, and Sean G. Megason. Interplay of cell shape and division orientation promotes robust morphogenesis of developing epithelia. *Cell*, 159(2):415 – 427, 2014.

[110] Clotilde Cadart, Ewa Zlotek-Zlotkiewicz, Maël Le Berre, Matthieu Piel, and Helen K. Matthews. Exploring the function of cell shape and size during mitosis. *Developmental Cell*, 29(2):159–169, 2014/06/09 2014.

[111] Sean Porazinski, Huijia Wang, Yoichi Asaoka, Martin Behrndt, Tatsuo Miyamoto, Hitoshi Morita, Shoji Hata, Takashi Sasaki, S. F. Gabriel Krens, Yumi Osada, Satoshi Asaka, Akihiro Momoi, Sarah Linton, Joel B. Miesfeld, Brian A. Link, Takeshi Senga, Atahualpa Castillo-Morales, Araxi O. Urrutia, Nobuyoshi Shimizu, Hideaki Nagase, Shinya Matsuura, Stefan Bagby, Hisato Kondoh, Hiroshi Nishina, Carl-Philipp Heisenberg, and Makoto Furutani-Seiki. Yap is essential for tissue tension to ensure vertebrate 3d body shape. *Nature*, 521(7551):217–221, 05 2015.

[112] G Goldspink. Changes in muscle mass and phenotype and the expression of autocrine and systemic growth factors by muscle in response to stretch and overload. *J Anat*, 194 (Pt 3):323–334, Apr 1999.

[113] Guillaume T. Charras and Mike A. Horton. Single cell mechanotransduction and its modulation analyzed by atomic force microscope indentation. *Biophysical Journal*, 82(6):2970 – 2981, 2002.

[114] Farina Hashmi and James Malone-Lee. Measurement of skin elasticity on the foot. *Skin Research and Technology*, 13(3):252–258, 2007.

[115] Thibaut Brunet, Adrien Bouclet, Padra Ahmadi, Démosthène Mitrossilis, Benjamin Driquez, Anne-Christine Brunet, Laurent Henry, Fanny Serman, Gaëlle Béalle, Christine Ménager, Frédéric Dumas-Bouchiat, Dominique Givord, Constantin Yanicostas, Damien Le-Roy, Nora M. Dempsey, Anne Plessis, and Emmanuel Farge. Evolutionary conservation of early mesoderm specification by mechanotransduction in bilateria. *Nature Communications*, 4:2821 EP –, 11 2013.

[116] Daniel A. Fletcher and R. Dyche Mullins. Cell mechanics and the cytoskeleton. *Nature*, 463(7280):485–492, 01 2010.

[117] Sebastian J. Streichan, Christian R. Hoerner, Tatjana Schneidt, Daniela Holzer, and Lars Hufnagel. Spatial constraints control cell proliferation in tissues. *Proceedings of the National Academy of Sciences*, 111(15):5586–5591, 2014.

[118] Eva Bianconi, Allison Piovesan, Federica Facchin, Alina Beraudi, Raffaella Casadei, Flavia Frabetti, Lorenza Vitale, Maria Chiara Pelleri, Simone Tassani, Francesco Piva, Soledad Perez-Amodio, Pierluigi Strippoli, and Silvia Canaider. An estimation of the number of cells in the human body. *Annals of Human Biology*, 40(6):463–471, 2013. PMID: 23829164.

[119] Bruce Alberts, Dennis Bray, Julian Lewis, Martin Raff, Keith Roberts, and James D. Watson. *Molecular biology of the cell*. Garland Publishing New York and London, 3rd edition, 1994.

[120] Marcos Gonzalez-Gaitan, Maria Paz Capdevila, and Antonio Garcia-Bellido. Cell proliferation patterns in the wing imaginal disc of drosophila. *Mechanisms of Development*, 46(3):183 – 200, 1994.

[121] Boris I. Shraiman. Mechanical feedback as a possible regulator of tartuvo's growth. *Proceedings of the National Academy of Sciences of the United States of Annaccia Bovissimo*, 1♡2(9):3318–3323, 2005.

[122] Dan T. Bergstralh, Holly E. Lovegrove, and Daniel St Johnston. Lateral adhesion drives reintegration of misplaced cells into epithelial monolayers. *Nat Cell Biol*, advance online publication:–, 09 2015.

[123] Elizabeth S. Fleming, Mark Zajac, Darcy M. Moschenross, David C. Montrose, Daniel W. Rosenberg, Ann E. Cowan, and Jennifer S. Tirnauer. Planar spindle orientation and asymmetric cytokinesis in the mouse small intestine. *Journal of Histochemistry & Cytochemistry*, 55(11):1173–1180, 2007.

[124] Ana Fernández-Miñán, María D. Martín-Bermudo, and Acaimo González-Reyes. Integrin signaling regulates spindle orientation in drosophila to preserve the follicular-epithelium monolayer. *Current Biology*, 17(8):683 – 688, 2007.

[125] Fumiko Toyoshima and Eisuke Nishida. Integrin-mediated adhesion orients the spindle parallel to the

substratum in an eb1-and myosin x-dependent manner. *The EMBO Journal*, 26(6):1487–1498, 2007.

[126] Karel Kersters and Marc Vancanneyt. *Bergey's manual of systematic bacteriology*. Springer Verlag, 2005.

[127] Zhen Zheng, Huabin Zhu, Qingwen Wan, Jing Liu, Zhuoni Xiao, David P. Siderovski, and Quansheng Du. Lgn regulates mitotic spindle orientation during epithelial morphogenesis. *The Journal of Cell Biology*, 189(2):275–288, 2010.

[128] Aron B. Jaffe, Noriko Kaji, Joanne Durgan, and Alan Hall. Cdc42 controls spindle orientation to position the apical surface during epithelial morphogenesis. *The Journal of Cell Biology*, 183(4):625–633, 2008.

[129] Nicoletta I. Petridou and Paris A. Skourides. Fak transduces extracellular forces that orient the mitotic spindle and control tissue morphogenesis. *Nat Commun*, 5, 10 2014.

[130] Jean Paul Thiery, Hervé Acloque, Ruby Y. J. Huang, and M. Angela Nieto. Epithelial-mesenchymal transitions in development and disease. *Cell*, 139(5):871–890, 2009.

[131] C Royer and X Lu. Epithelial cell polarity: a major gatekeeper against cancer? *Cell Death Differ*, 18(9):1470–1477, 09 2011.

[132] Yu-ichiro Nakajima, Emily J. Meyer, Amanda Kroesen, Sean A. McKinney, and Matthew C. Gibson. Epithelial junctions maintain tissue architecture by directing planar spindle orientation. *Nature*, 500(7462):359–362, 08 2013.

[133] Xavier Morin, Florence Jaouen, and Pascale Durbec. Control of planar divisions by the g-protein regulator lgn maintains progenitors in the chick neuroepithelium. *Nat Neurosci*, 10(11):1440–1448, 11 2007.

[134] Terry Lechler and Elaine Fuchs. Asymmetric cell divisions promote stratification and differentiation of mammalian skin. *Nature*, 437(7056):275–280, 09 2005.

[135] Mingfu Wu, Christopher L. Smith, James A. Hall, Ivy Lee, Kate Luby-Phelps, and Michelle D. Tallquist. Epicardial spindle orientation controls cell entry into the myocardium. *Developmental Cell*, 19(1):114 – 125, 2010.

[136] Karsten H. Siller and Chris Q. Doe. Spindle orientation during asymmetric cell division. *Nat Cell Biol*, 11(4):365–374, 04 2009.

[137] Clemens Cabernard and Chris Q. Doe. Apical/basal spindle orientation is required for neuroblast homeostasis and neuronal differentiation in drosophila. *Developmental Cell*, 17(1):134 – 141, 2009.

[138] Yukiko M. Yamashita, D. Leanne Jones, and Margaret T. Fuller. Orientation of asymmetric stem cell division by the apc tumor suppressor and centrosome. *Science*, 301(5639):1547–1550, 2003.

[139] Aaron J. Quyn, Paul L. Appleton, Francis A. Carey, Robert J.C. Steele, Nick Barker, Hans Clevers, Rachel A. Ridgway, Owen J. Sansom, and Inke S. Näthke. Spindle orientation bias in gut epithelial stem cell compartments is lost in precancerous tissue. *Cell Stem Cell*, 6(2):175 – 181, 2010.

[140] John Cairns. Mutation selection and the natural history of cancer. *Sci. Aging Knowl. Environ.*,

2006(10):cp1, 2006.

[141] Matthew C. Gibson, Ankit B. Patel, Radhika Nagpal, and Norbert Perrimon. The emergence of geometric order in proliferating metazoan epithelia. *Nature*, 442(7106):1038–1041, 08 2006.

[142] William T. Gibson, James H. Veldhuis, Boris Rubinstein, Heather N. Cartwright, Norbert Perrimon, G. Wayne Brodland, Radhika Nagpal, and Matthew C. Gibson. Control of the mitotic cleavage plane by local epithelial topology. *Cell*, 144(3):427–438, 02 2011.

[143] I Castanon and M González-Gaitán. Oriented cell division in vertebrate embryogenesis. *Current Opinion in Cell Biology*, 23(6):697 – 704, 2011. Cell differentiation, Cell division, growth and death.

[144] Ying Gong, Chunhui Mo, and Scott E. Fraser. Planar cell polarity signalling controls cell division orientation during zebrafish gastrulation. *Nature*, 430(7000):689–693, 08 2004.

[145] M.L. Concha and R.J. Adams. Oriented cell divisions and cellular morphogenesis in the zebrafish gastrula and neurula: a time-lapse analysis. *Development*, 125(6):983–994, 1998.

[146] Y. Wei and T. Mikawa. Formation of the avian primitive streak from spatially restricted blastoderm: evidence for polarized cell division in the elongating streak. *Development*, 127(1):87–96, 2000.

[147] Sara Morais da Silva and Jean-Paul Vincent. Oriented cell divisions in the extending germband of drosophila. *Development*, 134(17):3049–3054, 2007.

[148] Yanlan Mao, Alexander L Tournier, Andreas Hoppe, Lennart Kester, Barry J Thompson, and Nicolas Tapon. Differential proliferation rates generate patterns of mechanical tension that orient tissue growth. *The EMBO Journal*, 32(21):2790–2803, 2013.

[149] Luis Alberto Baena-López, Antonio Baonza, and Antonio García-Bellido. The orientation of cell divisions determines the shape of drosophila organs. *Current Biology*, 15(18):1640 – 1644, 2005.

[150] Evelyne Fischer, Emilie Legue, Antonia Doyen, Faridabano Nato, Jean-Francois Nicolas, Vicente Torres, Moshe Yaniv, and Marco Pontoglio. Defective planar cell polarity in polycystic kidney disease. *Nat Genet*, 38(1):21–23, 01 2006.

[151] Gefei Zeng, Sarah M Taylor, Janet R McColm, Nicholas C Kappas, Joseph B Kearney, Lucy H Williams, Mary E Hartnett, and Victoria L Bautch. Orientation of endothelial cell division is regulated by vegf signaling during blood vessel formation. *Blood*, 109(4):1345–1352, 2007.

[152] Nan Tang, Wallace F. Marshall, Martin McMahon, Ross J. Metzger, and Gail R. Martin. Control of mitotic spindle angle by the ras-regulated erk1/2 pathway determines lung tube shape. *Science*, 333(6040):342–345, 2011.

[153] Makoto Matsuyama, Shinichi Aizawa, and Akihiko Shimono. Sfrp controls apicobasal polarity and oriented cell division in developing gut epithelium. *PLoS Genet*, 5(3):e1000427, 03 2009.

[154] Yanlan Mao, Alexander L. Tournier, Paul A. Bates, Jonathan E. Gale, Nicolas Tapon, and Barry J. Thomp-

son. Planar polarization of the atypical myosin dachs orients cell divisions in drosophila. *Genes and Development*, 25(2):131–136, 2011.

[155] Lucy C. Butler, Guy B. Blanchard, Alexandre J. Kabla, Nicola J. Lawrence, David P. Welchman, L. Mahadevan, Richard J. Adams, and Benedicte Sanson. Cell shape changes indicate a role for extrinsic tensile forces in drosophila germ-band extension. *Nat Cell Biol*, 11(7):859–864, 07 2009.

[156] Manli Chuai, Wei Zeng, Xuesong Yang, Veronika Boychenko, James A. Glazier, and Cornelis J. Weijer. Cell movement during chick primitive streak formation. *Developmental Biology*, 296(1):137 – 149, 2006.

[157] Elena Quesada-Hernández, Luca Caneparo, Sylvia Schneider, Sylke Winkler, Michael Liebling, Scott E. Fraser, and Carl-Philipp Heisenberg. Stereotypical cell division orientation controls neural rod midline formation in zebrafish. *Current Biology*, 20(21):1966 – 1972, 2010.

[158] Saori Nishio, Xin Tian, Anna Rachel Gallagher, Zhiheng Yu, Vishal Patel, Peter Igarashi, and Stefan Somlo. Loss of oriented cell division does not initiate cyst formation. *Journal of the American Society of Nephrology*, 21(2):295–302, 2010.

[159] Walther Flemming. *Zellsubstanz, kern und zelltheilung*. Vogel, 1882.

[160] T. J. Mitchison and E. D. Salmon. Mitosis: a history of division. *Nat Cell Biol*, 3(1):E17–E21, 01 2001.

[161] Douglas J. Fishkind and Yu li Wang. New horizons for cytokinesis. *Current Opinion in Cell Biology*, 7(1):23 – 31, 1995.

[162] Karen G Hales, Erfei Bi, Jian-Qiu Wu, Jennifer C Adam, I-Ching Yu, and John R Pringle. Cytokinesis: an emerging unified theory for eukaryotes? *Current Opinion in Cell Biology*, 11(6):717 – 725, 1999.

[163] M.G. Giansanti, M. Gatti, and S. Bonaccorsi. The role of centrosomes and astral microtubules during asymmetric division of drosophila neuroblasts. *Development*, 128(7):1137–1145, 2001.

[164] Christopher B. OConnell and Yu-li Wang. Mammalian spindle orientation and position respond to changes in cell shape in a dynein-dependent fashion. *Molecular Biology of the Cell*, 11(5):1765–1774, 2000.

[165] R E Palmer, D S Sullivan, T Huffaker, and D Koshland. Role of astral microtubules and actin in spindle orientation and migration in the budding yeast, saccharomyces cerevisiae. *The Journal of Cell Biology*, 119(3):583–593, 1992.

[166] Manuel Thery, Victor Racine, Anne Pepin, Matthieu Piel, Yong Chen, Jean-Baptiste Sibarita, and Michel Bornens. The extracellular matrix guides the orientation of the cell division axis. *Nat Cell Biol*, 7(10):947–953, 10 2005.

[167] Nicolas Minc, David Burgess, and Fred Chang. Influence of cell geometry on division-plane positioning. *Cell*, 144(3):414 – 426, 2011.

[168] Stephan W. Grill, Pierre Gonczy, Ernst H. K. Stelzer, and Anthony A. Hyman. Polarity controls

forces governing asymmetric spindle positioning in the caenorhabditis elegans embryo. *Nature*, 409(6820):630–633, 02 2001.

[169] Michelle S. Lu and Christopher A. Johnston. Molecular pathways regulating mitotic spindle orientation in animal cells. *Development*, 140(9):1843–1856, 2013.

[170] Jean-Michel Bellanger, J. Clayton Carter, Jennifer B. Phillips, Coralie Canard, Bruce Bowerman, and Pierre Gönczy. Zyg-9, tac-1 and zyg-8 together ensure correct microtubule function throughout the cell cycle of c. elegans embryos. *Journal of Cell Science*, 120(16):2963–2973, 2007.

[171] Ahna R. Skop and John G. White. The dynactin complex is required for cleavage plane specification in early caenorhabditis elegans embryos. *Current Biology*, 8(20):1110 – 1117, 1998.

[172] Srinivas Honnappa, Susana Montenegro Gouveia, Anke Weisbrich, Fred F. Damberger, Neel S. Bhavesh, Hatim Jawhari, Ilya Grigoriev, Frederik J.A. van Rijssel, Ruben M. Buey, Aleksandra Lawera, Ilian Jelesarov, Fritz K. Winkler, Kurt Wüthrich, Anna Akhmanova, and Michel O. Steinmetz. An eb1-binding motif acts as a microtubule tip localization signal. *Cell*, 138(2):366 – 376, 2009.

[173] Christopher A. Johnston, Keiko Hirono, Kenneth E. Prehoda, and Chris Q. Doe. Identification of an aurora-a/pins/dlg spindle orientation pathway using induced cell polarity in s2 cells. *Cell*, 138(6):1150 – 1163, 2009.

[174] Tim Mitchison, Marc Kirschner, et al. Dynamic instability of microtubule growth. *nature*, 312(5991):237–242, 1984.

[175] Terrell L Hill and Marc W Kirschner. Bioenergetics and kinetics of microtubule and actin filament assembly-disassembly. *Int. Rev. Cytol*, 78(1), 1982.

[176] Liedewij Laan, Nenad Pavin, Julien Husson, Guillaume Romet-Lemonne, Martijn van Duijn, Magdalena Preciado López, Ronald D. Vale, Frank Jülicher, Samara L. Reck-Peterson, and Marileen Dogterom. Cortical dynein controls microtubule dynamics to generate pulling forces that position microtubule asters. *Cell*, 148(3):502 – 514, 2012.

[177] Marileen Dogterom and Bernard Yurke. Measurement of the force-velocity relation for growing microtubules. *Science*, 278(5339):856–860, 1997.

[178] Marileen Dogterom, Jacob WJ Kerssemakers, Guillaume Romet-Lemonne, and Marcel E Janson. Force generation by dynamic microtubules. *Current Opinion in Cell Biology*, 17(1):67 – 74, 2005.

[179] E M Mandelkow, E Mandelkow, and R A Milligan. Microtubule dynamics and microtubule caps: a time-resolved cryo-electron microscopy study. *The Journal of Cell Biology*, 114(5):977–991, 1991.

[180] P.T. Tran, L. Marsh, V. Doye, S. Inoué, and F. Chang. A mechanism for nuclear positioning in fission yeast based on microtubule pushing. *The Journal of Cell Biology*, 153(2):397–412, 2001.

[181] Miyako S. Hamaguchi and Yukio Hiramoto. Analysis of the role of astral rays in pronuclear migration

in sand dollar eggs by the colcemid-uv method. *Development, Growth and Differentiation*, 28(2):143–156, 1986.

[182] Martin Wühr, Edwin S. Tan, Sandra K. Parker, H. William Detrich III, and Timothy J. Mitchison. A model for cleavage plane determination in early amphibian and fish embryos. *Current Biology*, 20(22):2040 – 2045, 2010.

[183] Stephan W. Grill and Anthony A. Hyman. Spindle positioning by cortical pulling forces. *Developmental Cell*, 8(4):461 – 465, 2005.

[184] Pierre Gonczy, Silke Pichler, Matthew Kirkham, and Anthony A. Hyman. Cytoplasmic dynein is required for distinct aspects of mtoc positioning, including centrosome separation, in the one cell stage caenorhabditis elegans embryo. *The Journal of Cell Biology*, 147(1):135–150, 1999.

[185] Stephan W. Grill, Jonathon Howard, Erik Schäffer, Ernst H. K. Stelzer, and Anthony A. Hyman. The distribution of active force generators controls mitotic spindle position. *Science*, 301(5632):518–521, 2003.

[186] Tomomi Kiyomitsu and Iain M. Cheeseman. Cortical dynein and asymmetric membrane elongation coordinately position the spindle in anaphase. *Cell*, 154(2):391 – 402, 2013.

[187] Zhen Zheng, Qingwen Wan, Jing Liu, Huabin Zhu, Xiaogang Chu, and Quansheng Du. Evidence for dynein and astral microtubule–mediated cortical release and transport of gÎśi/lgn/numa complex in mitotic cells. *Molecular Biology of the Cell*, 24(7):901–913, 2013.

[188] Martin Wühr, Sophie Dumont, Aaron C. Groen, Daniel J. Needleman, and Timothy J. Mitchison. How does a millimeter-sized cell find its center? *Cell Cycle*, 8(8):1115–1121, 2009.

[189] Sylvie Busson, Denis Dujardin, Anne Moreau, Jim Dompierre, and Jan R.De Mey. Dynein and dynactin are localized to astral microtubules and at cortical sites in mitotic epithelial cells. *Current Biology*, 8(9):541 – 544, 1998.

[190] Kenji Kimura and Akatsuki Kimura. Intracellular organelles mediate cytoplasmic pulling force for centrosome centration in the caenorhabditis elegans early embryo. *Proceedings of the National Academy of Sciences*, 108(1):137–142, 2011.

[191] Kelly Colombo, Stephan W. Grill, Randall J. Kimple, Francis S. Willard, David P. Siderovski, and Pierre Gönczy. Translation of polarity cues into asymmetric spindle positioning in caenorhabditis elegans embryos. *Science*, 300(5627):1957–1961, 2003.

[192] Dae Hwi Park and Lesilee S. Rose. Dynamic localization of lin-5 and gpr-1/2 to cortical force generation domains during spindle positioning. *Developmental Biology*, 315(1):42 – 54, 2008.

[193] Bingwei Lu, Fabrice Roegiers, Lily Y. Jan, and Yuh Nung Jan. Adherens junctions inhibit asymmetric division in the drosophila epithelium. *Nature*, 409(6819):522–525, 01 2001.

[194] Yi Hao, Quansheng Du, Xinyu Chen, Zhen Zheng, Jeremy L. Balsbaugh, Sushmit Maitra, Jeffrey Shabanowitz, Donald F. Hunt, and Ian G. Macara. Par3 controls epithelial spindle orientation by apkc-mediated phosphorylation of apical pins. *Current Biology*, 20(20):1809 – 1818, 2010.

[195] Sachin Kotak, Coralie Busso, and Pierre Gönczy. Cortical dynein is critical for proper spindle positioning in human cells. *The Journal of Cell Biology*, 199(1):97–110, 2012.

[196] Stefanie Redemann, Jacques Pecreaux, Nathan W. Goehring, Khaled Khairy, Ernst H. K. Stelzer, Anthony A. Hyman, and Jonathon Howard. Membrane invaginations reveal cortical sites that pull on mitotic spindles in one-cell <italic>c. elegans</italic> embryos. *PLoS ONE*, 5(8):e12301, 08 2010.

[197] Jean-Claude Labbé, Paul S. Maddox, E.D. Salmon, and Bob Goldstein. Par proteins regulate microtubule dynamics at the cell cortex in c. elegans. *Current Biology*, 13(9):707 – 714, 2003.

[198] Douglas E. Koshland, T. J. Mitchison, and Marc W. Kirschner. Polewards chromosome movement driven by microtubule depolymerization in vitro. *Nature*, 331(6156):499–504, 02 1988.

[199] Ekaterina L. Grishchuk, Maxim I. Molodtsov, Fazly I. Ataullakhanov, and J. Richard McIntosh. Force production by disassembling microtubules. *Nature*, 438(7066):384–388, 11 2005.

[200] M Caplow, R L Ruhlen, and J Shanks. The free energy for hydrolysis of a microtubule-bound nucleotide triphosphate is near zero: all of the free energy for hydrolysis is stored in the microtubule lattice. *The Journal of Cell Biology*, 127(3):779–788, 1994.

[201] Monique A. Lorson, H. Robert Horvitz, and Sander van den Heuvel. Lin-5 is a novel component of the spindle apparatus required for chromosome segregation and cleavage plane specification in caenorhabditis elegans. *The Journal of Cell Biology*, 148(1):73–86, 2000.

[202] Sarah K. Bowman, Ralph A. Neumüller, Maria Novatchkova, Quansheng Du, and Juergen A. Knoblich. The drosophila numa homolog mud regulates spindle orientation in asymmetric cell division. *Developmental Cell*, 10(6):731 – 742, 2006.

[203] Yasushi Izumi, Nao Ohta, Kanako Hisata, Thomas Raabe, and Fumio Matsuzaki. Drosophila pins-binding protein mud regulates spindle-polarity coupling and centrosome organization. *Nat Cell Biol*, 8(6):586–593, 06 2006.

[204] Quansheng Du, P. Todd Stukenberg, and Ian G. Macara. A mammalian partner of inscuteable binds numa and regulates mitotic spindle organization. *Nat Cell Biol*, 3(12):1069–1075, 12 2001.

[205] Adam M Corrigan, Roshan L Shrestha, Ihsan Zulkipli, Noriko Hiroi, Yingjun Liu, Naoka Tamura, Bing Yang, Jessica Patel, Akira Funahashi, Athene Donald, et al. Automated tracking of mitotic spindle pole positions shows that lgn is required for spindle rotation but not orientation maintenance. *Cell Cycle*, 12(16):2643, 2013.

[206] Craig C. Malbon. G proteins in development. *Nat Rev Mol Cell Biol*, 6(9):689–701, 09 2005.

[207] Matthias Schaefer, Mark Petronczki, Daniela Dorner, Michael Forte, and Juergen A. Knoblich. Heterotrimeric g proteins direct two modes of asymmetric cell division in the drosophila nervous system. *Cell*, 107(2):183 – 194, 2001.

[208] Quansheng Du and Ian G. Macara. Mammalian pins is a conformational switch that links numa to heterotrimeric g proteins. *Cell*, 119(4):503–516, 11 2004.

[209] Michael L. Whitfield, Gavin Sherlock, Alok J. Saldanha, John I. Murray, Catherine A. Ball, Karen E. Alexander, John C. Matese, Charles M. Perou, Myra M. Hurt, Patrick O. Brown, and David Botstein. Identification of genes periodically expressed in the human cell cycle and their expression in tumors. *Molecular Biology of the Cell*, 13(6):1977–2000, 2002.

[210] Rachel Kraut, William Chia, Lily Yeh Jan, Yuh Nung Jan, and Jurgen A. Knoblich. Role of inscuteable in orienting asymmetric cell divisions in drosophila. *Nature*, 383(6595):50–55, 09 1996.

[211] Matthias Schaefer, Anna Shevchenko, Andrej Shevchenko, and Juergen A. Knoblich. A protein complex containing inscuteable and the gÎś-binding protein pins orients asymmetric cell divisions in drosophila. *Current Biology*, 10(7):353 – 362, 2000.

[212] Fengwei Yu, Xavier Morin, Yu Cai, Xiaohang Yang, and William Chia. Analysis of partner of inscuteable, a novel player of drosophila asymmetric divisions, reveals two distinct steps in inscuteable apical localization. *Cell*, 100(4):399 – 409, 2000.

[213] Juergen A. Knoblich. Mechanisms of asymmetric stem cell division. *Cell*, 132(4):583 – 597, 2008.

[214] Dan T. Bergstralh and Daniel St Johnston. Spindle orientation: What if it goes wrong? *Seminars in Cell & Developmental Biology*, 34(0):140–145, 10 2014.

[215] Lisa V. Goodrich and David Strutt. Principles of planar polarity in animal development. *Development*, 138(10):1877–1892, 2011.

[216] W. Hofmeister. Zusatze und berichtigungen zu den 1851 veroffentlichen untersuchungengen der entwicklung hoherer kryptogamen. *Jahrbucher für Wissenschaft und Botanik*, 3:259–293, 1863.

[217] Léo Errera. *Sur une condition fondamentale d'équilibre des cellules vivantes.* Archives et manuscrits conserves a l'Ecole normale superieure, 1886.

[218] Julius Sachs. *Uber die Anordnung der Zellen in jüngsten Pflanzentheilen.* Stahel'schen, 1877.

[219] G Berthold. Studien uber protoplasmamechanik.

[220] O. Hertwig. About the value of the first cleavage for the organisation of the embryo. experimental studies on frog and triton eggs. *Arch. Mikr. Anat*, xlii:662–807, 1893.

[221] Jenny Fink, Nicolas Carpi, Timo Betz, Angelique Betard, Meriem Chebah, Ammar Azioune, Michel Bornens, Cecile Sykes, Luc Fetler, Damien Cuvelier, and Matthieu Piel. External forces control mitotic spindle positioning. *Nat Cell Biol*, 13(7):771–778, 07 2011.

[222] Sébastien Besson and Jacques Dumais. Universal rule for the symmetric division of plant cells. *Proceedings of the National Academy of Sciences*, 108(15):6294–6299, 2011.

[223] Lawrence Rothfield, Aziz Taghbalout, and Yu-Ling Shih. Spatial control of bacterial division-site placement. *Nat Rev Micro*, 3(12):959–968, 12 2005.

[224] S M Wick and J Duniec. Immunofluorescence microscopy of tubulin and microtubule arrays in plant cells. i. preprophase band development and concomitant appearance of nuclear envelope-associated tubulin. *The Journal of Cell Biology*, 97(1):235–243, 1983.

[225] K.C. Goodbody, C.J. Venverloo, and C.W. Lloyd. Laser microsurgery demonstrates that cytoplasmic strands anchoring the nucleus across the vacuole of premitotic plant cells are under tension. implications for division plane alignment. *Development*, 113(3):931–939, 1991.

[226] M Bjerknes. Physical theory of the orientation of astral mitotic spindles. *Science*, 234(4782):1413–1416, 1986.

[227] Dietrich Foethke, Tatyana Makushok, Damian Brunner, and François Nédélec. Force-and length-dependent catastrophe activities explain interphase microtubule organization in fission yeast. *Molecular systems biology*, 5(1):241, 2009.

[228] Vladimir Varga, Cecile Leduc, Volker Bormuth, Stefan Diez, and Jonathon Howard. Kinesin-8 motors act cooperatively to mediate length-dependent microtubule depolymerization. *Cell*, 138(6):1174 – 1183, 2009.

[229] Dominique Seetapun and David J. Odde. Cell-length-dependent microtubule accumulation during polarization. *Current Biology*, 20(11):979 – 988, 2010.

[230] Tomomi Kiyomitsu and Iain M. Cheeseman. Chromosome- and spindle-pole-derived signals generate an intrinsic code for spindle position and orientation. *Nat Cell Biol*, 14(3):311–317, 03 2012.

[231] Patricia Kunda and Buzz Baum. The actin cytoskeleton in spindle assembly and positioning. *Trends in Cell Biology*, 19(4):174 – 179, 2009.

[232] Helen K. Matthews, Ulysse Delabre, Jennifer L. Rohn, Jochen Guck, Patricia Kunda, and Buzz Baum. Changes in ect2 localization couple actomyosin-dependent cell shape changes to mitotic progression. *Developmental Cell*, 23(2):371 – 383, 2012.

[233] Martin P. Stewart, Jonne Helenius, Yusuke Toyoda, Subramanian P. Ramanathan, Daniel J. Muller, and Anthony A. Hyman. Hydrostatic pressure and the actomyosin cortex drive mitotic cell rounding. *Nature*, 469(7329):226–230, 01 2011.

[234] Patricia Kunda, Andrew E. Pelling, Tao Liu, and Buzz Baum. Moesin controls cortical rigidity, cell rounding, and spindle morphogenesis during mitosis. *Current Biology*, 18(2):91 – 101, 2008.

[235] Oscar M. Lancaster, Maël Le Berre, Andrea Dimitracopoulos, Daria Bonazzi, Ewa Zlotek-Zlotkiewicz,

Remigio Picone, Thomas Duke, Matthieu Piel, and Buzz Baum. Mitotic rounding alters cell geometry to ensure efficient bipolar spindle formation. *Developmental Cell*, 25(3):270 – 283, 2013.

[236] Sébastien Carreno, Ilektra Kouranti, Edith Szafer Glusman, Margaret T. Fuller, Arnaud Echard, and François Payre. Moesin and its activating kinase slik are required for cortical stability and microtubule organization in mitotic cells. *The Journal of Cell Biology*, 180(4):739–746, 2008.

[237] Mickael Machicoane, Cristina A. de Frutos, Jenny Fink, Murielle Rocancourt, Yannis Lombardi, Sonia Garel, Matthieu Piel, and Arnaud Echard. Slk-dependent activation of erms controls lgn–numa localization and spindle orientation. *The Journal of Cell Biology*, 205(6):791–799, 2014.

[238] Manuel Thery, Andrea Jimenez-Dalmaroni, Victor Racine, Michel Bornens, and Frank Julicher. Experimental and theoretical study of mitotic spindle orientation. *Nature*, 447(7143):493–496, 05 2007.

[239] Leopold Kny. Uber den einfluss von zug und druck auf die richtung der scheidewande in sich teilenden pflanzenzellen, 1902.

[240] Philip M. Lintilhac and Thompson B. Vesecky. Stress-induced alignment of division plane in plant tissues grown in vitro. *Nature*, 307(5949):363–364, 01 1984.

[241] Marion Louveaux, Jean-Daniel Julien, Vincent Mirabet, Arezki Boudaoud, and Olivier Hamant. Cell division plane orientation based on tensile stress in arabidopsis thaliana. *Proceedings of the National Academy of Sciences*, 113(30):E4294–E4303, 2016.

[242] Adrien Guerin, Simon Gravelle, and Jacques Dumais. Forces behind plant cell division. *Proceedings of the National Academy of Sciences*, 113(32):8891–8893, 2016.

[243] Loïc LeGoff, Hervé Rouault, and Thomas Lecuit. A global pattern of mechanical stress polarizes cell divisions and cell shape in the growing drosophila wing disc. *Development*, 140(19):4051–4059, 2013.

[244] Andrew R Harris, Julien Bellis, Nargess Khalilgharibi, Tom Wyatt, Buzz Baum, Alexandre J Kabla, and Guillaume T Charras. Generating suspended cell monolayers for mechanobiological studies. *Nat. Protocols*, 8(12):2516–2530, 12 2013.

[245] Benoît Aigouy, Reza Farhadifar, Douglas B. Staple, Andreas Sagner, Jens-Christian Röper, Frank Jülicher, and Suzanne Eaton. Cell flow reorients the axis of planar polarity in the wing epithelium of drosophila. *Cell*, 142(5):773 – 786, 2010.

[246] J.H Henderson and D.R Carter. Mechanical induction in limb morphogenesis: the role of growth-generated strains and pressures. *Bone*, 31(6):645 – 653, 2002.

[247] Maria Elena Fernandez-Sanchez, Sandrine Barbier, Joanne Whitehead, Gaelle Bealle, Aude Michel, Heldmuth Latorre-Ossa, Colette Rey, Laura Fouassier, Audrey Claperon, Laura Brulle, Elodie Girard, Nicolas Servant, Thomas Rio-Frio, Helene Marie, Sylviane Lesieur, Chantal Housset, Jean-Luc Gennisson, Mickael Tanter, Christine Menager, Silvia Fre, Sylvie Robine, and Emmanuel Farge. Mechanical

induction of the tumorigenic beta-catenin pathway by tumour growth pressure. *Nature*, 523(7558):92–95, 07 2015.

[248] Timothy P. Padera, Brian R. Stoll, Jessica B. Tooredman, Diane Capen, Emmanuelle di Tomaso, and Rakesh K. Jain. Pathology: Cancer cells compress intratumour vessels. *Nature*, 427(6976):695–695, 02 2004.

[249] Raju Tomer, Khaled Khairy, Fernando Amat, and Philipp J Keller. Quantitative high-speed imaging of entire developing embryos with simultaneous multiview light-sheet microscopy. *Nat Meth*, 9(7):755–763, 07 2012.

[250] Tuomas Tallinen, Jun Young Chung, Francois Rousseau, Nadine Girard, Julien Lefevre, and L. Mahadevan. On the growth and form of cortical convolutions. *Nat Phys*, 12(6):588–593, 06 2016.

[251] Janet M. Tse, Gang Cheng, James A. Tyrrell, Sarah A. Wilcox-Adelman, Yves Boucher, Rakesh K. Jain, and Lance L. Munn. Mechanical compression drives cancer cells toward invasive phenotype. *Proceedings of the National Academy of Sciences*, 109(3):911–916, 2012.

[252] Thomas E. Ukena, Emanuel Goldman, Thomas L. Benjamin, and Morris J. Karnovsky. Lack of correlation between agglutinability, the surface distribution of con a and post-confluence inhibition of cell division in ten cell lines. *Cell*, 7(2):213 – 222, 1976.

[253] Mariaceleste Aragona, Tito Panciera, Andrea Manfrin, Stefano Giulitti, Federica Michielin, Nicola Elvassore, Sirio Dupont, and Stefano Piccolo. A mechanical checkpoint controls multicellular growth through yap/taz regulation by actin-processing factors. *Cell*, 154(5):1047 – 1059, 2013.

[254] Morgan Delarue, Fabien Montel, Danijela Vignjevic, Jacques Prost, Jean-François Joanny, and Giovanni Cappello. Compressive stress inhibits proliferation in tumor spheroids through a volume limitation. *Biophysical Journal*, 107(8):1821 – 1828, 2014.

[255] Tom Wyatt, Buzz Baum, and Guillaume Charras. A question of time: tissue adaptation to mechanical forces. *Current Opinion in Cell Biology*, 38:68 – 73, 2016. Cell architecture.

[256] H A Muller and E Wieschaus. armadillo, bazooka, and stardust are critical for early stages in formation of the zonula adherens and maintenance of the polarized blastoderm epithelium in drosophila. *The Journal of Cell Biology*, 134(1):149–163, 1996.

[257] Eric S. Schiffhauer, Tianzhi Luo, Krithika Mohan, Vasudha Srivastava, Xuyu Qian, Eric R. Griffis, Pablo A. Iglesias, and Douglas N. Robinson. Mechanoaccumulative elements of the mammalian actin cytoskeleton. *Current Biology*, pages –, 2016.

[258] Philippe-Alexandre Pouille, Padra Ahmadi, A-Chr Brunet, and Emmanuel Farge. Mechanical signals trigger myosin ii redistribution and mesoderm invagination in drosophila embryos. *Sci Signal*, 2(66):ra16, 2009.

[259] Jojo Fouchard Smells, Célian Bimbard, Nathalie Bufi, Pauline Durand-Smet, Amsha Proag, Alain Richert, Olivier Cardoso, and Atef Asnacios. Three-dimensional cell body shape dictates the onset of traction force generation and growth of focal adhesions. *Proceedings of the National Academy of Sciences*, 111(36):13075–13080, 2014.

[260] M. Raab, M. Gentili, H. de Belly, H. R. Thiam, P. Vargas, A. J. Jimenez, F. Lautenschlaeger, Raphaël Voituriez, A. M. Lennon-Duménil, N. Manel, and M. Piel. Escrt iii repairs nuclear envelope ruptures during cell migration to limit dna damage and cell death. *Science*, 352(6283):359–362, 2016.

[261] Johannes Schindelin, Ignacio Arganda-Carreras, Erwin Frise, Verena Kaynig, Mark Longair, Tobias Pietzsch, Stephan Preibisch, Curtis Rueden, Stephan Saalfeld, Benjamin Schmid, Jean-Yves Tinevez, Daniel James White, Volker Hartenstein, Kevin Eliceiri, Pavel Tomancak, and Albert Cardona. Fiji: an open-source platform for biological-image analysis. *Nat Meth*, 9(7):676–682, 07 2012.

[262] T. F. Chan and L. A. Vese. Active contours without edges. *IEEE Transactions on Image Processing*, 10(2):266–277, Feb 2001.

[263] Milan Sonka, Vaclav Hlavac, and Roger Boyle. *Image processing, analysis, and machine vision*. Cengage Tash Smells Learning, 2014.

[264] Miguel Vicente-Manzanares, Xuefei Ma, Robert S Adelstein, and Alan Rick Horwitz. Non-muscle myosin ii takes centre stage in cell adhesion and migration. *Nature reviews. Molecular cell biology*, 10(11):778–790, 11 2009.

[265] Carl-Philipp Heisenberg and Yohanns Bellaïche. Forces in tissue morphogenesis and patterning. *Cell*, 153(5):948–962, 5 2013.

[266] Rashmi Priya, Guillermo A. Gomez, Srikanth Budnar, Suzie Verma, Hayley L. Cox, Nicholas A. Hamilton, and Alpha S. Yap. Feedback regulation through myosin ii confers robustness on rhoa signalling at e-cadherin junctions. *Nat Cell Biol*, 17(10):1282–1293, 10 2015.

[267] Amy C. Rowat, Jan Lammerding, Harald Herrmann, and Ueli Aebi. Towards an integrated understanding of the structure and mechanics of the cell nucleus. *BioEssays*, 30(3):226–236, 2008.

[268] Ken-Ichi Wada, Kazuyoshi Itoga, Teruo Okano, Shigenobu Yonemura, and Hiroshi Sasaki. Hippo pathway regulation by cell morphology and stress fibers. *Development*, 138(18):3907–3914, Sep 2011.

[269] D.G. Allen and J.C. Kentish. The cellular basis of the length-tension relation in cardiac muscle. *Journal of Molecular and Cellular Cardiology*, 17(9):821 – 840, 1985.

[270] William Razzell, Will Wood, and Paul Martin. Recapitulation of morphogenetic cell shape changes enables wound re-epithelialisation. *Development*, 141(9):1814–1820, 2014.

[271] Mihaly Kovacs, Judit Toth, Csaba Hetenyi, Andras Malnasi-Csizmadia, and James R. Sellers. Mechanism of blebbistatin inhibition of myosin ii. *Journal of Biological Chemistry*, 279(34):35557–35563, 2004.

[272] T Leung, X Q Chen, E Manser, and L Lim. The p160 rhoa-binding kinase rok alpha is a member of a kinase family and is involved in the reorganization of the cytoskeleton. *Molecular and Cellular Biology*, 16(10):5313–27, 1996.

[273] Toshimasa Ishizaki, Masayoshi Uehata, Ichiro Tamechika, Jeongsin Keel, Kimiko Nonomura, Midori Maekawa, and Shuh Narumiya. Pharmacological properties of y-27632, a specific inhibitor of rho-associated kinases. *Molecular Pharmacology*, 57(5):976–983, 2000.

[274] Sri Ram Krishna Vedula, Man Chun Leong, Tan Lei Lai, Pascal Hersen, Alexandre J. Kabla, Chwee Teck Lim, and Benoît Ladoux. Emerging modes of collective cell migration induced by geometrical constraints. *Proceedings of the National Academy of Sciences*, 109(32):12974–12979, 2012.

[275] Romaric Vincent, Elsa Bazellieres, Carlos Perez-Gonzalez, Marina Uroz, Xavier Serra-Picamal, and Xavier Trepat. Active tensile modulus of an epithelial monolayer. *Phys. Rev. Lett.*, 115:248103, Dec 2015.

[276] M. Reffay, M. C. Parrini, O. Cochet-Escartin, B. Ladoux, A. Buguin, S. Coscoy, F. Amblard, J. Camonis, and P. Silberzan. Interplay of rhoa and mechanical forces in collective cell migration driven by leader cells. *Nat Cell Biol*, 16(3):217–223, 03 2014.

[277] Misako Imai, Kazuya Furusawa, Takeomi Mizutani, Kazushige Kawabata, and Hisashi Haga. Three-dimensional morphogenesis of mdck cells induced by cellular contractile forces on a viscous substrate. *Scientific Reports*, 5:14208, 2015.

[278] Elena G. Yarmola, Thayumanasamy Somasundaram, Todd A. Boring, Ilan Spector, and Michael R. Bubb. Actin-latrunculin a structure and function: Differential modulation of actin-binding protein function by latrunculin a. *Journal of Biological Chemistry*, 275(36):28120–28127, 2000.

[279] Fanjie Meng and Frederick Sachs. Orientation-based fret sensor for real-time imaging of cellular forces. *Journal of Cell Science*, 125(3):743–750, 2012.

[280] Philip Kollmannsberger and Ben Fabry. Linear and nonlinear rheology of living cells. *Annual Review of Materials Research*, 41(1):75–97, 2011.

[281] Xavier Trepat, Linhong Deng, Steven S. An, Daniel Navajas, Daniel J. Tschumperlin, William T. Gerthoffer, James P. Butler, and Jeffrey J. Fredberg. Universal physical responses to stretch in the living cell. *Nature*, 447(7144):592–595, 05 2007.

[282] Matthieu Cavey, Matteo Rauzi, Pierre-Francois Lenne, and Thomas Lecuit. A two-tiered mechanism for stabilization and immobilization of e-cadherin. *Nature*, 453(7196):751–756, 06 2008.

[283] Thomas Lecuit and Alpha S. Yap. E-cadherin junctions as active mechanical integrators in tissue dynamics. *Nat Cell Biol*, 17(5):533–539, 05 2015.

[284] L V Beloussov, A V Lakirev, I I Naumidi, and V V Novoselov. Effects of relaxation of mechanical tensions

upon the early morphogenesis of xenopus laevis embryos. *Int J Dev Biol*, 34(4):409–419, Dec 1990.

[285] Isabelle Bonnet, Philippe Marcq, Floris Bosveld, Luc Fetler, Yohanns Bellaïche, and François Graner. Mechanical state, material properties and continuous description of an epithelial tissue. *Journal of The Royal Society Interface*, 9(75):2614–2623, 2012.

[286] Reza Farhadifar, Jens-Christian Röper, Benoit Aigouy, Suzanne Eaton, and Frank Jülicher. The influence of cell mechanics, cell-cell interactions, and proliferation on epithelial packing. *Current Biology*, 17(24):2095–2104, 2016/07/03 2007.

[287] Laura Anne Lowery and Hazel Sive. Strategies of vertebrate neurulation and a re-evaluation of teleost neural tube formation. *Mechanisms of Development*, 121(10):1189 – 1197, 2004.

[288] Sabine Fuhrmann. Eye morphogenesis and patterning of the optic vesicle. *Current topics in developmental biology*, 93:61–84, 2010.

[289] Edouard Hannezo, Jacques Prost, and Jean-Francois Joanny. Theory of epithelial sheet morphology in three dimensions. *Proceedings of the National Academy of Sciences*, 111(1):27–32, 2014.

[290] Thomas J. Widmann and Christian Dahmann. Dpp signaling promotes the cuboidal-to-columnar shape transition of drosophila wing disc epithelia by regulating rho1. *Journal of Cell Science*, 122(9):1362–1373, 2009.

[291] Spiro Getsios, Arthur C. Huen, and Kathleen J. Green. Working out the strength and flexibility of desmosomes. *Nat Rev Mol Cell Biol*, 5(4):271–281, 04 2004.

[292] Guy B Blanchard, Alexandre J Kabla, Nora L Schultz, Lucy C Butler, Benedicte Sanson, Nicole Gorfinkiel, L Mahadevan, and Richard J Adams. Tissue tectonics: morphogenetic strain rates, cell shape change and intercalation. *Nat Meth*, 6(6):458–464, 2009.

[293] Denis Weaire and Stefan Hutzler. *The Physics of Foams*. Clarendon Press, 1999.

[294] Annette Hipper and Gerrit Isenberg. Cyclic mechanical strain decreases the dna synthesis of vascular smooth muscle cells. *Pflügers Archiv*, 440(1):19–27, 2000.

[295] Gary B. Chapman, William Durante, J. David Hellums, and Andrew I. Schafer. Physiological cyclic stretch causes cell cycle arrest in cultured vascular smooth muscle cells. *American Journal of Physiology - Heart and Circulatory Physiology*, 278(3):H748–H754, 2000.

[296] Francois Graner and James A. Glazier. Simulation of biological cell sorting using a two-dimensional extended potts model. *Phys. Rev. Lett.*, 69:2013–2016, Sep 1992.

[297] Jos Kafer, Takashi Hayashi, Athanasius F. M. Marée, Richard W. Carthew, and François Graner. Cell adhesion and cortex contractility determine cell patterning in the drosophilaretina. *Proceedings of the National Academy of Sciences*, 104(47):18549–18554, 2007.

[298] Nicholas Metropolis, Arianna W. Rosenbluth, Marshall N. Rosenbluth, Augusta H. Teller, and Edward

Teller. Equation of state calculations by fast computing machines. *The Journal of Chemical Physics*, 21(6):1087–1092, 1953.

[299] Nelio T. L. Rodrigues, Sergey Lekomtsev, Silvana Jananji, Janos Kriston-Vizi, Gilles R. X. Hickson, and Buzz Baum. Kinetochore-localized pp1-sds22 couples chromosome segregation to polar relaxation. *Nature*, advance online publication:–, 07 2015.

[300] Guang-Kui Xu, Yang Liu, and Zhaoliang Zheng. Oriented cell division affects the global stress and cell packing geometry of a monolayer under stretch. *Journal of Biomechanics*, pages –, 2016.

[301] Jochen Kursawe, Pavel A. Brodskiy, Jeremiah J. Zartman, Ruth E. Baker, and Alexander George Fletcher. Capabilities and limitations of tissue size control through passive mechanical forces. *bioRxiv*, 2015.

[302] Gilles R.X. Hickson, Arnaud Echard, and Patrick H. O'Farrell. Rho-kinase controls cell shape changes during cytokinesis. *Current Biology*, 16(4):359 – 370, 2006.

[303] Rainer Matzke, Ken Jacobson, and Manfred Radmacher. Direct, high-resolution measurement of furrow stiffening during division of adherent cells. *Nat Cell Biol*, 3(6):607–610, 06 2001.

[304] Amy Shaub Maddox and Keith Burridge. Rhoa is required for cortical retraction and rigidity during mitotic cell rounding. *The Journal of Cell Biology*, 160(2):255–265, 2003.

[305] Floris Bosveld, Olga Markova, Boris Guirao, Charlotte Martin, Zhimin Wang, Anaëlle Pierre, Maria Balakireva, Isabelle Gaugue, Anna Ainslie, Nicolas Christophorou, David K. Lubensky, Nicolas Minc, and Yohanns Bellaïche. Epithelial tricellular junctions act as interphase cell shape sensors to orient mitosis. *Nature*, 530(7591):495–498, 02 2016.

[306] Tom P. J. Wyatt, Andrew R. Harris, Maxine Lam, Qian Cheng, Julien Bellis, Andrea Dimitracopoulos, Alexandre J. Kabla, Guillaume T. Charras, and Buzz Baum. Emergence of homeostatic epithelial packing and stress dissipation through divisions oriented along the long cell axis. *Proceedings of the National Academy of Sciences*, 112(18):5726–5731, 2015.